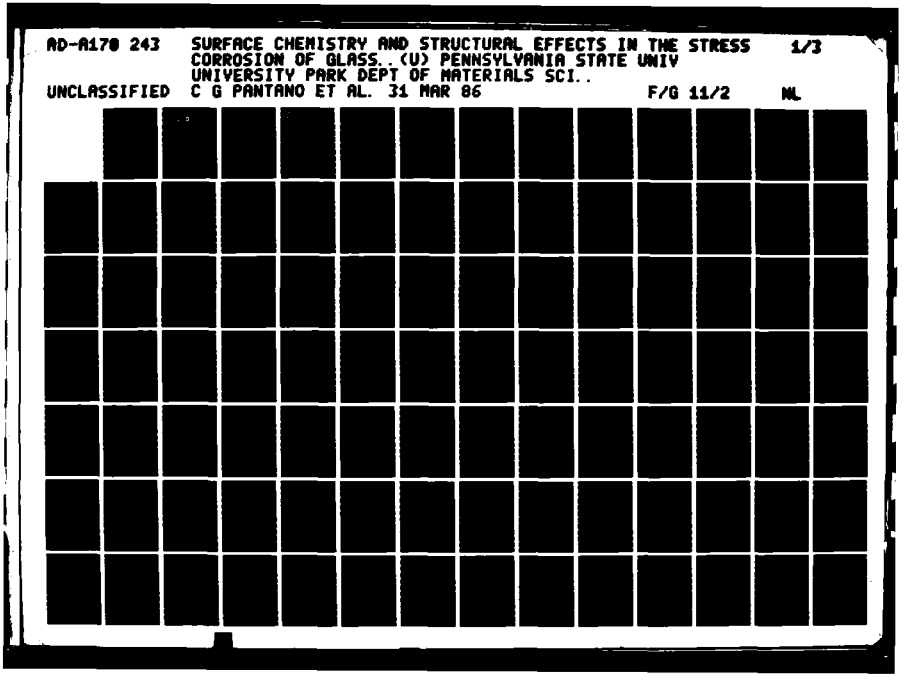
AD-A170 243 SURFACE CHEMISTRY AND STRUCTURAL EFFECTS IN THE STRESS 1/3
CORROSION OF GLASS..(U) PENNSYLVANIA STATE UNIV
UNIVERSITY PARK DEPT OF MATERIALS SCI..
UNCLASSIFIED C G PANTANO ET AL. 31 MAR 86 F/G 11/2 NL

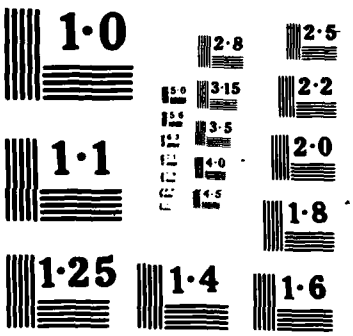
1·0
1·1
1·25
1·4
1·6
1·8
2·0
2·2
2·5
2·8
3·15
3·5
4·0
4·5
5·0

(2)

REPORT DOCUMENTATION PAGE

1b. RESTRICTIVE MARKINGS	
2b. DECLASSIFICATION/DOWNGRADING SCHEDULE	3. DISTRIBUTION/AVAILABILITY OF REPORT: Approved for public release, distribution unlimited
4. PERFORMING ORGANIZATION REPORT NUMBER(S)	5. MONITORING ORGANIZATION REPORT NUMBER(S): AFOSR-TR- 86-0502
6a. NAME OF PERFORMING ORGANIZATION: Dept. of Mat. Sci. & Eng. Pennsylvania State University	6b. OFFICE SYMBOL (If applicable)
6c. ADDRESS (City, State and ZIP Code): 123 Steidle Bldg. University Park, PA 16802	7a. NAME OF MONITORING ORGANIZATION: AFOSR/NC
	7b. ADDRESS (City, State and ZIP Code): Bldg 410 Bolling AFB, DC 20332-6448
8a. NAME OF FUNDING/SPONSORING ORGANIZATION: AFOSR/NC	8b. OFFICE SYMBOL (If applicable)
8c. ADDRESS (City, State and ZIP Code): Bldg 410 Bolling AFB, DC 20332-6448	9. PROCUREMENT INSTRUMENT IDENTIFICATION NUMBER: AFOSF-82-0013

10. SOURCE OF FUNDING NOS.

PROGRAM ELEMENT NO.	PROJECT NO.	TASK NO.	WORK UNIT NO.
61102F	2303	A3	

11. TITLE (Include Security Classification): Surface Chemistry and Structural Effects in the Stress Corrosion of Glass and Ceramic Materials.

12. PERSONAL AUTHOR(S): Carlo G. Pantano and John J. Mecholsky

13a. TYPE OF REPORT	13b. TIME COVERED	14. DATE OF REPORT (Yr., Mo., Day)	15. PAGE COUNT
Final	FROM 1/82 TO 1/86	March 31, 1986	107

16. SUPPLEMENTARY NOTATION

17 COSATI CODES			18. SUBJECT TERMS (Continue on reverse if necessary and identify by block number)
FIELD	GROUP	SUB GR	Glasses, Silicate, Velocity, Plateaus, Thresholds Aqueous, Parameter

19. ABSTRACT (Continue on reverse if necessary and identify by block number)

The fracture behavior of glasses in the system $Na_2O \cdot xAl_2O_3 \cdot (3-x)SiO_2$ (x=0.0,0.2,0.4,0.6,0.8 and 1.0) has been evaluated, and independently, their chemical corrosion in aqueous solutions was studied. It is to be noted that the alkali-concentration, which is usually assumed to be directly responsible for the chemical reactivity of silicate glasses, was held constant in this family of glasses. The changes imposed upon the Al_2O_3/SiO_2 ratio, on the other hand, were intended to influence the network structure of the glass. The V-K_I diagrams were obtained using the constant moment double cantilever beam technique in a wide variety of environments. The n-parameter in Region I was found to be independent of pH, whereas the presence of velocity plateaus and thresholds was shown to be very dependent upon the composition of the aqueous environment. This behavior was attributed to interactions between the fracture surfaces behind the crack-tip. The dependence of the n-parameter upon the bulk composition and structure of the glass was correlated with the elastic properties of the glass; i.e., the value of the n-parameter did not depend directly upon the corresponding corrosion resistance of the glass. Finally, the static fatigue limit, at least in the

20. DISTRIBUTION/AVAILABILITY OF ABSTRACT: UNCLASSIFIED/UNLIMITED ☒ SAME AS RPT ☒ DTIC USERS ☐	21. ABSTRACT SECURITY CLASSIFICATION: DTIC FILE COPY
22a. NAME OF RESPONSIBLE INDIVIDUAL: Lt Col Larry W. Burggraf	22b. TELEPHONE NUMBER (Include Area Code): 202-767-4960
	22c. OFFICE SYMBOL: NC

DD FORM 1473, 83 APR EDITION OF 1 JAN 73 IS OBSOLETE.

19. Abstract (continued)

case of the $Na_2O \cdot 3SiO_2$ (x=0.0) glass, could be explained in terms of crack-healing rather than crack-blunting. Altogether, this study of fracture within a systematic compositional series of glasses led to critical assessments of the existing models for environment-dependent crack growth in glass. The results of comparable - although less extensive - studies on fluorozirconate glasses and silica sol/gel materials are also reported.

THE COLLEGE OF EARTH AND MINERAL SCIENCES

Contract No. AFOSR-82-0013

Final Report
to
Air Force Office of Scientific Research
Bolling AFB, DC 20332

SURFACE CHEMISTRY AND STRUCTURAL EFFECTS IN THE STRESS CORROSION OF GLASS AND CERAMIC MATERIALS

C. G. Pantano and J. J. Mecholsky
Department of Materials Science and Engineering

The Pennsylvania State University

University Park, Pennsylvania

PREFACE

This report summarizes the work performed at The Pennsylvania State University during the period from 1 January 1982 to 29 January 1986, under Grant No. AFOSR-82-0013. The Principal Investigator was Carlo G. Pantano, Faculty Associates were Jack J. Mecholsky and Richard C. Bradt, Research Associate was Cheryl A. Houser, and Graduate-Student Research Assistants included J. Chesson, A. Tesar, D. Coon, M. Murtagh, A. Gonzalez and A. Phelps.

A major objective of this program was to evaluate the slow crack growth behavior of a systematic compositional series of glasses and to correlate these data with independent studies of the surface chemistry. This objective was, in fact, accomplished using the glass system $Na_2O \cdot xAl_2O_3 \cdot (3-x)SiO_2$. This endeavor led to new models for understanding stress corrosion susceptibility, chemical effects during crack growth and the static fatigue limit. After a general discussion of chemical effects in fracture (Chapter I), these new models are described in Chapters II, III, IV and V of this report. The development of these new concepts would not have been possible without the careful measurement and documentation of trends throughout a family of glasses. A comparable study of fluorozirconate glasses was initiated during the third year of this program; the results obtained to date are highlighted in Chapter VI. Finally, Chapter VII presents the first reported study of the mechanical behavior - and its dependence upon environment - of a silica sol/gel material.

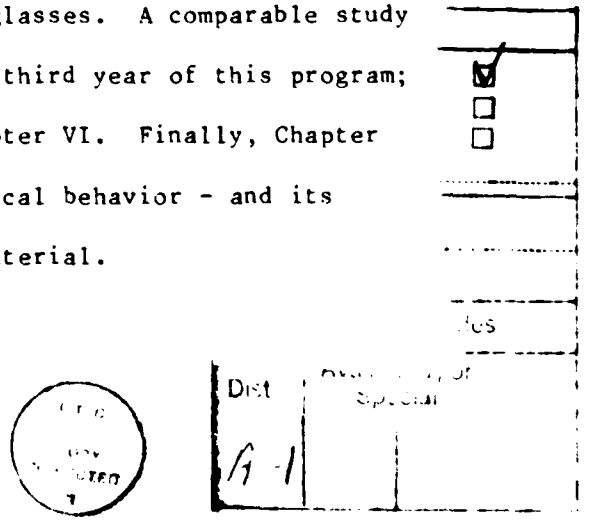

The following is a complete list of the publications, presentations and theses supported through this program.

Publications:

1. "Mechanical Properties of Silicon Oxynitride Glasses," J. Non-Cryst. Solids, 56, 161 (1983), by D. N. Coon, J. G. Rapp, R. C. Bradt and C. G. Pantano.

2. "Transformation Range Viscosity of Fluorozirconate Glasses," J. Am. Cer. Soc., 67, C164 (1984), by J. E. Shelby, C. G. Pantano and A. Tesar.

3. "Chemical Analysis of Fracture Surfaces," in Fractography of Ceramic and Metal Failures, ASTM STP 827, J. J. Mecholsky, Editor (ASTM, Phil, 1984) pp. 134-156, by C. G. Pantano and J. F. Kelso.

4. "Surface Chemistry in Relation to the Strength and Fracture of Silicate Glasses," in Strength of Inorganic Glasses, C. R. Kurkjian, Editor (Plenum, NY, 1985), pp. 37-66, by C. G. Pantano.

5. "Surface Chemistry and Fracture of Fluoride Glasses," Mater. Sci. Forum, 6, 285 (1985), by C. G. Pantano.

6. "Mechanical Property Testing in Fluoride Glasses: An Assessment," Mater. Sci. Forum, 6, 699 (1985), by J. J. Mecholsky, C. G. Pantano and A. C. Gonzalez.

7. "Mechanical and Physical Properties of Fluorozirconate Glasses," Mater. Sci. Forum, 6, 703 (1985), by J. J. Mecholsky, A. C. Gonzalez, C. G. Pantano and B. Bendow.

8. "Elastic Moduli of Silica Gels Prepared with Tetraethoxysilane," M. J. Murtagh, E. K. Graham and C. G. Pantano, accepted for publication in J. American Ceramic Society.

9. "Surface Chemistry and Slow Crack Growth Behavior of Fluorozirconate Glasses," Carlo G. Pantano, to appear in Infrared Fiberoptics (Proceedings of a NATO Advanced Research Workshop, 1986).

10. "The Relationship Between Elastic Properties and Slow Crack Growth in Sodium-Aluminosilicate Glasses", D. N. Coon, J. J. Mecholsky and C. G. Pantano, submitted for publication to J. American Ceramic Society.

11. "Slow Crack Crowth Behavior in the Threshold Region," D. N. Coon, J. J. Mecholsky and C. G. Pantano, submitted for publication to J. American Ceramic Society.

12. "Static Fatigue Limit Due to Crack Healing in $Na_2O \cdot 3SiO_2$ Glass," D. N. Coon, J. J. Mecholsky and C. G. Pantano, to be submitted.

13. "Stress Corrosion of Sodium-Aluminosilicate Glasses: A Comparison of Small and Large Cracks," D. N. Coon, J. J. Mecholsky and C. G. Pantano, to be submitted to J. Fracture Mechanics.

Presentations:

1. "Chemical Analysis of Fracture Surfaces," at the ASTM Symposium on Fractography of Ceramics, Philadelphia, PA, April 1982.

2. "Mechanical Properties of Sodium Aluminosilicate Glasses," at the 84th Annual Meeting of the American Ceramic Society, Cincinnati, OH, April 1982.

3. "Stress Corrosion of Sodium Aluminosilicate Glasses," at the Fall Meeting of the Glass Division of the American Ceramic Society, Bedford Springs, PA, October 1, 1982.

4. "Fluoride Glasses Based Upon Mixtures of PbF_2 with 3d-Transition Metal Fluorides," at the Fall Meeting of the Glass Division of the American Ceramic Society, Bedford Springs, PA, October 1, 1982.

5. "Surface Chemistry in Regard to the Strength and Fracture of Silicate Glasses," Invited paper at the NATO Advanced Research Workshop on Strength of Glass, Algarve, Portugal, March 1983.

6. "Mechanical Properties of Silicon Oxynitride Glasses," at the International and VIIth University Conference on Glass Science, Clausthal, FRG, July 1983.

7. "Effects of NaF Upon the Mechanical Properties of Fluorozirconate Glasses," at the 2nd International Symposium on Halide and Other Non-Oxide Glasses, Rennselear Polytechnic Institute, 2-5 August, 1983.

8. "Surface Studies of a Fluorozirconate Glass," at the 2nd International Symposium on Halide and Other Non-Oxide Glasses, Rennselear Polytechnic Institute, 2-5 August, 1983.

9. "Stress Corrosion Effects in Fluorozirconate Glasses," at the Glass Division Fall Meeting, Grossinger, NY, October 1984.

10. "Slow Crack Growth Behavior of Sodium Aluminosilicate Glasses," at the 87 th Annual Meeting of the American Ceramic Society, Cincinnati, OH, May 1985.

11. "The Elastic Properties of Silica Gels and Their Dependence on Relative Humidity," at the 87th Annual Meeting of the American Ceramic Society, Cincinnati, OH, May 1985.

12. "Surface Chemistry and Fracture of Fluoride Glasses," Invited paper at the 3rd International Symposium on Halide Glasses, Rennes, France, June 1985.

13. "Mechanical Property Testing in Fluoride Glasses: An Assessment," at the 3rd International Symposium on Halide Glasses, Rennes, France, June 1985.

14. "Mechanical and Physical Properties of Fluorozirconate Glasses," at the 3rd International Symposium on Halide Glasses, Rennes, France, June 1985.

15. "Surface Chemical Effects During the Fracture of Fluorozirconate Glasses," at the AF Workshop on Strength, Durability and Coating of Heavy Metal Fluoride Glasses, San Diego, CA, January 1986.

16. "Reliability of Fluoride Glasses: An Assessment," at the AF Workshop on Strength, Durability and Coating of Heavy Metal Fluoride Glasses, San Diego, CA, January 1986.

17. "Stress Corrosion of Fluorozirconate Glasses," at the NATO Advanced Research Workshop on Infrared Fiberoptics, Algarve, Portugal, April 1986.

Theses:

1. "Effects of Structure On the Fracture of $Na_2O \cdot xAl_2O_3 \cdot (3-x)SiO_2$ Glasses," Master of Science, Jeffrey Chesson, 1983.

2. "The Effects of Modifying Cation Substitutions on the Physical and Mechanical Properties of a Fluorozirconate Glass," Master of Science, Aleta A. Tesar, 1984.

3. "The Elastic Moduli of Silicon Alkoxide Gels by Pulse Superposition Interferometry," Master of Science, Martin J. Murtagh, 1985.

4. "Slow Crack Growth in Sodium Aluminosilicate Glasses," Doctor of Philosophy, Dennis N. Coon, 1986.

TABLE OF CONTENTS

CHAPTER I

SURFACE CHEMISTRY IN RELATION TO THE STRENGTH AND FRACTURE OF SILICATE GLASSES

by

Carlo G. Pantano

Department of Materials Science and Engineering

The Pennsylvania State University

University Park, PA 16802

in: Strength of Inorganic Glass, (C. R. Kirkjian, Editor, Plenum Publ. Corp., New York, 1985).

SURFACE CHEMISTRY IN RELATION TO THE STRENGTH AND FRACTURE OF SILICATE GLASSES

by

Carlo G. Pantano

Department of Materials Science & Engineering
The Pennsylvania State University
University Park, PA 16802

Introduction

The strength and fracture behavior of silica and silicate glasses can be influenced by surface chemistry in many different ways. It may be appropriate to start this discussion by attempting to identify the most important relationships.

(1) Surface chemical phenomena can result in compositional and structural changes at glass surfaces during high temperature fabrication processes. In the case of silica glass, this is limited to chemical adsorption of water and other gaseous species, as well as surface segregation and/or volatization of water and impurities from the bulk of the glass. In the case of multicomponent glasses, more dramatic composition changes may occur due to the mobility and reactivity of the modifier species. The extent of chemical and structural modification of the surface is a complex function of the bulk composition of the glass and the thermal and atmospheric history of the glass surface. Obviously, any high temperature chemical or structural alteration of the surface will influence subsequent adsorption and surface chemical behavior in a manner which cannot be predicted simply from a knowledge of the bulk glass composition. It will be shown, for example, that for a given glass composition, some high temperature fabrication processes enhance the hydration resistance of the surface while others degrade it.

(2) The chemisorption of gaseous species at surfaces and crack-tips under residual or applied stresses can contribute to the rupture of interatomic bonds. This phenomena is, of course, fundamental to slow crack growth and will not be treated in any detail here. However, it is worth pointing out that slow crack growth does exhibit a composition dependence. Thus, the strength behavior of real glass surfaces will be influenced by any in-depth modification of the surface during high temperature fabrication.

(3) Chemical reactions between the glass surface and adsorbed species can lead to broken bonds, hydration films and other structural heterogenities at the surface under ambient conditions. These reactions will undoubtedly be localized at high energy surface sites, especially those associated with strained bonds. And while all the bonds at the surface may be strained to some extent, the strain may be accentuated at regions associated with bulk topological features, phase separated regions, crystallites or impurities. The distinction between this phenomena and slow crack growth is perhaps philosophical since both involve bond breaking chemical reactions at high energy surface sites. However, it has a special significance in the sense that it may be a realistic source of flaws, or flaw-precursors, and may in some instances occur at high energy sites not associated with strained bonds per se. The alkali species in multicomponent glasses, for example, will preferentially react with water and carbon dioxide. The reaction and distribution of surface reaction products and corrosion pits will be non-uniform to an extent determined by the composition and thermal history of the glass.

In general, one expects these kinds of interactions to be auto-catalytic in the sense that any subsequent chemical reactions will also be localized at these sites. For example, the reaction between a strained siloxane linkage ($\equiv Si-O-Si\equiv$) and water not only leads to a broken bond, but the silanol groups ($\equiv Si-OH$) so-produced will enhance the physical adsorption of water at that same site. This relatively mobile water is then available to react with other siloxane linkages in that region whether they are strained or not.

(4) The mechanically induced 'flaws' at glass surfaces are high energy sites where the adsorption and/or condensation of mobile water can result in corrosion reactions. That is, the chemistry of the condensed water can be modified dramatically by the dissociation of surface silanol groups and ion-exchange reactions with modifier species due to the high ratio of surface area to solution volume. Thus, the geometry of the flaw may be modified by gel formation and swelling, non-uniform dissolution, and etching.

(5) The physical adsorption of mobile water or other gaseous species at pristine surfaces, at compositionally-modified surfaces, on surface reaction products, within pre-existing flaws or at the interface between the glass surface and organic coatings provides a reservoir of reactants for chemical interactions upon the application of stress. It is well known from a wide variety of fracture mechanics studies that the transport of water or other reactants can limit slow crack growth. It is possible that the most significant influence of hydrated surface layers - especially within microcracks - is their capacity to 'store' physically adsorbed water until a stress is applied. This 'reservoir of reactants' becomes especially significant when it exists at the interface between a glass fiber and organic coating.

Obviously, one cannot be too dogmatic about these classifications since they are all dependent upon the same fundamental phenomena. However, these classifications do facilitate the design of critical experiments, and perhaps most importantly, the interpretation of strength behavior for commercial glass products.

It becomes immediately evident that melt surfaces and fracture surfaces are most appropriate for experimental investigation. The melt surfaces of glass are among the strongest surfaces available and the most prevalent in practice. Most importantly, though, it is the strength behavior of these surfaces which is most dependent upon chemical interactions. Understanding the way in which these surfaces evolve at high temperature, during cooling, and during exposure to and service in the ambient atmosphere, is extremely important but not well established. Fracture surfaces, on the other hand, are most useful as 'model' surfaces for studying the evolution of melt surfaces and the behavior of cracks and crack-tips in the absence stress.

In this paper, we will not consider the stress enhanced surface chemical reactions associated with slow crack growth phenomena since these are addressed independently in these proceedings. Rather, the hydroxylation of silica and silicate glasses, the characteristics of melt surfaces, and the chemistry and structure of clean fracture surfaces will be emphasized. Finally the relationships between surface chemistry and fracture behavior will be considered. Although this discussion will refer to the use of a wide variety of analytical techniques for studying glass surfaces, the details associated with each of these methods will not be specifically addressed. The reader is referred to a number of review articles where the theory, instrumentation, applicability and shortcomings of these methods are presented with regard to glass surface studies[1-5].

HYDROXYL GROUPS AND HYDRATION AT GLASS SURFACES

Silica Glass

The chemisorption of water -commonly termed hydroxylation or hydrolysis- dominates the surface chemical behavior of clean or pristine silicate glasses. There are a number of sites where the chemisorption of water may occur; viz

$$\equiv Si^{+} + H_2O \rightarrow \equiv Si\text{-}OH + H^{+} \quad (1)$$

$$\equiv Si\text{-}O^{-} + H_2O \rightarrow \equiv Si\text{-}OH + OH^{-} \quad (2)$$

$$\equiv Si\text{-}O\text{-}Si \equiv + H_2O \rightarrow 2(\equiv Si\text{-}OH) \quad (3)$$

$$\equiv Si\text{-}OX + H_2O \rightarrow Si\text{-}OH + XOH \text{ where } X = Li, Na, K, Ca, Ba, Pb, \text{etc.} \quad (4)$$

These reactions are fundamental to the surface chemistry and fracture behavior of silicate glasses for two important reasons:

(1) regardless of how or where the chemisorption takes place, a silanol group -SiOH- is produced, where physical adsorption and clustering of water and other polar molecules will be localized, and

(2) hydroxylation of siloxane linkages ($\equiv Si\text{-}O\text{-}Si\equiv$) breaks those bonds which comprise the structural backbone of silicate glasses.

There has been considerable investigation of the behavior of surface silanol groups, but vanishingly little investigation of their creation at high or low temperatures on clean surfaces.

Much of the work concerning the behavior of silanol groups has been confined to high surface area silicas. These include silica gel, porous 'Vycor' glass and silica 'fume' (e.g. Cab-O-Sil). In addition to their technological application as dessicants and packing for chromatographic columns, the primary rationale for the extensive study of high surface area silicas is their adaptability to infrared absorption analysis[3]. This technique not only provides a qualitative and quantitative measure of the hydroxyl groups and molecular water at the surface, but also provides an indication of their configuration.

Extensive reviews are already available concerning infrared analysis and surface chemistry of high surface area silicas[6-8]. Here, only the most important observations are presented. The major objective of this section is to bring out those observations that are most relevant to the strength behavior of silica and silicate glasses.

It is well established that silica surfaces at ambient conditions are covered to varying degrees with physically adsorbed molecular water (often termed water of hydration). However, it is the underlying chemisorbed water (often termed hydroxyl or silanol groups) which is of most concern. There are two silanol configurations which can be readily distinguished:vicinal and isolated; viz,

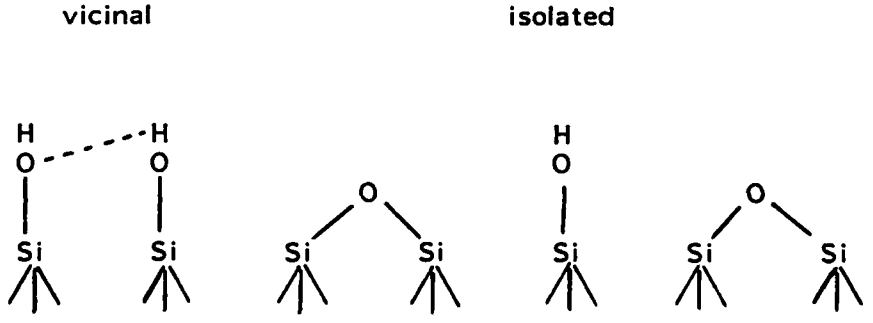

The vicinal hydroxyl groups are hydrogen bonded to one another due to their close proximity across pores, cracks and breaks in the silica ring structures. And in some instances, it is possible to distinguish between weakly-hydrogen bonded and strongly-hydrogen bonded vicinal hydroxyl groups. The point is that the concentration and configuration of the silanol groups determine the capacity for physical adsorption of molecular water; i.e. physical adsorption of molecular water occurs predominantly at the vicinal silanol groups:

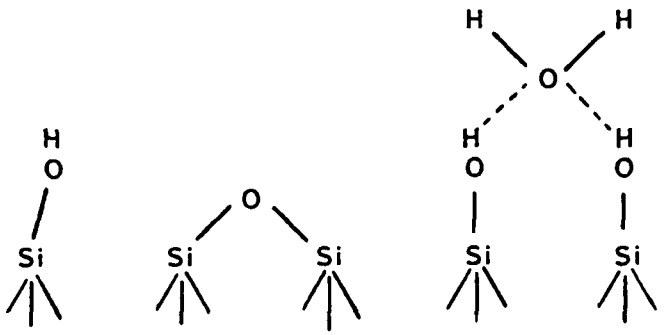

The molecular water of hydration, the vicinal silanol groups and the isolated silanol groups are readily identified with infrared absorption spectroscopy as shown in Figure 1.

The molecular water is physically adsorbed to the silica surface through hydrogen bonds with the vicinal silanol groups. Of course, multilayer adsorption and clustering of a molecular water can occur through intermolecular hydrogen bonding of the water molecules themselves. Nevertheless, upon vacuum evacuation or moderate heating, the molecular water is readily eliminated from the surface (see figure 1). On the other hand, removal of the underlying chemisorbed water is more difficult. Temperatures of the order 500C and higher are required to affect the chemisorbed water (see figure 1). Under these conditions, the vicinal hydroxyl groups can condense to liberate molecular water and thereby produce a siloxane linkage (≡Si-O-Si≡); viz

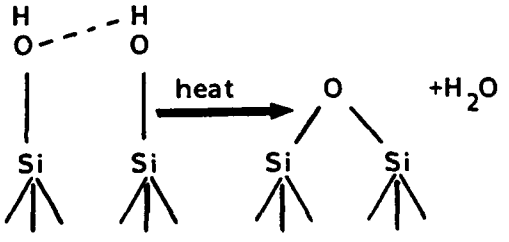

Obviously, the strongly hydrogen bonded groups condense more readily that the weakly hydrogen bonded groups. Most significant, though, is the fact that the siloxane linkages formed by the condensation can be 'strained' upon cooling to ambient temperatures. The amount of strain depends upon the original configuration of the vicinal hydroxyls and the maximum temperature of dehydration. Naturally, there is no mechanism for the removal of the isolated silanol groups during a high temperature dehydration (see Figure 1). That is, at temperatures of the order 850C-900C, the concentration of surface silanol

groups is less than 1 per 100 $Å^2$ and these remaining silanol groups are of the freely vibrating kind.

Since the silanol groups - particularly the vicinal variety - are responsible for the physical adsorption of molecular water, it is not surprising that silicas dehydrated at elevated temperatures can be extremely hydrophobic. Of course, they will re-hydrate upon exposure to water at a rate dependent upon the water vapor partial pressure, the amount of 'strain' in the siloxane linkages and the configuration of the siloxane linkages (see Figure 1). It is shown below that the application of an external stress accelerates the re-hydration.

The density of the silanol groups found on a silica glass surface obviously depends upon the thermal and atmospheric history of the sample but is typically 4-8 per 100 $Å^2$. It is worth pointing out that if one calculates the minimum number of terminal sites ($\equiv Si^+$ or $\equiv SiO^-$) required for the very existence of a surface on silica glass, one expects about 2-3 silanols per 100$Å^2$ to be formed via reactions (1) and (2). The additional silanols often found at silica surfaces may be due to roughness or porosity, but are probably due to the hydrolysis of siloxane bridges (reaction 3). Unfortunately, a measure of the initial and/or equilibrium silanol density at a melt or fracture surface of silica glass has never been reported under any conditions.

Since most of the experimental data used to formulate the conclusions summarized above were obtained using high surface area silicas, one must question the significance of these observations with regard to the surfaces of bulk or massive glasses. The internal microporosity of the silica gel and porous glass are of some concern. And although the silica fume -notably Cab-O-Sil- is a compact particulate silica which contains no internal porosity, its preparation for infared absorption analysis requires that it be mixed with

KBr and/or be pressed into a powder compact with extreme pressure. Thus, the studies of Bershtein[4,9,10] and co-workers are extremely significant. Here, attenuated total reflectance (ATR) infrared spectroscopy was used to monitor hydroxyl groups at the surface of massive silica glass specimens. In contrast to the use of high surface area microporous glasses, silica gels or powder compacts (Figure 2a), the multiple ATR element provides a more realistic glass surface for study (Figure 2b). Here, silica glass with a very low bulk water must be used. However, any adsorption of water on the surface is readily detected due to absorption of the infrared radiation at each internal reflection. Moreover, it is possible to hydrate these massive surfaces under an applied load, as well as, to subject them to strength measurements. This work has already been reviewed in the literature and need not be covered in detail here[9]; however, a summary of the most significant findings is appropriate.

These ATR studies showed that the surfaces of fused silica -after hydration at temperatures of the order 70°C to 600°C - contained both physically adsorbed molecular water and silanol groups. And, the concentration of silanol groups was much higher when the hydration was carried out under stress. Although the spectral resolution of the ATR data is inferior to the direct transmission data obtained with powder compacts, the published spectra do suggest the presence of both vicinal and freely vibrating hydroxyl groups.

Perhaps of greater significance was the conclusion of Bershtein, et al.[10] that the hydrolysis of siloxane linkages occurs preferentially at weakened ≡Si-O-Si≡ sites in the glass and that the concentration of these 'weakened' sites set a limit upon the number of sites which could be hydroxylated. They found, for example, that increasing the time of hydration increased the thickness of the hydrated layer but not the concentration of hydroxyls within it, typically 3-5 percent by weight. They showed further that

hydrolysis of the weakened bonds created 'passages' for the intrusion of molecular water. The 'passages' were observed even when the hydration was carried out in the absence of an applied stress. Using mercury porosimetry, they found that these 'passages' had widths less than 1 μm, with the majority possessing widths less than 600 Å. The 'weakened' bonds responsible for the preferential hydrolysis, intrusion of molecular water and corresponding creation of defects, were suggested to be associated with sub-microscopic 'ordered' regions in the glass structure. These investigators suggested that the presence of impurities -particularly bulk water-could reduce the stresses at the interfaces or boundaries of these ordered regions, whereas in high purity silica the non-uniform or localized weakening of siloxane bridges could be accentuated.

Finally, the Bershtein group[10,11] related the strength of the hydrated silicas to the measured distribution of hydroxyls in the surface. They showed a distinct reduction in strength due to the non-uniform hydrolysis of siloxane bonds, and an increase in strength upon acid etching of the hydrated layers. Nonetheless, they also showed that by carrying out the hydrolysis at elevated temperatures and in the presence of sufficient water, the strength could in fact be improved with hydration. This they attributed to the elimination of 'weakened' siloxane linkages, the creation of a 'microplastic' surface layer, and consequently a more uniform distribution of applied stress.

The work on high surface area silicas and compact silica plates emphasizes the importance of strained surface bonds, the configuration of silanols and siloxane linkages, and of course, the presence of an externally applied stress. Recently, Dunken and Hoffman[12] have attempted to shed light on these concepts using theoretical 'cluster' calculations. They essentially calculate the probability of a water molecule disrupting siloxane linkages as a function

of the geometry and composition of the cluster. Although this work, too, has been summarized in a recent review[13], some of the more important observations are included here. For example, calculations on a $(Si_2O_7H_2)$ cluster showed that the simultaneous interaction of the hydroxyl portion of a water molecule with a silicon atom, and the protonic end of the water molecule with the siloxane bridge, can be more favorable than an interaction between the water molecule and a silanol. Moreover, the calculations showed that siloxane bridges between tetrahedra already containing a silanol are most susceptible to hydrolysis. With regard to the geometry of the cluster, the calculations suggested that hydrolysis of a siloxane linkage with an angle $<115^{\circ}$ is more favorable than hydrolysis of a stretched siloxane linkage!

Some direct evidence for the presence of strained siloxane bonds, and their preferential hydrolysis, has been provided by Raman spectroscopy. The Raman spectra for vitreous silica[14], and for dehydrated silica gels[15,16], exhibit bands at 605 cm^{-1} and 495 cm^{-1} which are assigned to the vibration of three-membered and four-membered planar rings, respectively. The three-membered ring is of particular significance because it represents a high energy configuration consisting of strained siloxane bonds. Krol and van Lierop[15] examined dehydrated silica gel and found that the existence of these three- and four-membered rings correlated with the presence of freely vibrating silanol groups; i.e. the degree of freedom provided by the surface stabilizes these high energy planar-ring configurations. These authors also examined the re-hydration of silica gel with Raman spectroscopy[16]. Upon exposing the dehydrated gel to the ambient atmosphere, they observed a complete disappearance of the 605 cm^{-1} band with little or no corresponding attenuation of the band at 495 cm^{-1}.

Thus, it can be concluded that the highly strained siloxane bonds in the three-membered rings were preferentially hydrolyzed by water.

Obviously, the configuration of silica tetrahedra at the tip of a highly stressed crack will also have a strong influence on chemical reactivity and therefore upon slow crack growth phenomena. Although there is no way to describe or measure this characteristic at the present time, Wiederhorn[17] showed that the interaction between stressed crack tips and water was very different in normal vs anomalous glasses. Since a major difference between normal and anomalous glasses is the way in which =Si-O-Si= linkages are distorted under stress, the configuration dependence of hydrolysis reactions is further supported.

In general, then, we are at the point where additional understanding of the hydroxylation of silica glass will require more extensive characterization of the structure of glass - in the bulk and at the free surface. The schematic in Figure 3a emphasizes in a more realistic way the role of the bulk glass structure and ring statistics in determining the number of strained siloxane bridges at the surface, and consequently, the total number and configuration of silanol groups. Unfortunately, the ability to further develop these ideas is limited due to the lack of experimental techniques which are sensitive to the strain and configuration associated with siloxane bridges and hydroxyl groups, as well as to the network topology. Nonetheless, it is probably worth emphasizing the point that the hydroxyl groups are responsible for the adsorption of water, and in a sense, represent sites of preferential attack where water molecules gain access to the structure. In fact, the molecular water will 'cluster' at these regions due to hydrogen bonding interactions between the water molecules themselves. In principle, of course, the absence of silanol (or other polar) surface sites would greatly inhibit the adsorption of water.

Multicomponent Silicate Glasses

The formation of silanol groups on silica glass is usually limited to the outermost monolayer. In contrast, the hydroxylation and hydration of glasses containing modifier species -particularly alkali ions- occurs in depth[1,18,19]. The hydrogen depth profiles in Figure 4 show quite clearly that the ability to hydrate glass in water is enhanced for alkali containing glasses. In general, the extent of hydrogen incorporation correlates directly with the alkali content. Of course, these profiles provide little indication of the molecular form of the hydrogen, the configuration of the silanols, or the uniformity of hydration.

In-depth hydration of alkali containing glasses also occurs due to the water vapor in the ambient atmosphere[1,20,21]. Figure 5 shows schematically the concentration profiles observed for alkali and hydrogen at alkali-silicate glass surfaces. These reactions were proposed on the basis of AES (Auger electron spectroscopy), XPS (x-ray photoelectron spectroscopy) and SIMS (secondary ion mass spectroscopy) studies of fracture surfaces, sputter-cleaned surfaces, and a variety of glass commercial surfaces, all after exposure to the ambient atmosphere.

It is quite clear that the physical adsorption of molecular water is more extensive on these multicomponent silicate glasses than it is on pure silica glass. The reasons for this are demonstrated schematically in Figures 3b and 3c. In addition to the silanol groups (which form due to dangling Si^{+} and SiO^{-} sites), the alkali ions are also capable of adsorbing molecular water. The adsorbed molecular water can react with the non-bridging oxygens in the sub-surface to liberate the alkali ions and create free hydroxyl ions. The alkali ions are generally observed to diffuse out of the hydrated surface

whereas the hydroxyl ions will attack siloxane bridges to further depolymerize the silicate network. The enhanced attack of siloxane bonds under these alkaline conditions produces many more silanol groups. Thus, extensive in-depth hydration, and perhaps dissolution, of the surface is expected. The alkali ions liberated from the structure will accumulate at the glass-atmosphere interface where they react with CO_2 to form carbonate species (see Figure 5). The carbonate species and surface alkalinity are not observed for pure silica glass.

The existence of modified surface layers on multicomponent glasses as shown in Figure 5 - after even short exposure to the ambient atmosphere - seems to be a general phenomena. It is in this regard that the observations of Stavrinidis and Holloway[22] are quite interesting. They observed a narrow region (~12nm) of low reflectivity at the interface created by healing cracks in a soda-lime-silica glass. Since this interface was formed only when the crack surfaces were first exposed to a humid atmosphere, it is undoubtedly due to a hydrated surface film. Interestingly, these hydrated crack surfaces were able to be healed.

Also significant in the hydration of alkali containing glasses is the microporosity which can be generated within the modified surface layer. In some cases, the intrusion of molecular water, attack of siloxane linkages by free hydroxyl and molecular water, and condensation of some silanol groups, can all combine to transform and swell the surface into a microporous 'gel'. Sewell[23], and also Martin, Akinc and Oh [24], showed the presence of microporosity on the hydrated surfaces of E-glass and soda-lime-silica glass fibers. Nonetheless, it is important to emphasize that the hydroxylation of alkali containing glasses need not result in a 'gel' layer formation. Indeed, the alkali ions in the surface and sub-surface are replaced by hydrogen-bearing species to form a 'hydrogen' glass. However, it is the initial composition, and

particularly the network structure, of the surface which determines the extent to which it hydrates and is transformed into a swollen 'gel' layer via the 'solvation' of internal silanols by molecular water.

The dependence of hydration and 'gel' formation upon the subtle characteristics of the glass network structure is especially evident in the binary alkali-silicates. One can compare surface film formation on binary alkali silicate glasses whose molar alkali concentration - and therefore non-bridging oxygen density - are identical. The hydrated surface films are more stable in the order lithia-silica > soda-silica > potassia silical. This is due to the lower partial molar volume for the silica network in the glasses with smaller alkali ions. The reduced volume of pore space in the leached lithia silica glasses inhibits the intrusion of water and breakdown of the 'silica-rich' surface film which forms upon preferential release of the alkali component. In the potassia silica glasses, on the other hand, a large pore volume makes the intrusion of water and the hydrolysis of siloxane bridges easier; e.g. the ionic radius of K^+ is approximately equal to that of H_3O^+. This enhances the production of a soluble, colloidal silica 'gel' film at the surface.

In general, then, one expects the hydration of multicomponent silicate glasses to occur in stages as shown schematically in Figure 6. The relative rates of 'hydrogen-glass' formation vs 'gel' formation will depend upon the glass composition and structure, the solution pH and the temperature. The simultaneous creation of mechanical stresses, and the extent to which they are transmitted to the sub-surface, will be dependent upon the details. However, the spontaneous cracking of glass due to hydration and surface film formation has been reported[25].

MELT SURFACES

It has been pointed out that the hydration of glass surfaces is very much dependent upon composition and structure. During the formation and cooling of a melt surface, reorientation of the silicate structure, segregation of impurities, volatilization of modifiers, water, and other impurities and chemisorption phenomena determine the final characteristics of the glass surface. It is generally observed that melt surfaces have better hydration resistance and lower chemical reactivity than ground, polished or fractured surfaces. The 'purification' of the surface due to volatization of water, impurities and alkali, and the more favorable molecular orientation of the silica structure, are possible reasons for this. The presence of residual stress at the melt surface due to non-uniform cooling or composition gradients can also influence the chemical reactivity. Otherwise, very little is known in detail about these phenomena.

Silica Glass

The direct surface analysis of silica 'melt' surfaces has not been prevalent for a couple of reasons. Primarily, it is the chemical structure of the silica surface and its hydroxyl content which is of most interest. With the exception of infared absorption spectroscopy, none of the available surface analysis techniques are especially sensitive to these characteristics[1]. In addition, the geometry of the sample becomes important for many surface analyses. Silica fibers which exhibit very high strengths, for example, would be most interesting to study. However, their dimensions and geometry are not appropriate for most surface analytical methods. The ATR technique would be most appropriate providing that flat, plane parallel sheets with pristine melt surfaces could be formed.

Another factor which has contributed to the lack of fundamental studies of silica melt surfaces is the difficulty in preparing and preserving surfaces for study. Although surface reactions of silica are slow in the ambient atmosphere, they do occur. Obviously, they must be prevented in order to positively identify those phenomena which occur at high temperature.

One indication of the chemistry at silica 'melt' surfaces is provided by glass capillary gas chromatography $(GC)^2$. This method is sensitive to the adsorption of nanogram quantities of gaseous species on the inside 'melt' surfaces of glass capillaries. Figure 7 compares the gas chromatograms for polar test mixtures analyzed in fused quartz and high purity silica[26]. The tails and reduced intensity of the peaks obtained in the fused quartz capillary indicate that some of the gaseous species are being adsorbed whereas the high purity silica provides an almost perfect chromatogram. The point is that even the trace levels of impurities present in the fused quartz have influenced the surface chemistry. Quite likely, some of the impurities and bulk hydroxyl groups have 'segregated' at the inside surface of the capillary during the high temperature manufacture. In a sense, the use of $(GC)^2$ to study the chemistry of pristine melt surfaces is ideally suited for comparison with the strength behavior of fibers. Here, the inside surface of a 25 meter capillary is 'sampled' by the polar test mixture. Surely, the same high energy sites responsible for these adsorption phenomena will play a role in the fatigue of glass fibers.

It should also be emphasized that both temporary and permanent stresses can exist at melt surfaces and these will surely influence the surface chemistry. All forming methods subject the molten glass to tensile stresses which are maximized at the surface. Even after cooling, the surface will be under stress due to the reduced interatomic distances expected there[13].

Multicomponent Silicate Glasses

Due to the high mobility and reactivity of modified species, compositional and structural differences are more prevalent at the melt surfaces of multicomponent glasses. A considerable number of surface studies have been reported for the melt surfaces of fibers, bottles, flat glass etc[1]. In general, it has been found that the composition profiles and hydration susceptibility of multicomponent melt surfaces can be quite variable.

Figure 8 presents SIMS depth profiles for the surface of an E-glass ribbon. The ribbons were prepared with a special bushing simply to provide flat surfaces amenable for study. These ribbons provide a convenient 'model' for understanding the high temperature chemistry associated with fiber glass surfaces. Although the quench rate may be somewhat less for the ribbons, one notes that this surface -prepared in air- is modified in depth. The outermost 5 nm are enriched in boron, and to some extent sodium, while the sub-surface region is enriched in calcium and silicon. These profiles -expressed as cation to oxygen ratios- were compared with the profiles measured for a 'bulk' fracture surface of the same E-glass. All of the ribbon profiles matched the bulk profiles at depths greater than 40 nm with the exception of sodium. The Na/O ratio was 2 to 3 times lower in the outermost 200 to 600 nm of the ribbon than in the bulk E-glass standard. Thus, the ribbon surface exhibits a modified layer at the outermost 20 nm -where sodium and boron are enriched- and a sodium depleted region extending to 600 nm. Although the profiles in the outermost 20 nm may be due in part to sputtering effects associated with the analysis[2], the sodium depletion extending to 600 nm is independent of sputtering effects.

In contrast, the inside surface of an alumina-borosilicate glass tube exhibits a dealkalized layer which extends to only 40 nm. The profiles in

Figure 9 show that the degree of dealkalization is quite dramatic; the sodium concentration was reduced by two orders of magnitude here, in contrast to a 2 to 3 times reduction for the ribbon surface. In contrast to many other 'commercial surfaces', the inside surface of tubing exhibits the most extensive surface depletion of alkali (with the exception of intentionally dealkalized products). This is undoubtedly related to the fabrication process which involves a high flow of 'air' through the hot glass tubing and thereby enhances the volatilization of alkali species.

Of course, one can intentionally modify the composition of glass surfaces through surface treatments. It has been demonstrated, for example, that the inside surface of soda-lime capillary can be improved for $(GC)^2$ by passing sulfur dioxide or difluoroethane through the preform and capillary during the fabrication[27]. The use of sulfur dioxide[28] or difluoroethane[29] is well-known for treating the internal surfaces of glass containers. All of these treatments enhance the hydration resistance of the glass surface. In fact, it was recently shown that the combined use of sulfur dioxide and difluoroethane could further enhance the hydration resistance of the glass surface[30]. It is quite clear that these modified surfaces are dealkalized after the high temperature treatment. However, it is also observed that the hydrogen content in the surface is reduced. Therefore, the alkali species are not simply replaced by hydrogen during these treatments. It is primarily the high temperature polymerization and relaxation of the silicate network near the surface which is responsible for the improved hydration resistance after these treatments. Thus, it is important to recognize that not only the composition, but particularly the network structure of the glass, may be modified by the treatment of surfaces at high temperatures.

Obviously the critical question is whether or not the high temperature modification of thin surface layers can influence strength behavior. Budd, et al.[31] measured the stress corrosion susceptibility for the internal surfaces of glass bottles with and without internal sulfur treatment. His results are duplicated in Table 1. They indicate that modification of even a 50nm surface layer -at least for a melt surface- can have a dramatic influence on the strength and dynamic fatigue behavior. Yashchishin and Sharagov[32] examined the impact toughness of plate glass treated at elevated temperatures with sulfur dioxide and also difluorodichloromethane. They, too, observed an increase in the fracture resistance due to a modification of thin surface layers. The reasons for the increased strength and fatigue resistance are by no means clear, although the enhanced hydration resistance provided by these treatment points to the importance of surface chemistry. Here, it can only be stated that the surface composition and structure has been modified by a high temperature treatment, and at the same time, a measurable improvement in the strength and fatigue behavior are observed.

CLEAN SURFACES

It is quite noticeable that little effort has been directed at understanding the fundamental nature of glass surfaces via the spectroscopic study of 'ideal' or 'clean' surfaces. Here, the objective might be to understand the nature of the dangling bonds at a fresh fracture surface produced in ultra high vacuum and the relative effects of surface reconstruction, adsorption of bulk impurities, and adsorption of gaseous species during its passivation. In a sense, a more fundamental understanding of 'ideal' surfaces is required to fully define the reaction mechanisms responsible for the properties exhibited by 'real' surfaces during processing in, or exposure to, particular atmospheres.

Hochstrasser and Antonini[33] crushed silica glass in an ultra high vacuum environment (~10^{-10} torr). They used electron spin resonance (ESR) to characterize the paramagnetic dangling bonds and adsorption-desorption measurements to examine interactions with CO_2. Silica fracture surfaces are expected to contain approximately 2-3 dangling bonds per 100 $Å^2$. The ESR analysis detected only 4% to 10% of the expected number of $\equiv Si^{\cdot}$ dangling bonds, and failed to detect the presence of any $\equiv SiO^{\cdot}$ dangling bonds. The investigators concluded that most of the dangling bonds were eliminated by a self-reconstruction process during and/or after the fracture event. This occurred even at temperatures as low as -150°C. It is most interesting that the number of dangling bonds detected by ESR increased with the purity of the silica. This suggests that impurities in the glass are responsible -at least in part- for the elimination of dangling bonds. At temperatures of the order 300°C, all of the dangling bonds were eliminated by surface reconstruction and the out-diffusion of impurities.

More recently, Lacharme et al.[34] used Auger electron spectroscopy to examine the fracture surfaces of silica glass and binary sodium and potassium silicate glasses. They found a local enrichment of alkali at the fracture surfaces created in a vacuum of 10^{-10} torr. They concluded that the fracture of the glasses had followed zones of local alkali enrichment already present in the bulk glass. This interpretation is inconsistent with the random network theory for glass structure, but interestingly, it would be consistent with the cluster models of silicate glass structure where alkali ions preferentially "decorate" the interfaces between clusters. Thus, fracture surfaces could be enriched in alkali if the crack follows a path between the clusters. Nonetheless, other investigators have offered a different interpretation for the local enrichment of alkali observed at clean fracture surfaces.

Pantano, et al.[2] have used ion scattering spectrometry (ISS) to examine fracture surfaces of alkali-silicate glasses created in ultra high vacuum. The ISS method is unique because it is sensitive only to the outermost monolayer of the solid. In fact, by scattering ions off the surfaces at a glancing angle only those atoms which 'protrude' from the surface structure are detected. Unfortunately, conventional ISS is insensitive to hydrogen. Nonetheless, these data show quite clearly that alkali ions do, in fact, dominate the outermost monolayer of these clean fracture surfaces. Under the conditions where the ISS spectra for pure silica glass exhibited the stoichiometric ratio of Si and O, the spectra for the alkali silicate glasses exhibit little or no detectable Si and O. Obviously, these 'ideal' fracture surfaces are not a simple projection of the bulk structure. These investigators have proposed that the alkali ions assume new positions in the outermost monolayer wherein they shield the silicate tetrahedra. It is likely that this atomic rearrangement requires only relaxation or a 'jump' of alkali species into the surface monolayer, and not a long range diffusion process. And while the presence of localized charges at the dangling surface bonds would enhance this outward relaxation of alkali ions, the presence of charged surface sites is not a necessity. Any highly deformable cation will have a tendency to relax into the surface monolayer because it can reduce the force field perpendicular to the surface and provide a more complete coordination structure.

Kelso, et al.[35] compared the experimental ISS spectra for clean fracture surfaces of silica and potassium silicate glass with the results of a molecular dynamics (MD) simulation of a surface monolayer. A fracture surface was created in the MD simulation by removing the periodic boundary conditions in one dimension and then allowing the glass to relax at 300K. The MD calculations suggested that oxygen would dominate the outermost monolayer of silica glass

while potassium and oxygen would dominate the outermost monolayer of potassium trisilicate. The MD results were in reasonable agreement with the experimental ISS data. Interestingly, the MD simulations showed a distinct depletion of potassium in the sub-surface. The profile was reminiscent of a 'double-layer'.

The most significant conclusion to be drawn from these studies of clean surfaces is that in the absence of external environmental species, the glass surface will lower its free energy state by reconstruction processes. The studies described in a later section of this paper suggest that this rearrangement may occur during a fracture event. In the case of melt surfaces, the rearrangement will be enhanced due to the elevated temperatures, for example, during fiber drawing. Obviously, any attempt to 'passivate' surfaces by attaching chemical species to dangling bonds at the surface must be carried out simultaneously with the creation of the surface, or by an internal 'Gibbsian' adsorption process.

RELATIONSHIPS BETWEEN BULK COMPOSITION AND STRUCTURE, SURFACE CHEMISTRY AND FRACTURE OF GLASS

It should be quite clear at this point that the surface chemistry is dependent upon both the environmental conditions and bulk composition and structure of the glass. Ideally, then, one would like to examine the fracture of glass specimens whose surface chemistry -and its dependence upon bulk composition and structure- could be controlled and characterized. This could provide very fundamental information about the fracture behavior of glasses. Indeed, there have been many measurements of strength distributions and slow crack growth in controlled environments, and these measurements have been made on glasses of various 'bulk' compositions. But none of these studies have been coupled with direct analysis of, for example, fracture surfaces prepared at

sub-critical velocities in various chemical environments. Moreover, few of these studies have attempted to examine the strength and fracture behavior and its dependence on surface chemistry in glasses whose composition and structure are systematically modified. Obviously, these are not easy tasks, but may be necessary in order to provide insight to the micromechanisms of crack growth.

In this regard, Kaplow[36] attempted to prepare clean silica films under ultra high vacuum conditions, analyze the surfaces directly with Auger electron spectroscopy, and then measure their strengths with a fracture-bend device. He proposed further to modify these atomically clean silica surfaces by exposure to various chemical environments, and to correlate the resulting surface composition directly with the measured strengths. It was his intention to 'passivate' the surface by reacting the dangling $\equiv Si^{+}$ and $\equiv SiO^{-}$ surface sites in these chemical environments. Unfortunately, the silica films he prepared -although atomically clean- contained thermal and structural flaws whose magnitude insensitized the strength behavior to chemical effects. Of course, the studies of Antonni and Hochstrasser[33], and also Kelso[35], have already shown that these dangling bonds are rapidly eliminated even under ultra-high vacuum by a self-reconstruction. Thus, it is unlikely that they would have been available for passivation under these conditions.

Martin, et al.[24] and also Donnett, et al[37] measured the strengths and adsorption isotherms for E-glass and soda-lime-silicate glass fibers which were drawn under varying -but controlled- conditions. In principle, at least, this affords one the highest probability of 'passivating' the surface, as well as understanding the way high temperature surface chemistry influences strength behavior. Unfortunately, neither study utilized direct surface analysis to characterize the composition and structure of the fiber surfaces. The adsorption isotherms provide only an indirect measure of these surface

properties, and moreover, the adsorbates used can very often modify the surface under study. Nonetheless, it is worth emphasizing that both groups observed that the development of surface microporosity was a key factor in the correlation between drawing atmosphere and strength behavior.

Chesson[38] and Kerly[39] have taken a different approach in attempting to correlate bulk composition and structure, surface chemistry and fracture behavior. Here, a systematic compositional series of sodium aluminosilicate glasses have been studied so that the influence of various chemical and structural features could be evaluated with regard to fracture and stress corrosion behavior. In the system $Na_2O \cdot xAl_2O_3 \cdot (3-x)SiO_2$, the bulk density of non-bridging oxygen sites can be varied independent of the sodium concentration. Based upon the current understanding of hydration - already summarized in this paper - these structural variations should cause systematic changes in the surface pH, type of surface film formation, water transport mechanism and dissolution kinetics.

Figures 10, 11 and 12 reveal that the chemical properties[39] of these glasses are, in fact, very sensitive to the Al_2O_3/Na_2O ratio (which controls the non-bridging oxygen density). It can be seen that these glasses exhibit a wide range of 'equilibrium' pH values (Figure 10). Thus, the crack-tip chemistry in each of these glasses will be very different in aqueous environments. Although one might argue that the pH at the tip of a moving crack may not reach its 'equilibrium' value, the equilibrium pH for a given glass characterizes its 'tendency' to react with water. Indeed, the pH of the solution contained in the crack tip may be of little importance; rather, the surface pH - that is, the number of ionized silanol groups - may be of more significance. Of course, the implications of equilibrium pH with regard to the

aging of surfaces and pre-existing flaws - even in the absence stress - are more straightforward.

The soda and silica dissolution rates are also extremely sensitive to the Na_2O/Al_2O_3 ratio as shown in Figure 11. This is an intrinsic property and not a pH effect. That is, the dissolution rates were measured in water - where the pH could drift - and at constant pH using a buffer. The dissolution rates were slightly higher under constant pH conditions, but the dependence upon the Al_2O_3/Na_2O ratio was not affected. This strong dependence of dissolution rate upon the Al_2O_3/Na_2O ratio - independent of 'solution pH' - lends validity to the suggested importance of 'surface pH'.

The hydrogen profiles in Figure 12 provide some insight to surface pH effects, the transport of water and surface film formation. They show that the glasses with $x = 0$ and $x = .2$ form distinct hydrated layers at the surface, whereas the glasses with $x \geq .4$ exhibit reduced hydrogen penetration. Moreover, the amount of hydrogen incorporated in the leached layer decreases with the Al_2O_3/Na_2O ratio. These same glasses were examined with diffuse reflectance Fourier transform infared spectroscopy. These data revealed that the sodium ions at non-bridging oxygen sites were released at a much higher rate than those at $(AlO_4)^-$ sites. Thus, although all of these glasses have the same number of sodium ions - and therefore the same number of sites where protonic species may be immobilized - it is primarily the non-bridging oxygen sites which influence the hydration phenomena and surface pH. That is, it is the non-bridging oxygen site, and not the sodium ion per se, which is responsible for the reaction with water.

The large effect of the first alumina substitution ($x = 0.2$) on the chemical properties suggests that the Al_2O_3 does not substitute randomly in the $Na_2O\ 3SiO_2$ glass structure. Rather, it occupies those sites where the

transport and attack of water is most significant, for example within a topological network of non-bridging oxygens. This conclusion is consistent with the results of Smets and Lommen[40] who measured the diffusion coefficient for water (D_{H_2O}) during hydration of a similar compositional series of aluminosilicate glasses. They report that a change in the Al_2O_3/Na_2O ratio from 0 to .25 in $Na_2O.4SiO_2$ reduced D_{H_2O} by a factor of 400.

A wide variety of mechanical properties are also being evaluated in this same series of glasses[38]. Here, only the fracture toughness (K_{IC}) and stress stress intensity exponent (n) are reported in Figures 13 and 14. The fracture toughness - measured in liquid nitrogen via the controlled microflaw technique - increased with the first substitution of Al_2O_3 in $Na_2O{\cdot}3SiO_2$ and then decreased with additional substitution. The initial increase in K_{IC} is consistent with the idea that the first additions of Al_2O_3 to $Na_2O{\cdot}3SiO_2$ do not substitute randomly in the structure, but rather occupy the weakest sites - topological or otherwise - in the $Na_2O{\cdot}3SiO_2$ structure. The decrease in K_{IC} with further polymerization of the network structure is more surprising - particularly since the elastic modulus increases steadily with Al_2O_3/Na_2O. However, it is notable that the activation energy for sodium ion motion (@T<Tg) exhibits the same dependence upon the Al_2O_3/Na_2O ratio. The activation energies were obtained independently for this same series of glasses via internal friction measurements[45]. This correlation suggests that the motion of alkali ions may be involved in the propagation of cracks - at least in the absence of external chemical effects. This is consistent with the observations made on the alkali-silicate fracture surfaces created in vacuum where an alkali-ion rearrengement was observed. It leads naturally to the conclusion that the atomic rearrangement observed at those clean fracture surfaces occurred during the crack propagation in ultra high vacuum. The fact that the glasses with Al_2O_3/Na_2O = 1 have fully polymerized

networks such as pure silica glass - but exhibit lower fracture toughnesses than pure silica glass - is also consistent with the idea that sodium ions can be involved in the fracture process. Interestingly, the notion that alkali ions play a role in fracture was first suggested by Cox in 1969[46]. Later, Rauschenbach and Hinz[47] considered the stress-induced segregation of sodium to crack-tips in glass.

The stress intensity exponents in Figure IV-14 were measured in deionized water using the stressing rate technique. These data suggest that it is the combined effect of crack tip pH and network structure - and not the mere presence of alkali - which controls the susceptibility to stress corrosion. That is, the $Na_2O \cdot Al_2O_3 \cdot 2SiO_2$ glass exhibits a susceptibility to stress corrosion which is comparable to SiO_2. It should be recalled that the glasses have isostructural networks and that the equilibrium surface pH of the aluminosilicate is extremely low in spite of the soda. Of course, additional studies, particularly slow crack growth experiments carried out in solutions buffered to the 'equilibrium pH', are needed to fully rationalize this behavior.

SUMMARY

It is quite clear that chemical reactions at glass surfaces - under ambient conditions as well as during high temperature fabrication processes - will modify the composition, molecular structure and morphology of the surface to varying degrees. It is also evident that the bulk glass composition and structure will influence the reaction mechanisms, and in particular, the 'depth' of interaction. However, the extent to which these surface chemical phenomena directly affect strength and fracture behavior has not been established. Indeed, correlations may be drawn between the surface chemical reactivity and hydration susceptibility of various glasses and glass surfaces and their

strength and fracture behavior. Nonetheless, the fundamental processes which underly these apparent correlations are not accessible simply from a surface analysis. Even the reconstruction processes observed to occur at fracture surfaces of alkali-containing glasses may be a consequence - and not the means - by which fracture occurs.

It is likely that surface chemical reactions which occur under stress are the critical phenomena influencing the strength and fracture behavior of glass. Of course, these stresses need not be limited to an applied stress but undoubtedly include the intrinsic 'monolayer' stresses associated with the very existence of a surface, surface stresses due to thermal history and dealkalization of multicomponent glass surfaces, and the stressed bonds associated with the topology and impurities in the surface region. The important point to be made is that the classical and modern-day spectroscopic approaches to surface science are insensitive to the presence of the stresses. That is, surface analyses *cannot* be localized at microscopic regions of high stress. And, uniform surface stresses whose magnitude is of significance in fracture cannot be achieved <u>in situ</u> on specimens which are convenient for surface studies (with the possible exception of fibers and ribbons). Even the direct analysis of surfaces created in a slow crack growth experiment is of questionable value because the surface species produced at fracture may be intermediate to the surface species found by an analysis after fracture.

These comments are not meant to discourage surface chemical studies for understanding strength and fracture behavior. To be sure, knowledge of the composition of glass surfaces and their sensitivity to water, pH effects and the bulk glass properties is necessary. And in a practical sense, these approaches are required for the characterization of surfaces, surface treatments and protective coatings. However, the direct relationships which can be drawn

between classical surface chemistry and surface analyses, and the fundamental micromechanisms of fracture, may be limited. Nevertheless, it is hoped that this review provides a useful summary of glass surface chemistry, as it might relate to the strength and fracture of silicate glasses.

ACKNOWLEDGMENTS

The author thanks the Air Force Office of Scientific Research (AFOSR-82-0013) and the National Science Foundation (DMR-80-18473) for financial support of the work reviewed here, as well as the following students for their contributions: J. Chesson, C. A. Houser, J. Kelso and T. Kerly. Finally, the author achnowledges B. Smets for his comments and helpful suggestions.

REFERENCES

1. C. G. Pantano, Am. Cer. Soc. Bull., 60 (11), 1154 (1981).

2. C. G. Pantano, J. F. Kelso and M. J. Suscavage, in Advances in Materials Characterization - Vol. 15 (Plenum, New York, 1983).

3. M.L.Hair, Infared Spectroscopy in Surface Chemistry (Dekker, New York, 1967).

4. V. A. Bershtein and V. V. Nikitin, Sov. Phys-Doklady, 15 (2), 163 (1970).

5. M. Novotny and K.D. Bartle, Chromatographia, 7 (3), 122 (1974).

6. M. L. Hair, J. Non-Cryst. Sol., 19, 299 (1975).

7. T. H. Elmer, and also D. L. Eaton, in Silylated Surfaces (Gordon and Breach, New York, 1980.)

8. R. K. Iller, The Chemistry of Silica (J. Wiley & Sons, New York, 1979).

9. V. A. Bershtein & V. V. Nikitin, Proc. of Xth Intl. Cong. Glass, 9, 105 (1974).

10. V. A. Bershtein, S. N. Novikov & V. V. Nikitin, Sov. Phys. Solid State, 15 (2), 348 (1973).

11. V. A. Bershtein, Y. A. Emelyanov & V. A. Stepanov, Fiz. Khim. Stekla, 4(5), 549 (1978).

12. H. H. Dunken & R. Hoffman, Z Phys. Chem., 260(5), 913 (1979).

13. H. H. Dunken, in Treatise on Materials Science & Technology - Vol. 22 (Academic Press, New York, 1982.)

14. F. L. Galeener, Sol. State Comm., 44(77), 1037 (1982).

15. D. M. Krol and J. G. van Lierop, J. Non-Cryst. Sol., to appear 1984.

16. D. M. Krol and J. G. van Lierop, J. Non-Cryst. Sol., to appear 1984.

17. S. M. Wiederhorn, H. Johnson, A. M. Diness & A. H. Heuer, J. Am. Ceram. Soc. 57, 336 (1974).

18. W. A. Landford, in Advances in Materials Characterization -Vol. 15 (Plenum Press, New York, 1983.)

19. I. S. T. Tsong, C. A. Houser & S. S. C. Tong, Phys. Chem. Glasses 21 (5), 197 (1980).

20. J. E. Shelby, J. Vitko & C. G. Pantano, Solar Energy Mater., 3, 97 (1980).

21. D. E. Clark, C. G. Pantano & L. L. Hench, Corrosion of Glass (Books for Industry, New York, 1979.)

22. B. Stavrinidis & D. G. Holloway, Phys. Chem. Glasses, 24 (1), 19 (1983).

23. P. A. Sewell, Glass Techn., 8 (4), 108 (1967).

24. D. M. Martin, M. Akinc & S. M. Oh, J. Am. Cer. Soc., 61 (7), 308 (1978).

25. A. G. Metcalfe, M. E. Gulden & G. K. Schmitz, Glass Tech., 12 (11), 15 (1971).

26. S. R. Lipsky, W. J. McMurray & M. Hernandez, J. Chromat. Sci., 18, 1 (1980).

27. W. E. Dirkes, W. A. Rubey & C. G. Pantano, J. High Res. Chromotog & Chromatog. Comm, 3, 303 (1980).

28. R. W. Douglas & J. O. Isard, J. Soc. Glass Tech., 33, 289 (1949).

29. J. P. Poole, H. C. Snyder & R. J. Ryder, U.S.P. 3,314,772 (1967).

30. R. J. Ryder, W. J. Poad & C. G. Pantano, J. Can. Ceram. Soc., 51, 21(1982).

31. S. M. Budd & W. P. Cornelius, Glass Tech., 20 (5), 170 (1979).

32. I. N. Yashchishin & V. A. Sharagov, Steklo Keram., 9, 12 (1978).

33. G. Hochstrasser & J. F. Antonini, Surf. Sci., 32, 644 (1972).

34. J. P.. Lacharme, P. Champion & D. Leger, Scanning Elect. Micr., 1981, p. 237.

35. J. F. Kelso, C. G. Pantano & S. H. Garofalini, to appear in Surf. Sci. Lett.

36. R. Kaplow, RADC-TR-81-292, 1981.

37. J. B. Donnet, R. Battistella & B. Chatenet, Glass Tech., 16 (6), 139 (1975).

38. J. Chesson, M. S. Thesis, Pennsylvania State University, 1983.

39. T. A. Kerly, M. S. Thesis, Pennsylvania State University, 1983.

40. B. M. J. Smets & T. P. A. Lommen, Phys. Chem. Glasses, 23, 83 (1982).

41. R. J. Eagen & J. C. Swearengen, J. Am. Cer. Soc., 61 (1), 27 (1978).

42. S. M. Wiederhorn, J. Am. Cer. Soc., 52 (2), 99 (1969).

43. J. E. Ritter and C. L. Sherburne, J. Am. Ceram. Soc., 54 (12), 601 (1971).

44. S. M. Wiederhorn and L. H. Bolz, J. Am. Ceram. Soc., 53 (10), 543 (1970).

45. D. E. Day & G. E. Rindone, J. Am. Cer. Soc., 45 (10), 496 (1962).

46. S. M. Cox, Phys. Chem. Glasses, 10 (6), 226 (1969).

47. B. Rauschenbach and W. Hinz, Silikattechnik, 30 , 329 (1979).

TABLE 1

	$S_o(\frac{MN}{M^2})$	C	n
internal surface untreated	307	.13	17
internal surface treated	440	.06	35

S_o = instaneous failure stress

C and n = stress corrosion factors

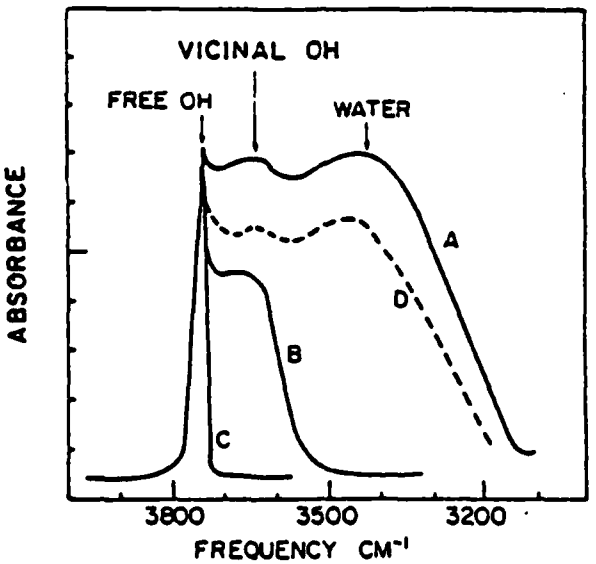

Figure 1. Infrared spectra for porous glass showing absorption bands for molecular water, vicinal hydroxyl groups and freely-vibrating hydroxyl groups; (A) heated to 100°C (B) heated to 300°C (C) heated to 500°C (D) re-hydrated after heating to 500°C (from 7).

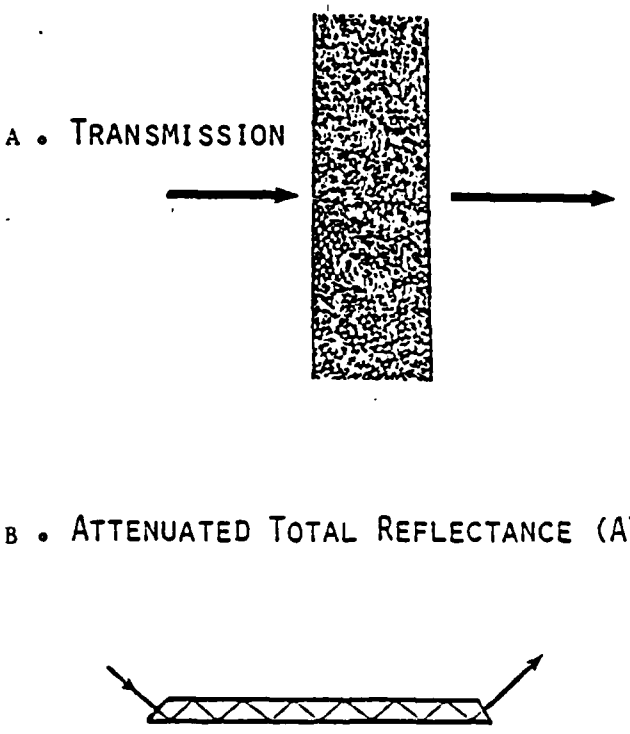

Figure 2. Methods of infrared absorption analysis which are 'surface sensitive'
(A) transmission through a microporous compact where many surfaces are sampled
(B) attenuated total reflectrance (ATR) where the surface is sampled by multiple internal reflections.

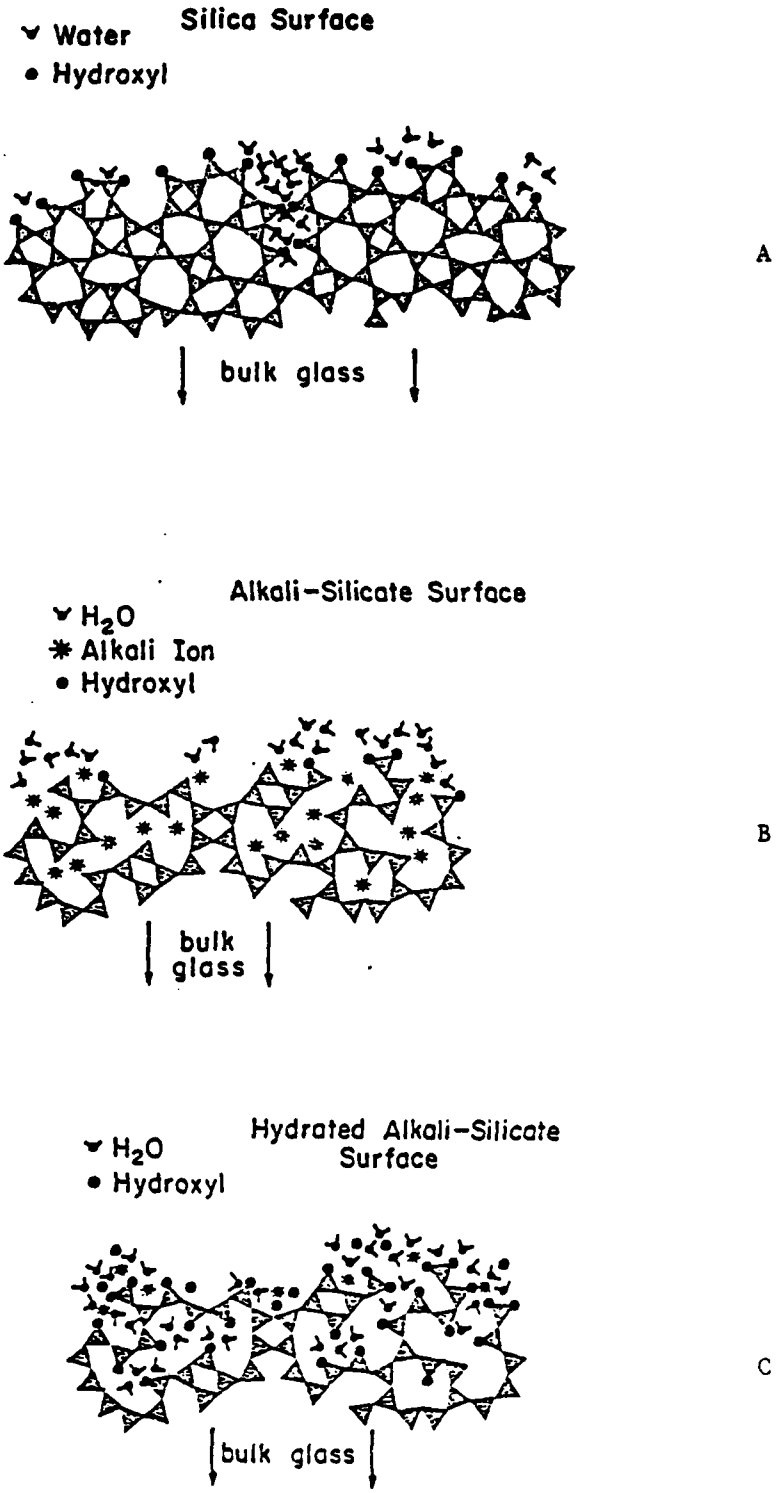

Figure 3. Schematic representations of silicate glass surface structures containing silanol groups and adsorbed molecular water (a) silica surface under ambient conditions (b) alkali-silicate surface under ambient conditions (c) alkali-silicate surface hydrated in water. (The ideal random networks in these schematics were generated with triangle rafts.)

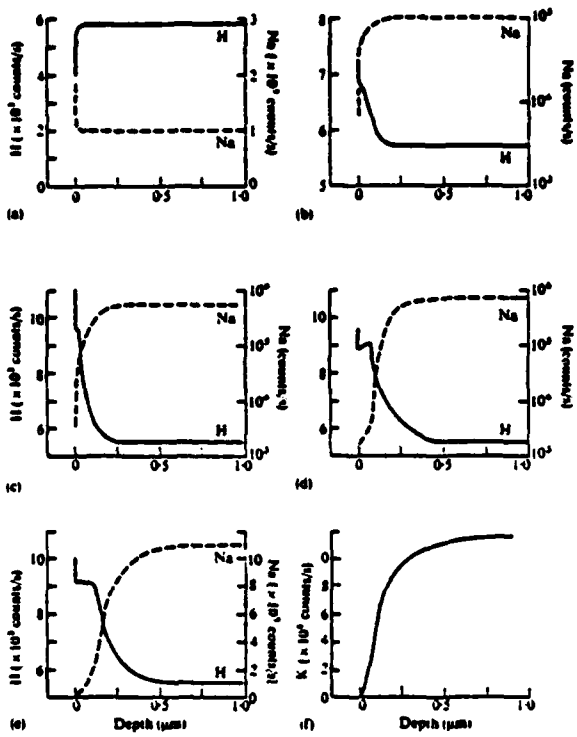

Figure 4. Hydrogen and alkali depth-profiles obtained with sputter-induced photon spectroscopy (SIPS) after soaking commercial glasses in water for 48h at 90°C (a) Corning code 7190 (trace alkali) (b) Corning code 7740 (4% soda) (c) sheet glass (12.8% soda) (d) Corning code 0160 (11.3% pottasia, 2.6% soda) (e) Corning code 0080 (16.2% soda) (f) K-profile for Corning code 0160. (from 19).

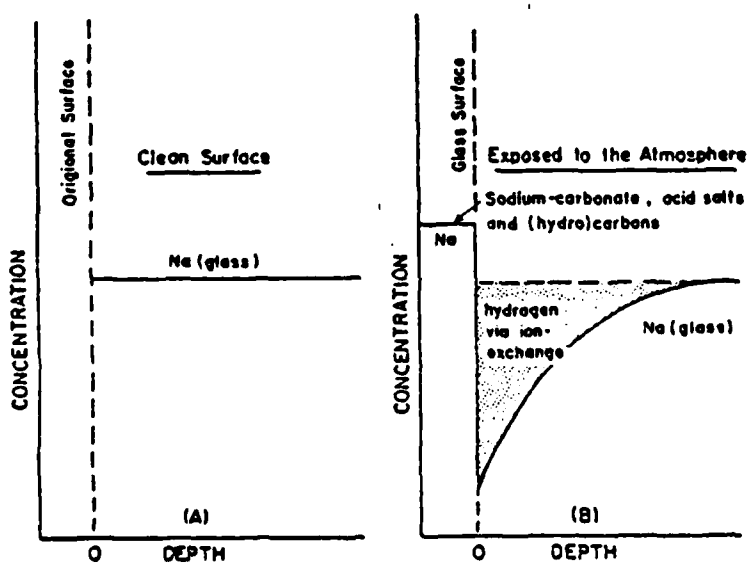

Figure 5. Model for the reaction between a clean sodium-silicate glass surface and water vapor in the ambient atmosphere (A) sodium depth-profile for the clean surface (B) idealized sodium depth-profile after reaction with adsorbed water and carbonaceous species, and the corresponding hydrogen incorporation.

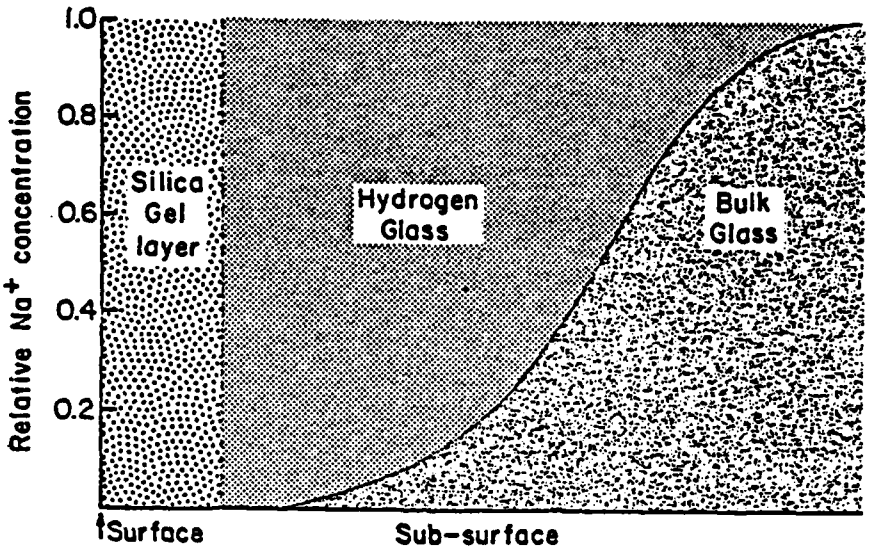

Figure 6. Surface layer formation on sodium-silicate glass. Hydrogen glass corresponds to the initial replacement of the alkali species with hydrogen to produce silanol groups at, and within, the glass surface. The gel is due to the incorporation of molecular water (at the silanol groups in the hydrogen glass) and the subsequent transformation of the surface into a swollen layer of colloidal silica.

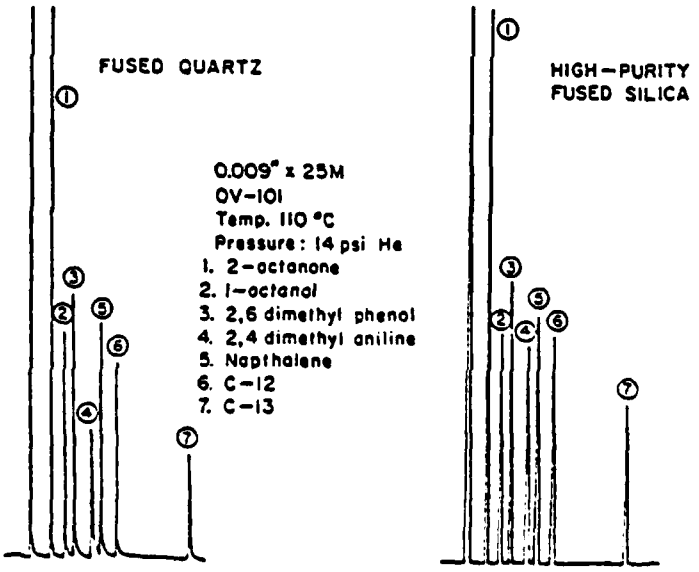

Figure 7. Glass capillary gas chromatographic $(GC)^2$ analysis of a nonpolar test mixture in fused quartz and high-purity silica; tails on the peaks and their reduced intensity in the fused quartz indicates 'adsorption' of these species (from 26).

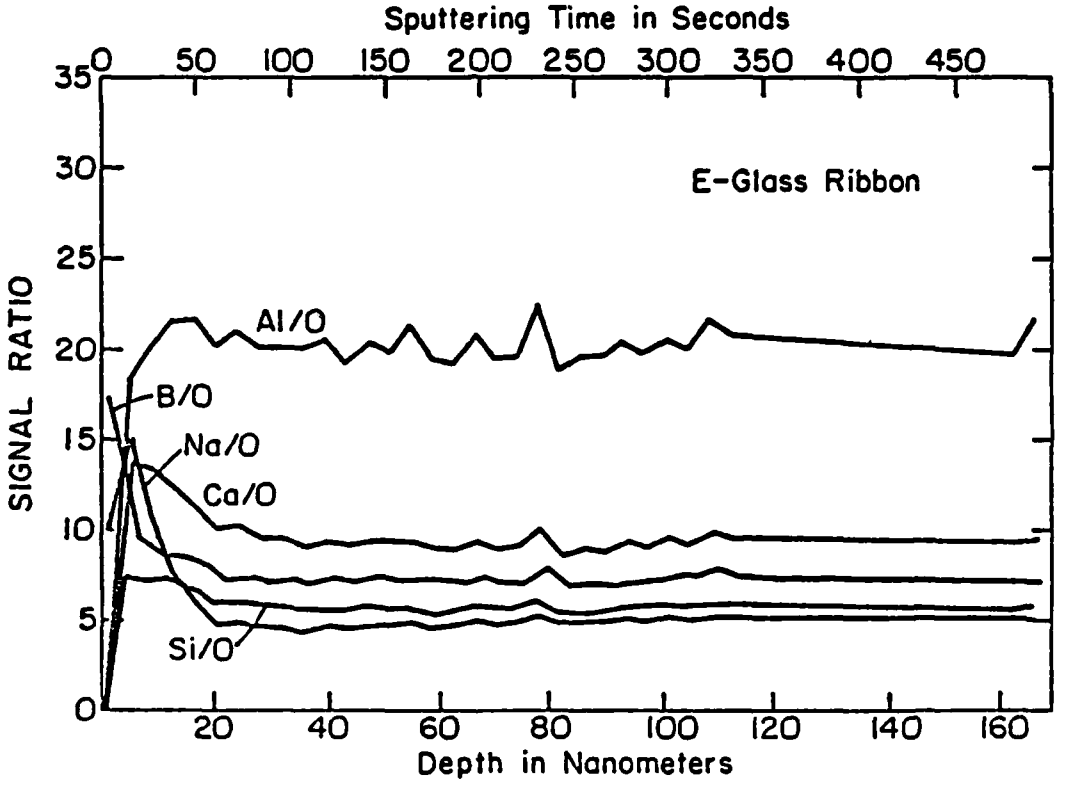

Figure 8. Depth profiles obtained with secondary ion mass spectroscopy (SIMS) at the surface of an E-glass ribbon. (The Na/O intensity ratio measured on a bulk standard of E-glass is ≈15.)

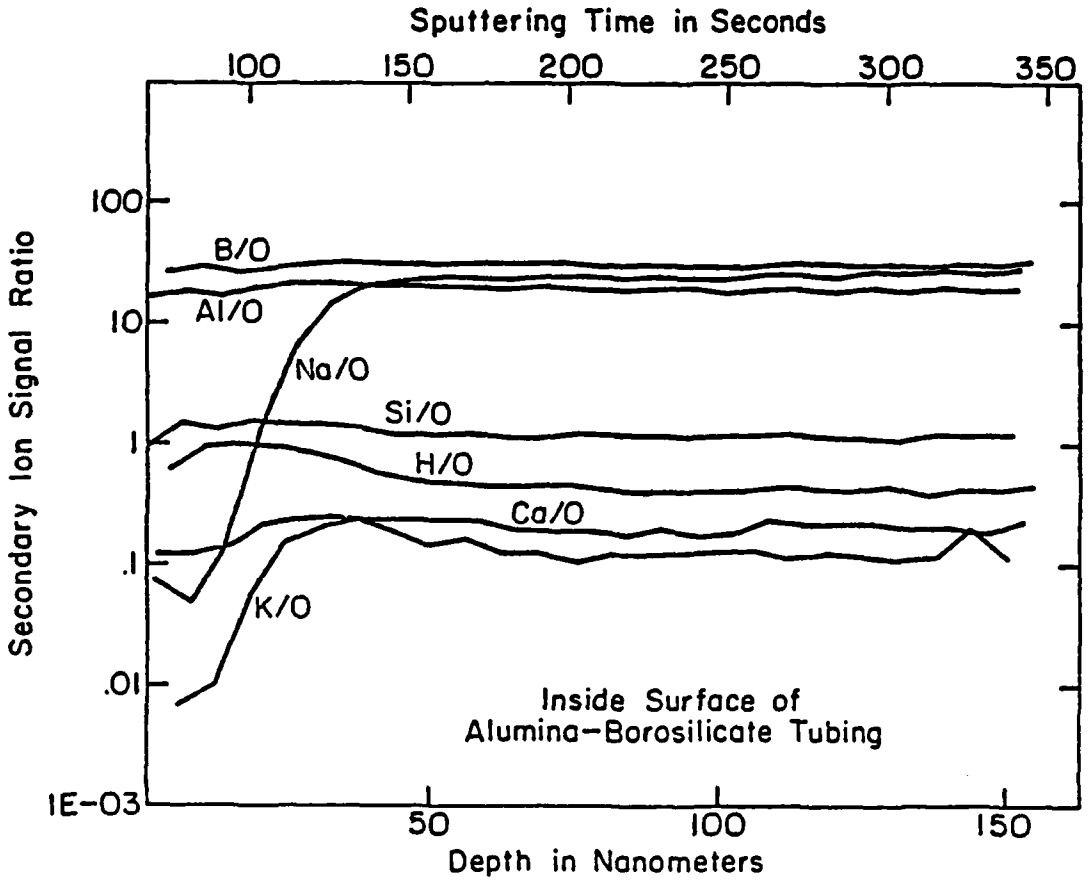

Figure 9. Depth profiles obtained with secondary ion mass spectroscopy (SIMS) at the inside surface of commercial glass tubing.

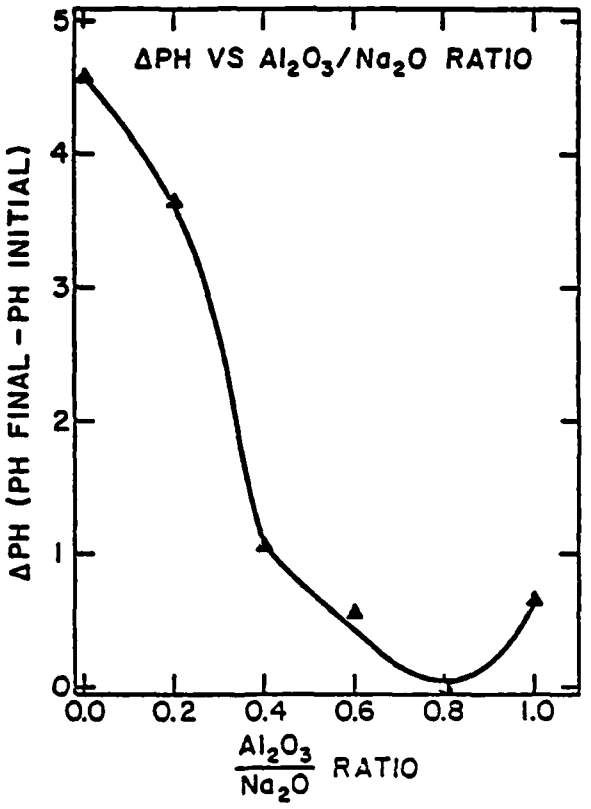

Figure 10. The 'equilibrium' pH changes observed in water at 30°C during exposure to glasses in the system $Na_2O \cdot xAl_2O_3 \cdot (3-x)SiO_2$.

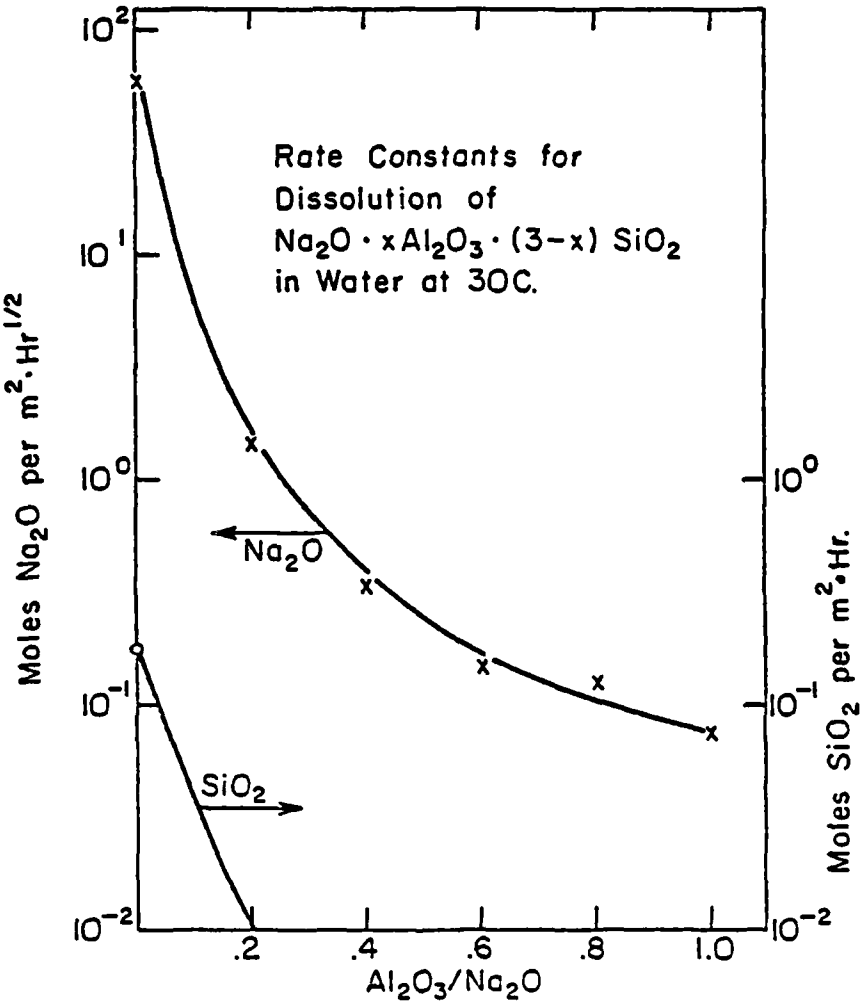

Figure 11. The rate constants for release of Na_2O and SiO_2 from glasses in the system $Na_2O \cdot xAl_2O_3 \cdot (3-x)SiO_2$.[2] The Na_2O was released with parabolic kinetics while the SiO_2 was released with linear kinetics.

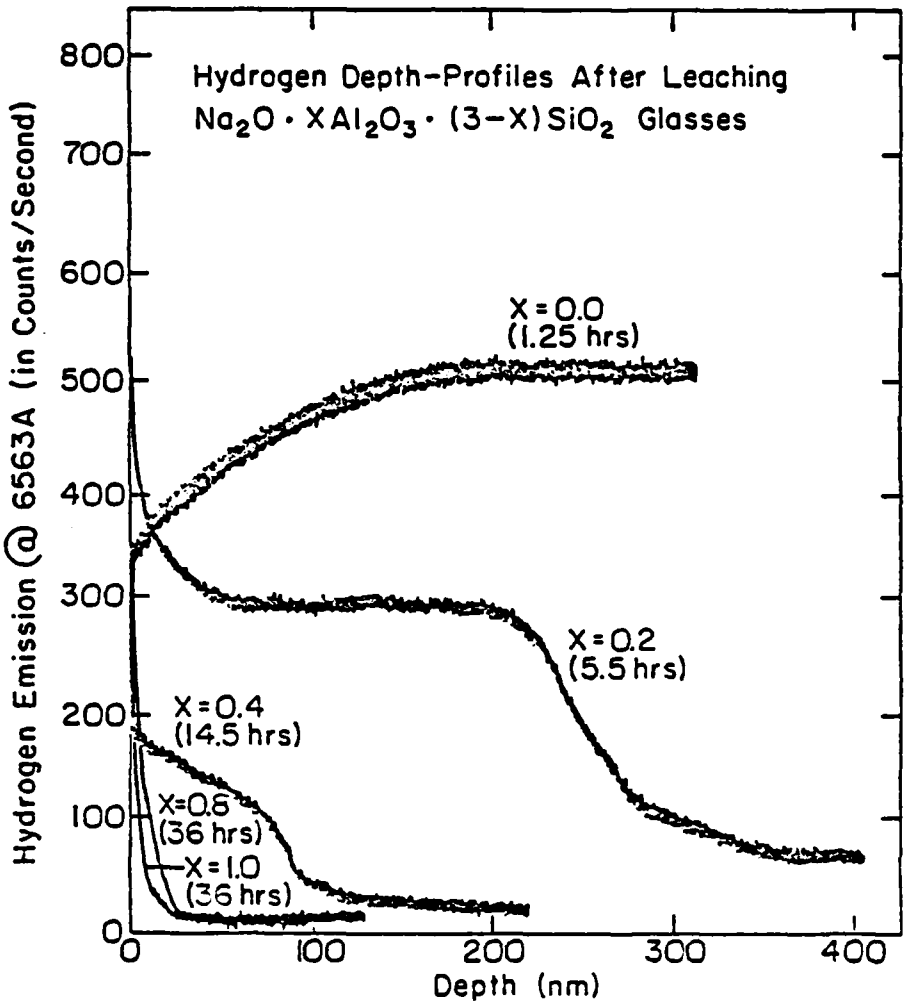

Figure 12. Hydrogen depth-profiles obtained with sputter induced photon spectroscopy (SIPS) for glasses soaked in water at 30°C for various times.

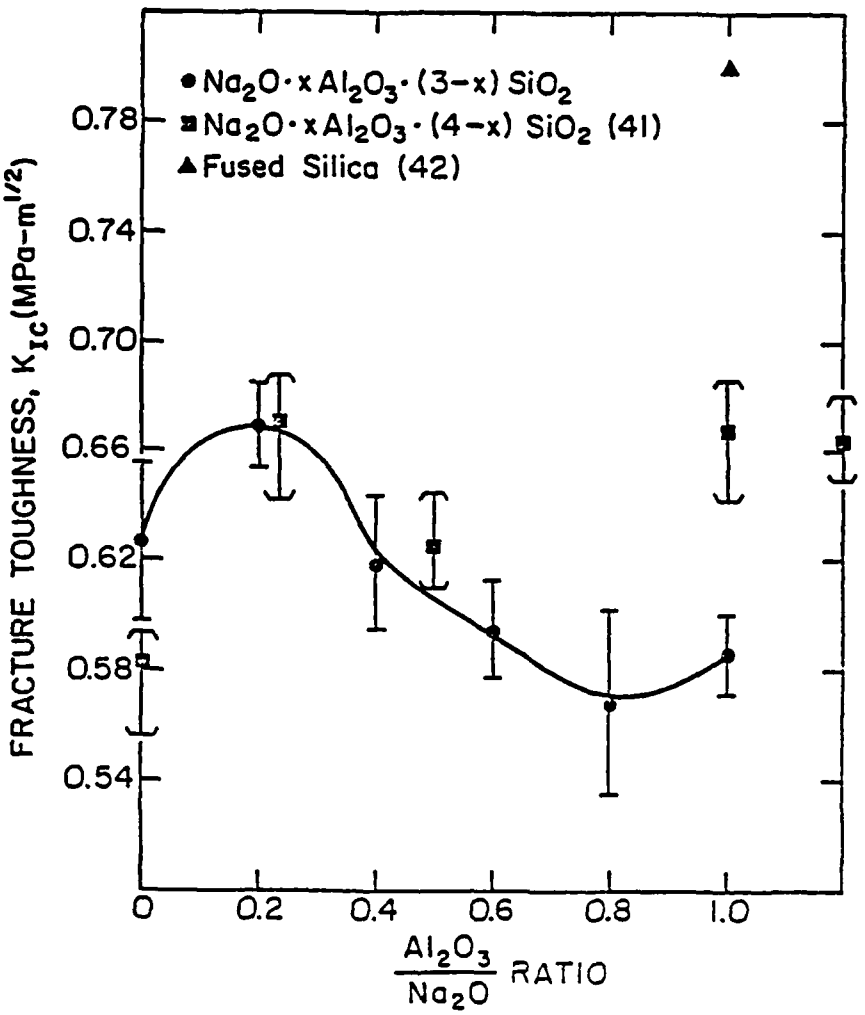

Figure 13. The fracture toughness measured by the controlled microflaw technique in a variety of aluminosilicate glasses. The value for fused silica is compared with the values for glasses with Al_2O_3/Na_2O = 1 since they all have fully polymerized silicate networks.

CHAPTER II

THE RELATIONSHIP BETWEEN ELASTIC PROPERTIES AND SLOW CRACK GROWTH IN SODIUM-ALUMINOSILICATE GLASSES

by

D. N. Coon, J. J. Mecholsky and C. G. Pantano

Department of Materials Science and Engineering

Pennsylvania State University

University Park, PA 16802

Submitted for publication to J. American Ceramic Society.

THE RELATIONSHIP BETWEEN ELASTIC PROPERTIES AND SLOW CRACK GROWTH IN SODIUM-ALUMINOSILICATE GLASSES

D. N. Coon,[+] J. J. Mecholsky and C. G. Pantano
Department of Materials Science and Engineering
Pennsylvania State University
University Park, PA 16802

ABSTRACT

Crack velocity, V, was measured as a function of stress intensity, K_I, for a series of sodium-aluminosilicate glasses corresponding to compositions represented by $Na_2O \cdot xAl_2O_3 \cdot (3-x)SiO_2$ with x values of 0.0, 0.2, 0.4, 0.6, 0.8 and 1.0. Thus, the molar concentration of Na_2O was held constant while Al_2O_3 was substituted for an equimolar amount of SiO_2. Although the corrosion resistance of these glasses varies by at least three orders of magnitude, the slopes (n) of the log V-log K_I curves only changed from ~17 to ~25. These observations indicate that ion exchange, leaching and dissolution are not the primary factors which control slow crack growth.

Although the underlying mechanism of slow crack growth is a chemical reaction between environmental species and crack tip bonds, it is suggested that the rate of the chemical reaction is controlled through the elastic strain. Under the assumption that the slope (n) of the log V-log K_I curve varies as the stiffness in the crack tip region, an expression was derived for the stiffness in terms of Young's elastic modulus (E). An excellent correlation was observed between n and E for sodium aluminosilicate, soda-lime-silica and fused silica glasses in agreement with our hypotheses. Altogether, this implies that the expression for the relation between crack velocity and stress intensity could be written as:

$$V = V_o K_I^{n SE}$$

where V_o and n are constants and S and E are material parameters determined by the elastic constants. Thus, the composition dependence of the stress corrosion susceptibility is due to the composition dependence of the elastic constants and not the chemical corrosion properties.

[+] Now with EG&G Idaho, Idaho Falls, ID

INTRODUCTION

The dependence of mechanical strength upon time and environment has been known for some time (1). The mechanism of strength degradation in glasses has been reported to be crack extension at sub-critical velocities (2). The rate of crack extension, and hence the magnitude of strength degradation, is governed primarily by the applied stress and stress-corrosion susceptibility. The objective of this study was to establish the dependence of this slow-crack growth behavior upon the composition and network structure of the glass.

BACKGROUND

It is generally accepted that crack extension occurs via a chemical reaction between the material and the environment surrounding it. Charles and Hillig (3) proposed that the rate at which such a reaction proceeds is altered by the application of an external stress. Wiederhorn (2) suggested that the external stress offsets a portion of the required activation energy in such a manner to increase the reaction rate. Since the applied stress is intensified at the crack tip, the reaction rate at the tip would be expected to be large compared to the surrounding planar surfaces. Under these conditions, Wiederhorn proposed the following model:

$$V = V_o \exp [(-E_o + bK_I)/RT] \qquad (1)$$

where V = rate of crack extension

V_o = constant

E_o = activation energy in the stress free state

b = constant

K_I = stress intensity

while R and T are the gas constant and absolute temperature.

This model has been reported to describe experimental stress intensity - crack velocity data very well (4,5) and, consequently, has gained widespread acceptance. Nevertheless, most researchers characterize the slow crack growth behavior by the n-parameter which relates the stress intensity to the crack velocity through the following relationship:*

$$V = V_o (K_I)^n \qquad (2)$$

The n parameters reported for silicate based glasses range from 10 to 40 (6).

A number of attempts have been made to determine the feature or property of a glass which is fundamental to the observed n-parameter. The tendency of a glass to react with an aqueous environment or undergo slow crack growth has been examined through the aqueous corrosion behavior (7,9). One of these studies showed that the leaching rate of sodium ions varied inversely with the n-parameter (7). The linear thermal expansion coefficient, which is related to the molecular structure of the material, was also shown to vary inversely with the n-parameter for many oxide glasses. These observation suggest that the two properties which play a major role in determining the slow crack growth behavior are chemical corrosion and molecular structure. In the present study, the effects of these two characteristics were separated in an effort to determine which is dominant in the slow crack growth process. Sodium-

* It can be argued that Eq (1) has more fundamental meaning than Eq (2) because it relates crack velocity to the activation energy and activation volume; nonetheless, it is more common and convenient to use n, the slope of the log velocity-log stress intensity curve, as a measure of the resistance to slow crack growth.

aluminosilicate glasses were chosen for investigation because the structure and corrosion behavior can be systematically varied by changing the soda to alumina composition ratio.

EXPERIMENTAL PROCEDURE

Sodium-aluminosilicate glasses corresponding to compositions represented by the general formula:

$$Na_2O \cdot x\ Al_2O_3 \cdot (3-x)\ SiO_2 \qquad (3)$$

were prepared with x values of 0.0, 0.2, 0.4, 0.6, 0.8 and 1.0. In this series, the molar concentration of Na_2O was held constant while Al_2O_3 was substituted for an equimolar amount of SiO_2. These glasses are identified by their Al_2O_3/Na_2O molar ratios; thus, $Na_2O \cdot 3SiO_2$ is labeled 0.0 glass and $Na_2O \cdot Al_2O_3 \cdot 2SiO_2$ is labeled 1.0 glass.

All of the glasses were melted in platinum or irridium crucibles using silica (5 μm Minusil) and reagent grade aluminum hydroxide and sodium carbonate. The high alumina glasses were crushed and remelted two or three times to insure homogeneity. After annealing, the glasses were cut into plates approximately 7.5 cm x 1.27 cm x 0.25 cm; a groove was machined down the center of the specimen. The depth of the groove was approximately one-half of the plate thickness and the width was 0.00075 to 0.001 cm. After cutting and grooving, the specimens were re-annealed to remove any residual stresses, and then were pre-stressed to initiate a sharp crack.

The stress intensity-crack velocity relationship for each composition was obtained by the constant moment double cantilever beam technique (CM-DCB) as described by Freiman, Mullville, and Mast (10). The aluminum arms, through

which the moment was applied, were attached to the glass specimens with epoxy. The applied stress intensity, K_I, was calculated from the relationship derived by Freiman, Mullville, and Mast:

$$K_I = [PL]/[2\sqrt{It}\,] \qquad (4)$$

where P = applied load

L = length of moment arm

I = moment of inertia

t = specimen thickness in the groove (1.25 mm).

The crack extension was monitored with a 40X travelling microscope equipped with a filar eyepiece.

The crack growth behavior of each composition was examined in both deionized water (pH 5) and in 10^{-3}M NaOH solution (pH 11). At least two, and up to five, specimens of each glass were tested at each condition. Each specimen generally provided 10-40 individual data points. The solution pH was checked periodically throughout each test.

RESULTS

Crack Velocity Data in Water

The results of constant moment double cantilever beam experiments in deionized water (pH 5) on 0.0, 0.2, 0.4, 0.6, 0.8, and 1.0 glasses are given in Figures 1a, 1b, 1c, 1d, 1e, and 1f, respectively. The results have been plotted according to the classical reaction model (Equation 1) of Wiederhorn (2). The corresponding regression lines are depicted in each figure, as well as the values of the slope (b/RT) and the 95% confidence intervals calculated from the linearized version of Equation 1:

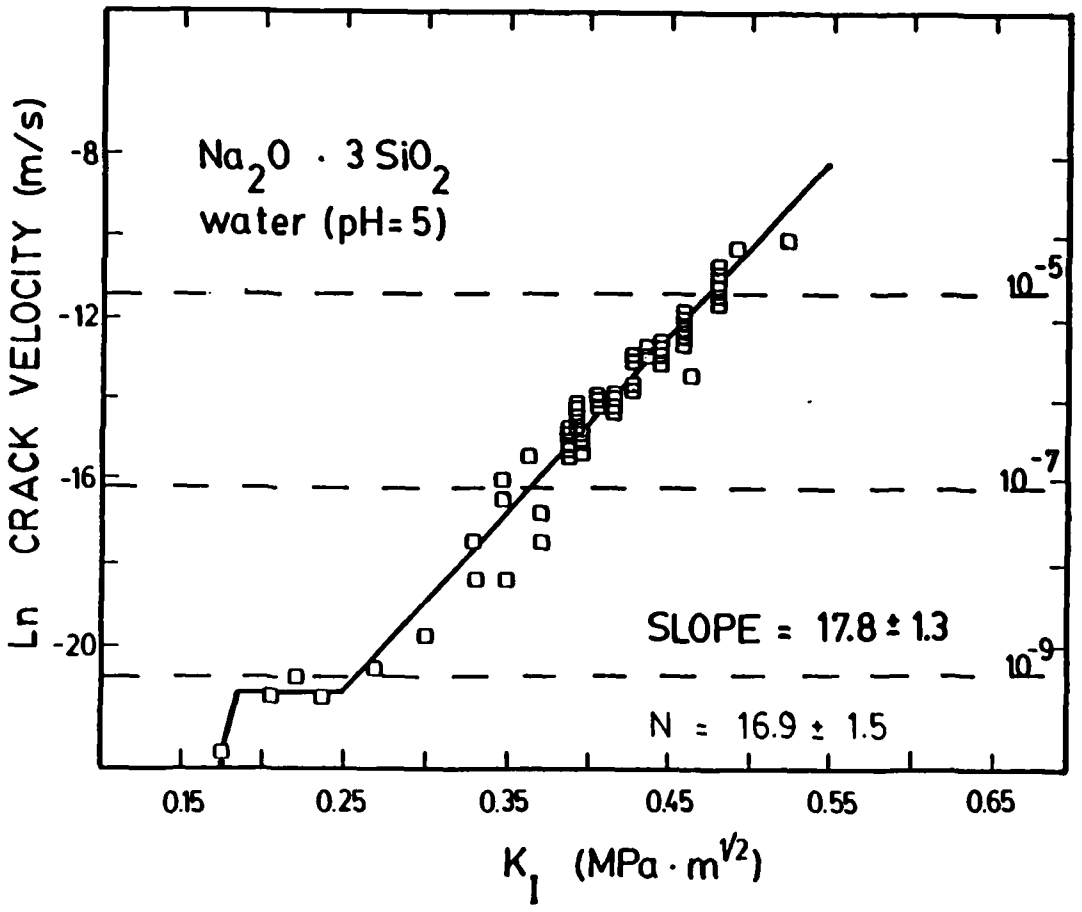

Figure 1a. Stress intensity-crack velocity data for 0.0 glass in water.

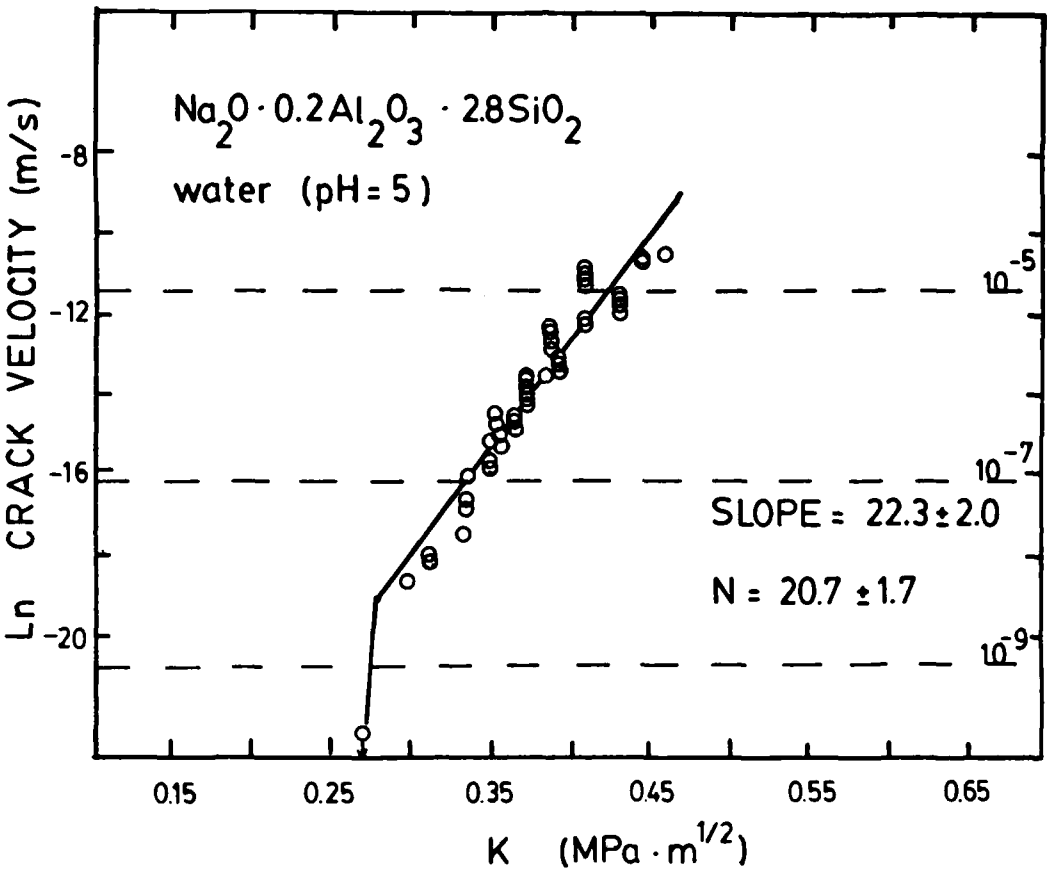

Figure 1b. Stress intensity-crack velocity data for 0.0 glass in water.

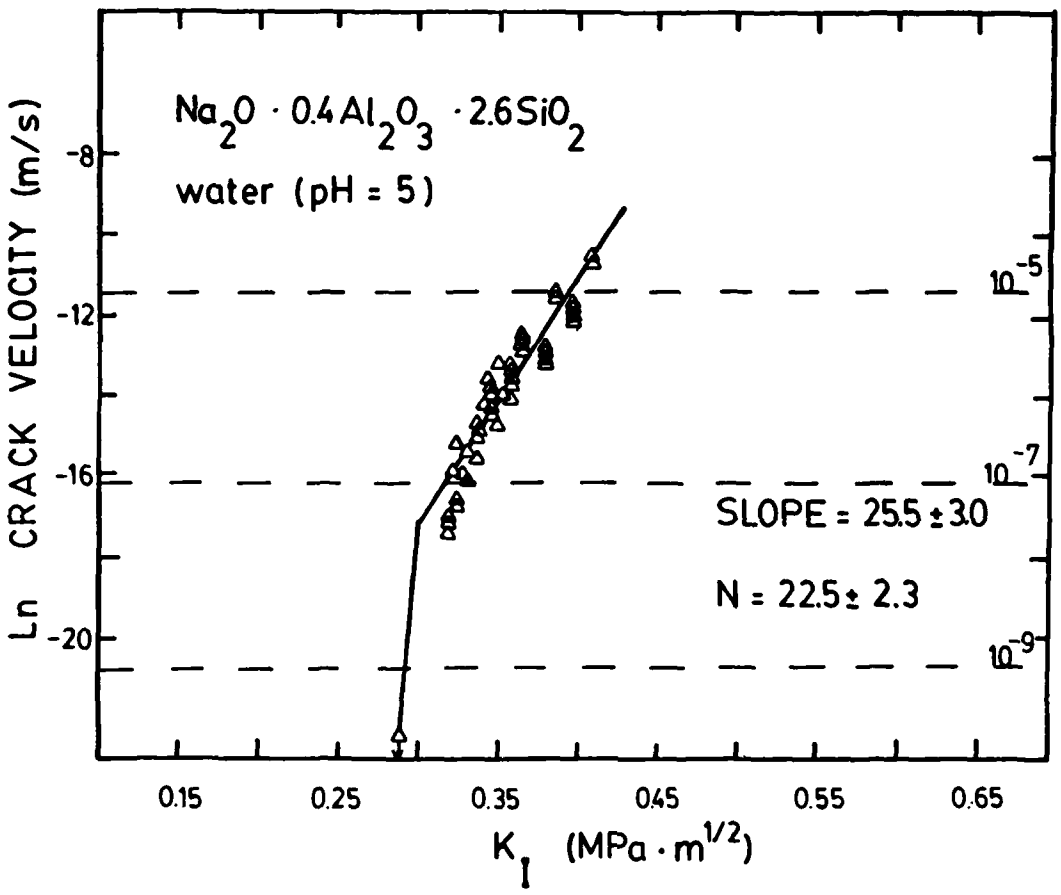

Figure 1c. Stress intensity-crack velocity data for 0.2 glass in water.

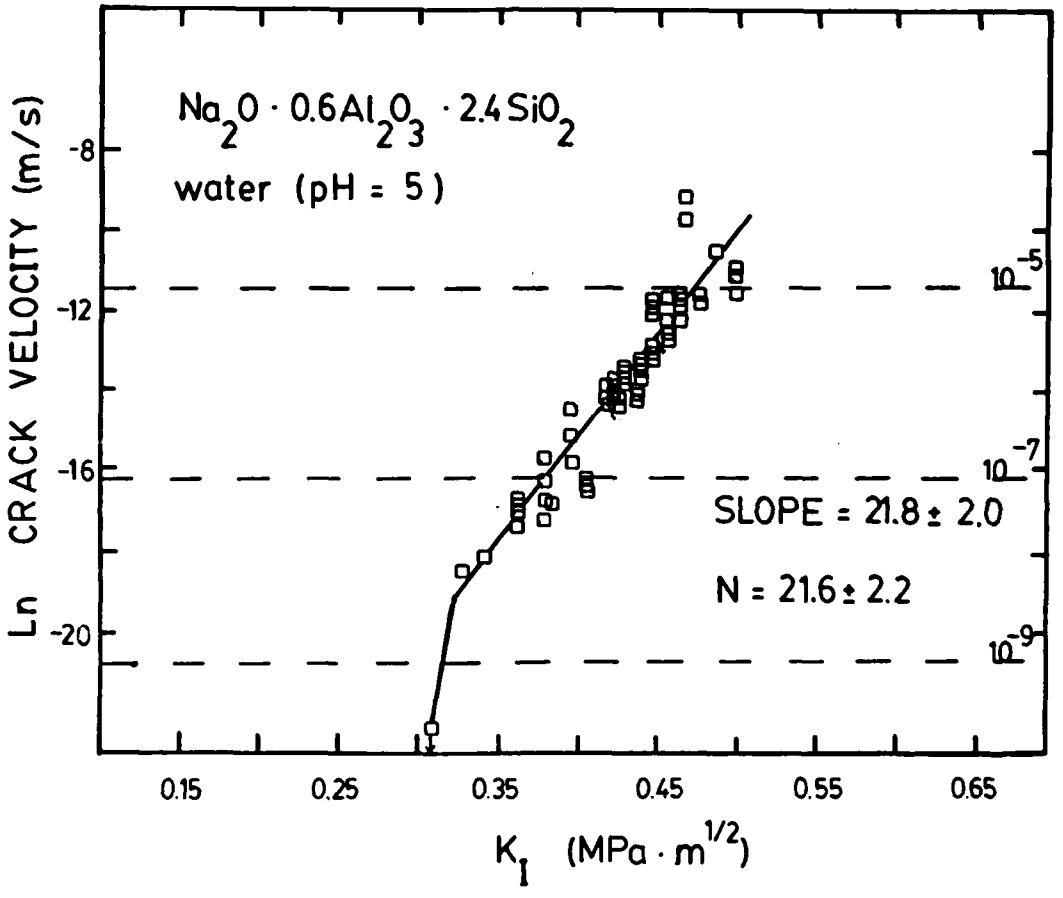

Figure 1d. Stress intensity-crack velocity data for 0.4 glass in water.

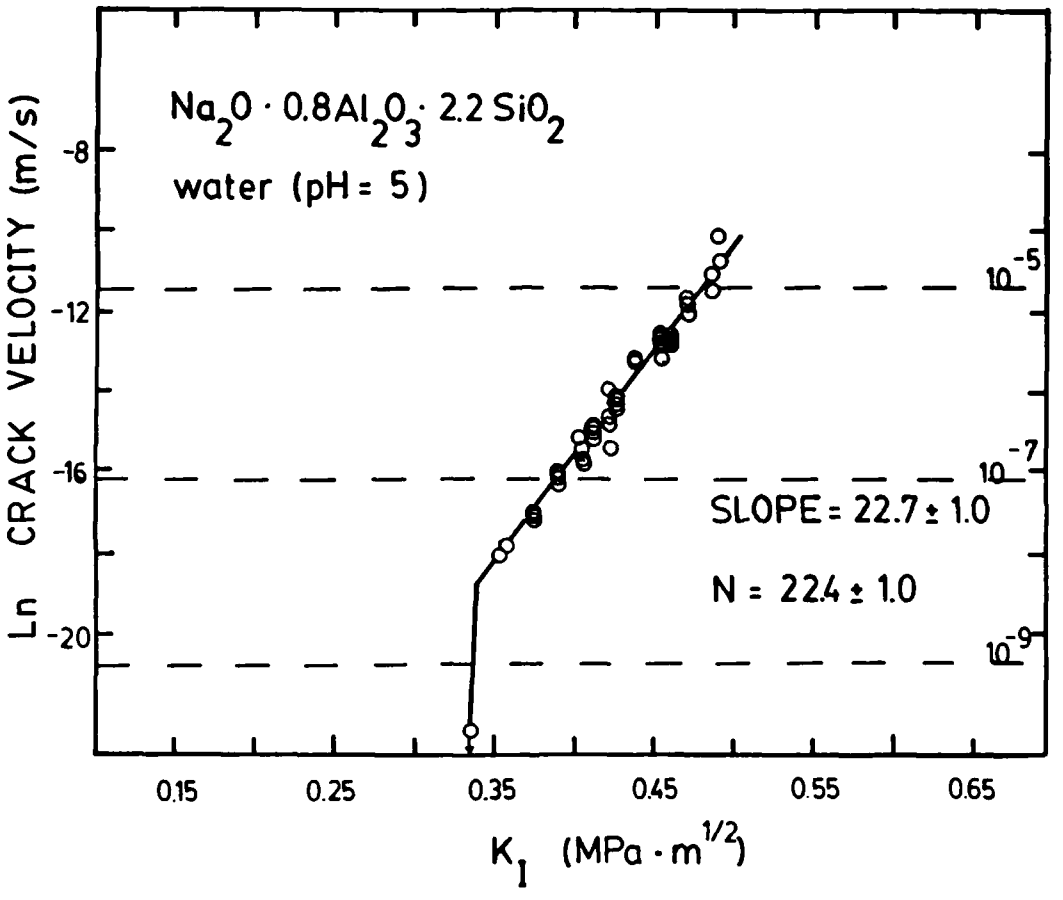

Figure 1e. Stress intensity-crack velocity data for 0.8 glass in water.

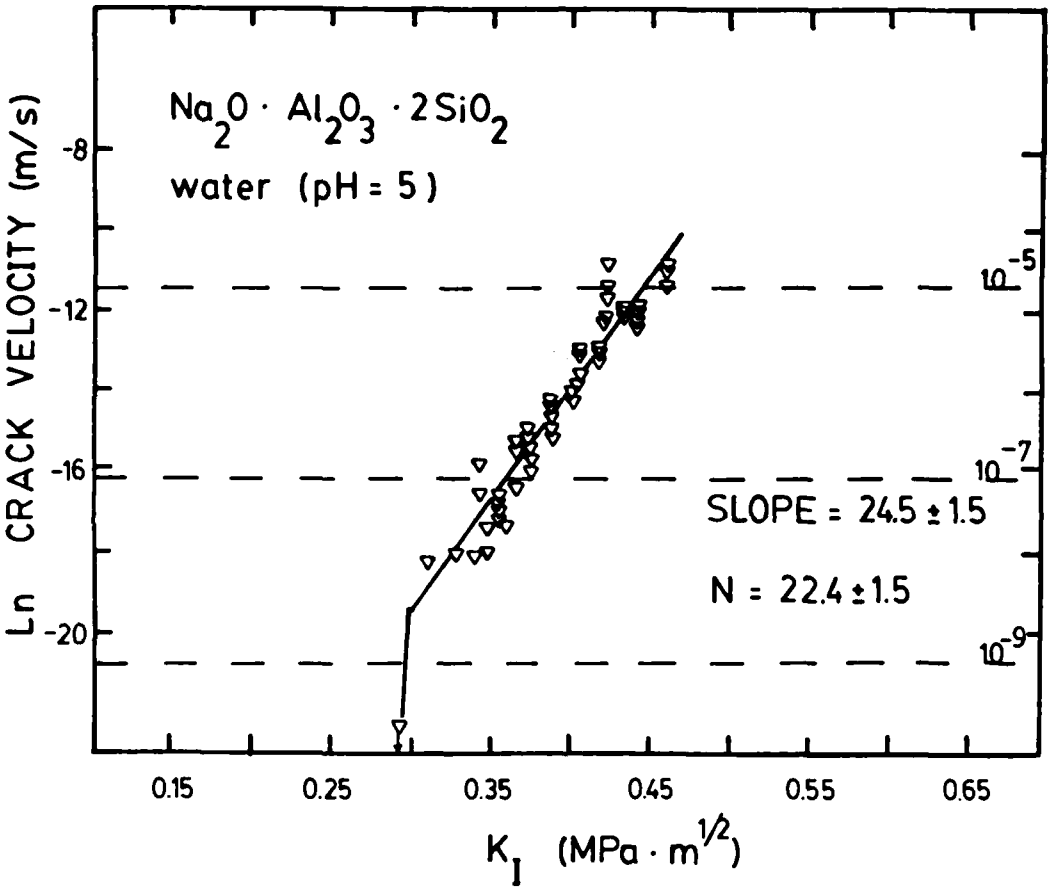

Figure 1f. Stress intensity-crack velocity data for 1.0 glass in water.

$$\text{Log } V = [(\text{Log } V_o) - E_1^*/RT] + [b/RT]K_I \qquad (5)$$

The n-parameters of the linearized power law relationship:

$$\text{Log } V = \text{Log } V_o + [n] \text{ Log } K_I \qquad (6)$$

are also given in the plots. In each case, the data were fit to a two parameter regression model (11). For convenience, the slopes and n-values have been listed in Table I.

All compositions exhibited a linear trend between the log of the crack velocity and the applied stress intensity in the range K_I = .25-.55 MPa·$m^{1/2}$; the corresponding crack velocities were in the range 10^{-9} to 10^{-4} m/s. The 0.0 glass exhibited a plateau in the range K_I = 0.2-0.25 MPa·$m^{1/2}$ at a velocity of 10^{-9} m/s. This type of behavior has been reported to occur in this composition by others (9). All of the glasses exhibited thresholds at low K_I (commonly termed the stress corrosion limit or static fatigue limit). An interpretation of these thresholds on the basis of crack healing has been reported (12).

Crack Velocity Data in 10^{-3} M NaOH

Figures 2a, 2b, 2c, 2d, 2e and 2f show the stress intensity-crack velocity data sets obtained in a 10^{-3} M NaOH aqueous solution (pH 11) for 0.0, 0.2, 0.4, 0.6, 0.8, and 1.0 glasses, respectively. The slopes and n-parameters for each composition are also given.

None of the glasses showed any significant change in slope or n-parameter at this higher pH. However, the velocity plateau in the 0.0 glass occured at a higher velocity (10^{-8} m/s) and extended up to a stress intensity of 0.38 MPa·$m^{1/2}$.

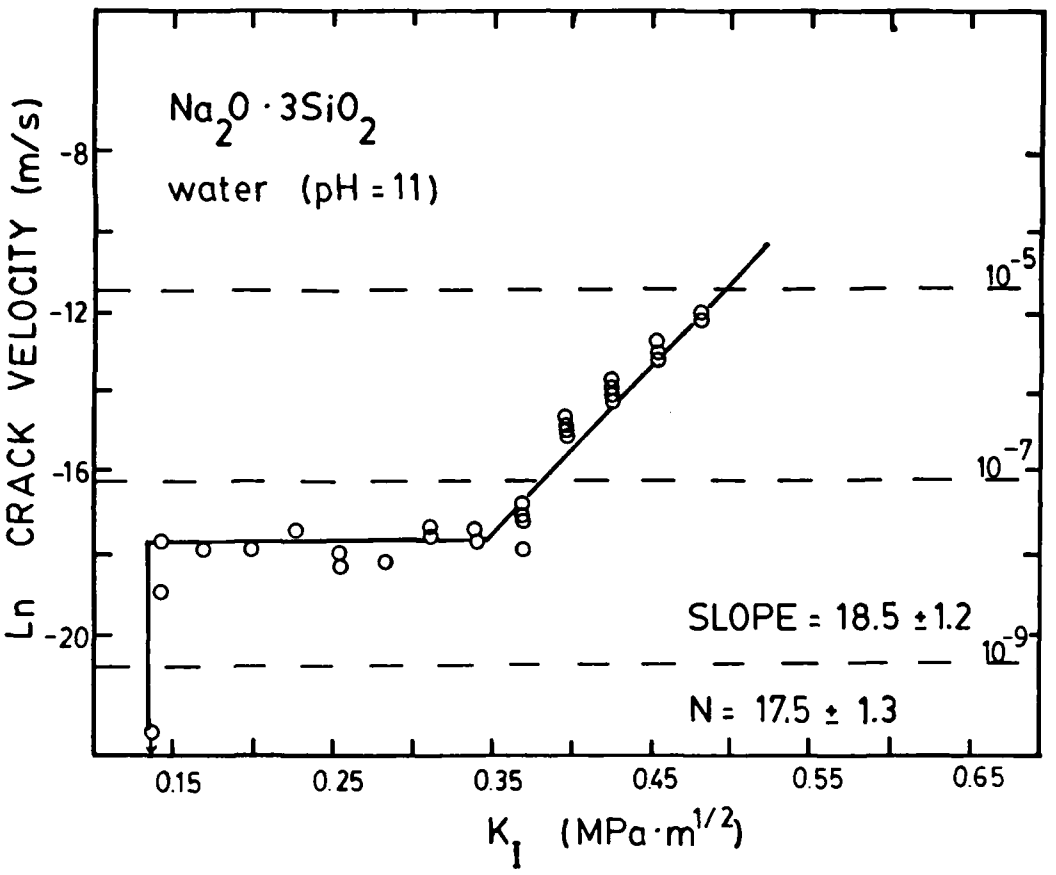

Figure 2a. Stress intensity-crack velocity data for 0.0 glass in NaOH solution.

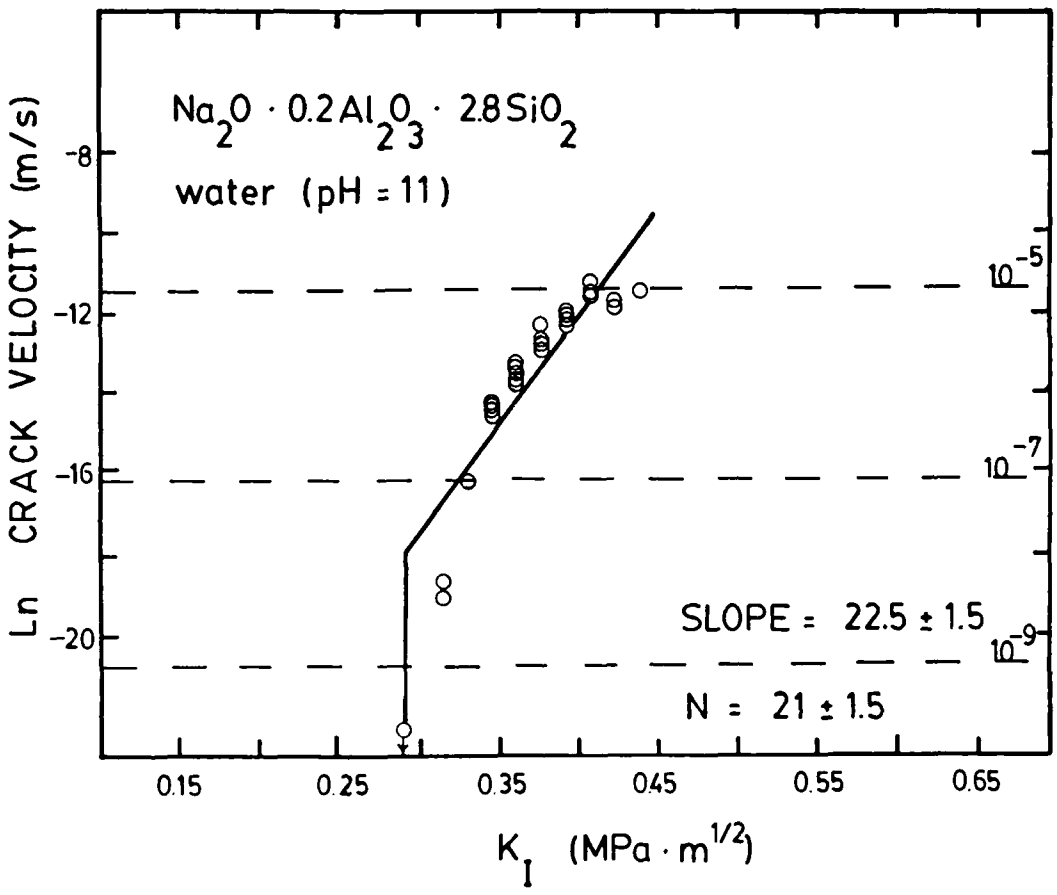

Figure 2b. Stress intensity-crack velocity data for 0.2 glass in NaOH solution.

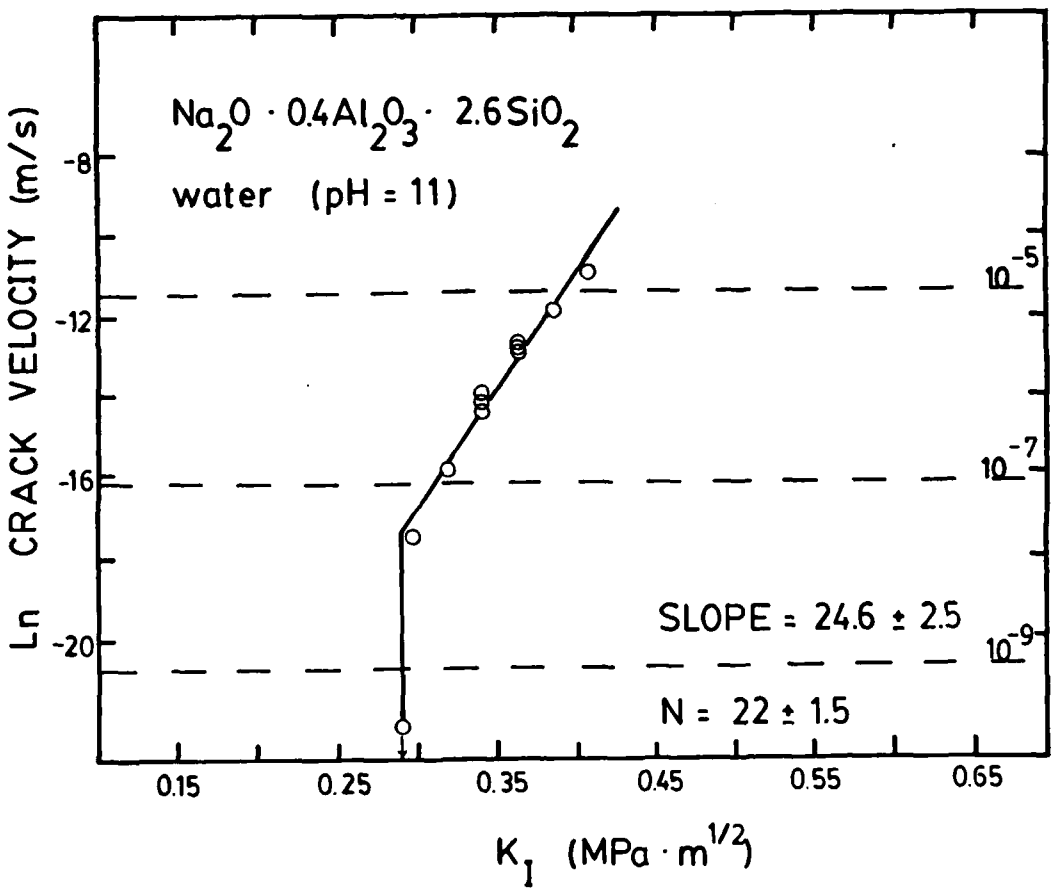

Figure 2c. Stress intensity-crack velocity data for 0.4 glass in NaOH solution.

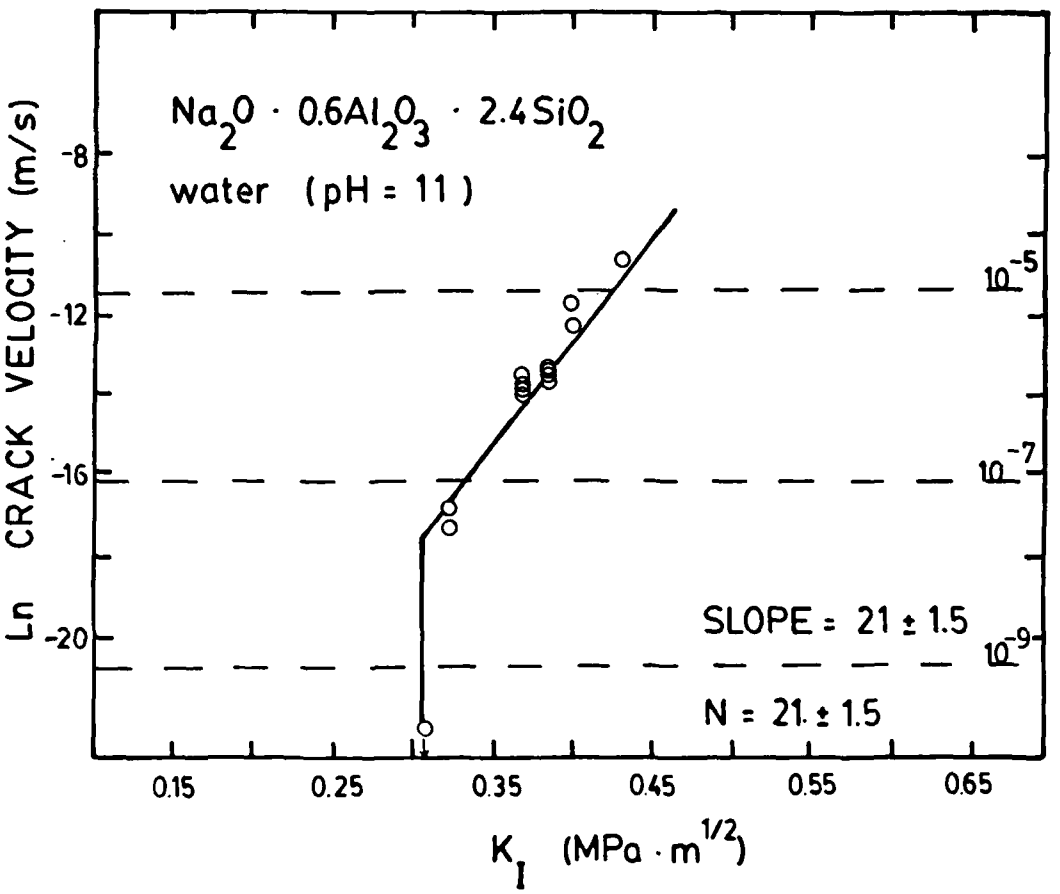

Figure 2d. Stress intensity-crack velocity data for 0.6 glass in NaOH solution.

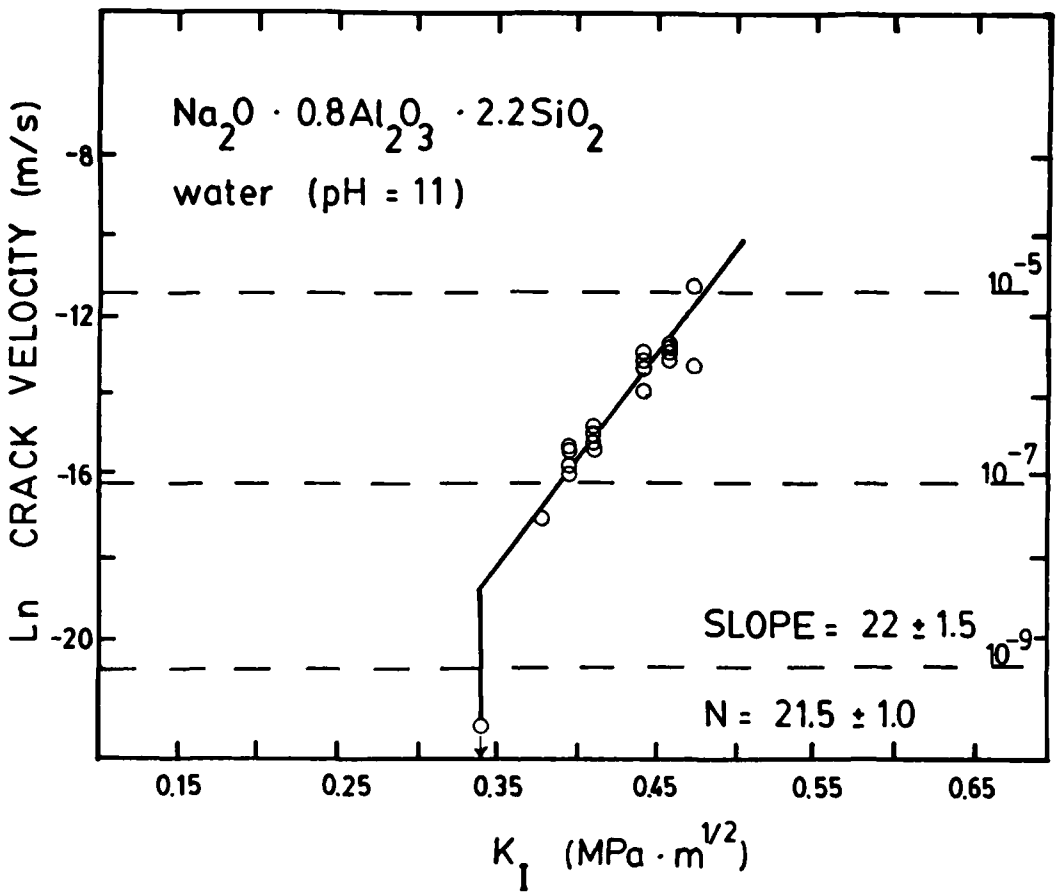

Figure 2e. Stress intensity-crack velocity data for 0.8 glass in NaOH solution.

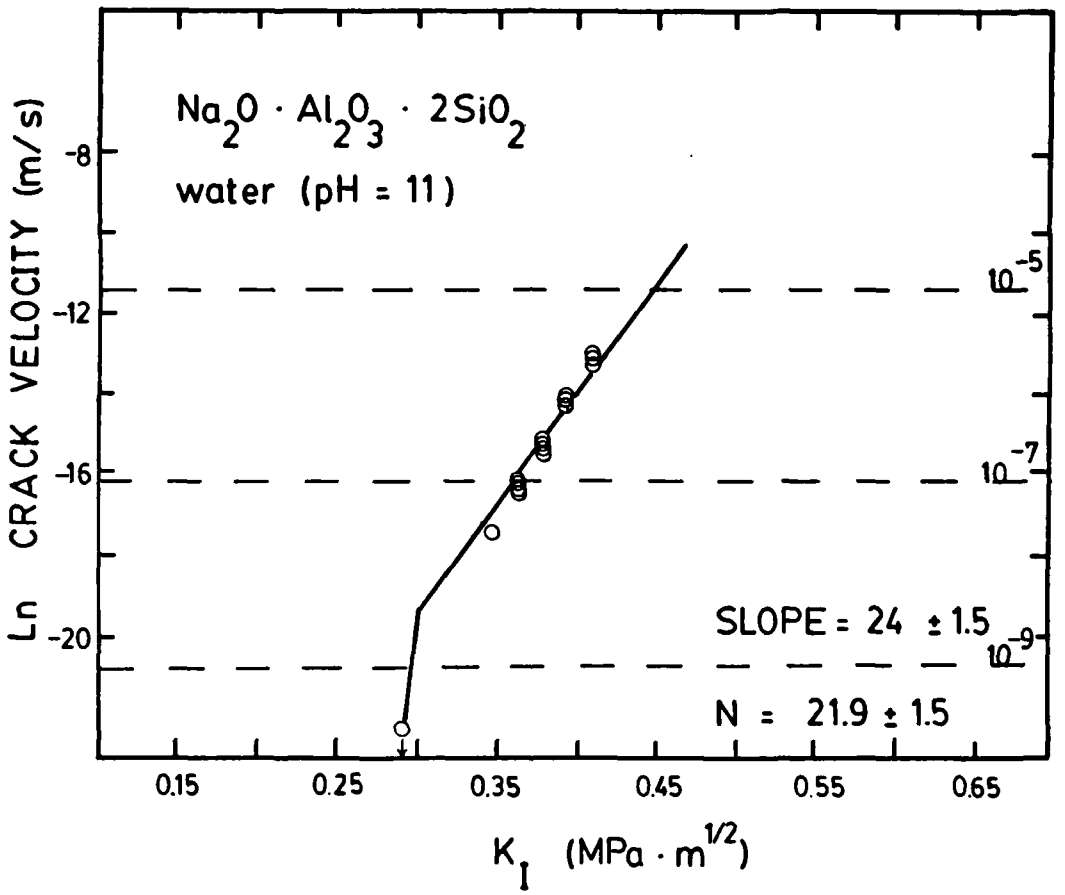

Figure 2f. Stress intensity-crack velocity data for 1.0 glass in NaOH solution.

DISCUSSION

Figure 3 plots n-parameters of the cumulative data sets versus the composition of the specimens expressed as the Al/Na ratios. The n-parameters range from 16 to 23 which is typical of silica-based glasses (6). The n-parameter increased with Al_2O_3 concentration up to an Al/Na molar ratio of 0.6. The n-parameter was invariant for compositions with Al/Na molar ratios in excess of 0.6.

The two characteristics which are expected to play a major role in determining the slow crack growth behavior are the glass structure and the chemical corrosion. First, the corrosion behavior of these glasses will be addressed, and then the structural characteristics will be considered. Finally, a relationship will be established between the elastic properties and the slow crack growth parameter. It will be shown that the glass structure is the determining factor in the slow crack growth behavior whereas corrosion effects are important only at very low K_I.

Corrosion Effects

It is now well accepted that the attack of alkali-silicate glasses in aqueous solution is due to two pH-dependent mechanisms (13,14). In solutions of pH less than 9.8, ion exchange and hydration of the glass surface are the dominant effects whereas in solutions of pH >7, dissolution of the glass occurs. The corrosion behavior of alkali-silicate glass can be explained over a wide range of conditions by a combination of these two mechanisms.

In acidic and neutral pH solutions, the primary corrosion mechanism is one of ion exchange between sodium ions in the glass and hydrogen or hydronium ions in the solution. Such an exchange can be represented by the following reaction:

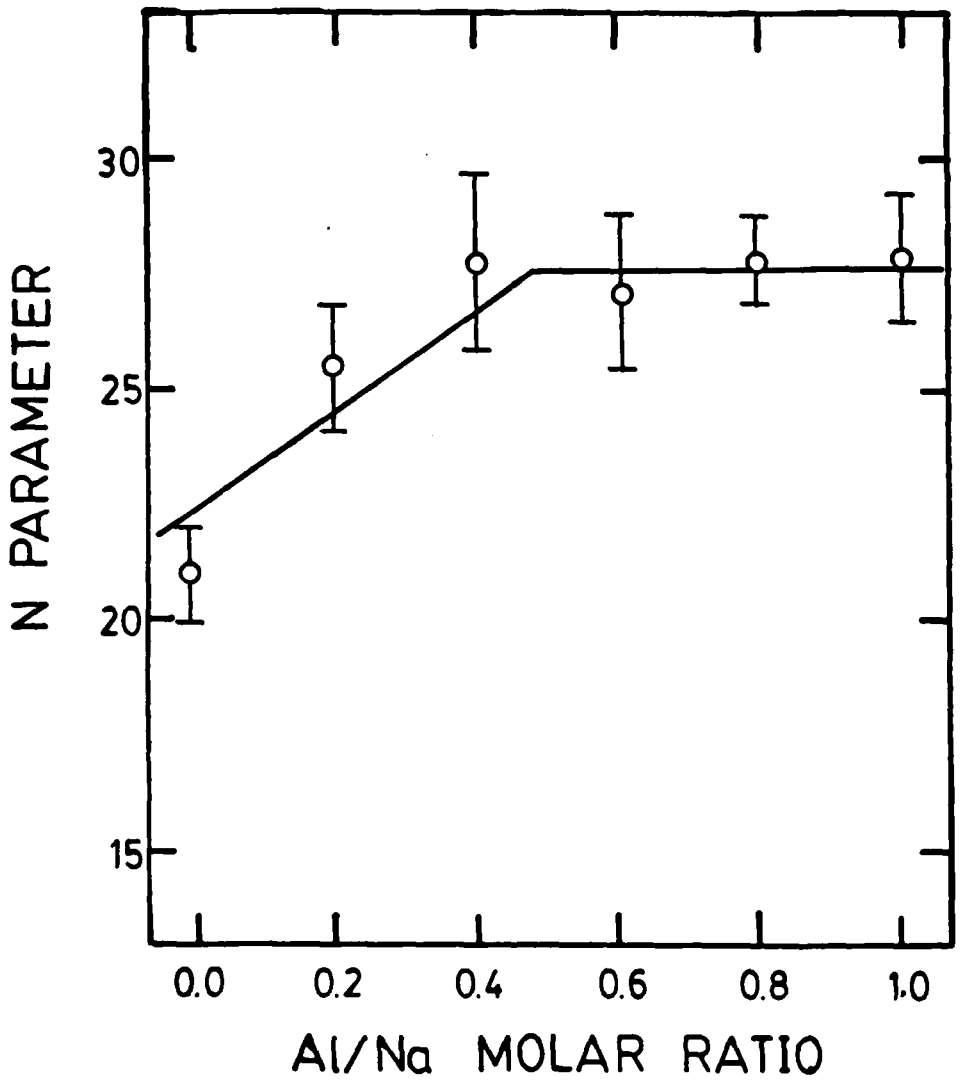

Figure 3. n-parameter as a function of composition in the glass system $Na_2O \cdot xAl_2O_3 \cdot (3-x)SiO_2$.

$$\equiv SiONa_{glass} + H^+ \cdot (H_2O)_{solution} \rightarrow \equiv SiOH_{glass} + Na^+ \cdot (H_2O)_{solution} \quad (7)$$

Although the exchange process does not directly affect the silicate network, the concentration of hydrogen ions in solution is lowered and the glass surface is depleted of sodium ions. Under dynamic conditions, the contacting solution can be replenished such that a 'pure water' solution is present at the surface at all times. In this case, the exchange would occur continually and be limited only by the interdiffusion of hydrogen species and sodium ions in the glass surface. Conversely, under static conditions the attacking solution is not replenished and the pH of the contacting solution increases to an equilibrium value which is in excess of the original pH. The magnitude of this equilibrium pH is determined by the composition of the glass and the glass surface area to solution volume ratio.

In high pH solutions, and to some extent in all aqueous solutions, hydroxyl ions attack siloxane bonds and dissolution of the silicate network occurs; e.g.

$$(\equiv Si - O - Si\equiv)_{glass} + (OH^-)_{solution} \rightleftarrows (\equiv Si-O^-)_{glass} + (HO - Si\equiv)_{solution} \quad (8)$$

The silicate solution species whose solubility controls this dissolution reaction is monosilicic acid (H_4SiO_4). Thus, the pH dependence of the dissolution reaction can be represented in terms of the equilibrium constant for its ionization; i.e.

$$H_4SiO_4 \rightleftarrows H_3SiO_4^- + H^+ \quad (9)$$

The equilibrium constant for this reaction is $10^{-9.8}$, and so:

$$\frac{[H_3SiO_4^-]\ [H^+]}{[H_4SiO_4]} = 10^{-9.8} \qquad (10)$$

The expression can be rewritten to yield:

$$10^{-9.8} + pH = \frac{[H_3SiO_4^-]}{[H_4SiO_4]} \qquad (11)$$

The concentration of monosilicic acid in solution decreases due to ionization, and in order to maintain equilibrium, more silicate network is dissolved. Since the ionization becomes substantial at pH >9.8 (see equation 11), so too does dissolution of the silicate network.

Qualitatively, the corrosion mechanism in the sodium-aluminosilicate glasses will follow the general description presented above for the simple alkali silicate glasses. However, the presence of the aluminate species influences the pH dependence of the dissolution; i.e. at low pH, the soluble aluminum ion (Al^{3+}) can form. This enhances the solubility and dissolution of aluminosilicate glasses in acidic solutions. Otherwise, the behavior in water and basic solutions are comparable.

Figures 4 and 5 present the equilibrum pH values and dissolution rate constants for the sodium-aluminosilicate glasses in water. It is quite clear that the reactivity of these glasses - in water - decreases with increasing Al/Na ratio. The equilibrium hydrogen ion activity varies by 4-5 orders of magnitude through the compositional series, while the sodium leach rate and silica dissolution rate varies by 3 orders of magnitude. All these aluminosilicate glasses had an identical concentration of soda; namely, 25 mole percent. Nevertheless, they exhibited wide variations in corrosion resistance

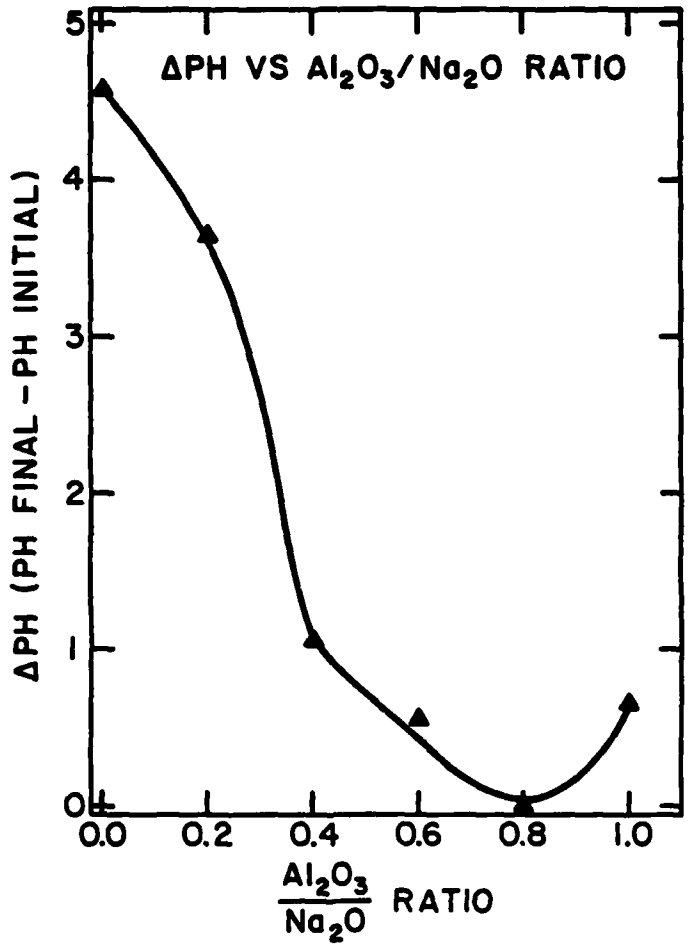

Figure 4. The equilibrium of pH of $Na_2O \cdot xAl_2O_3 \cdot (3-x)SiO_2$ glasses in contact with water at 30°C; bulk glass specimens where the surface area of glass-to-solution volume ratio was 10^{-1} cm^{-1}.

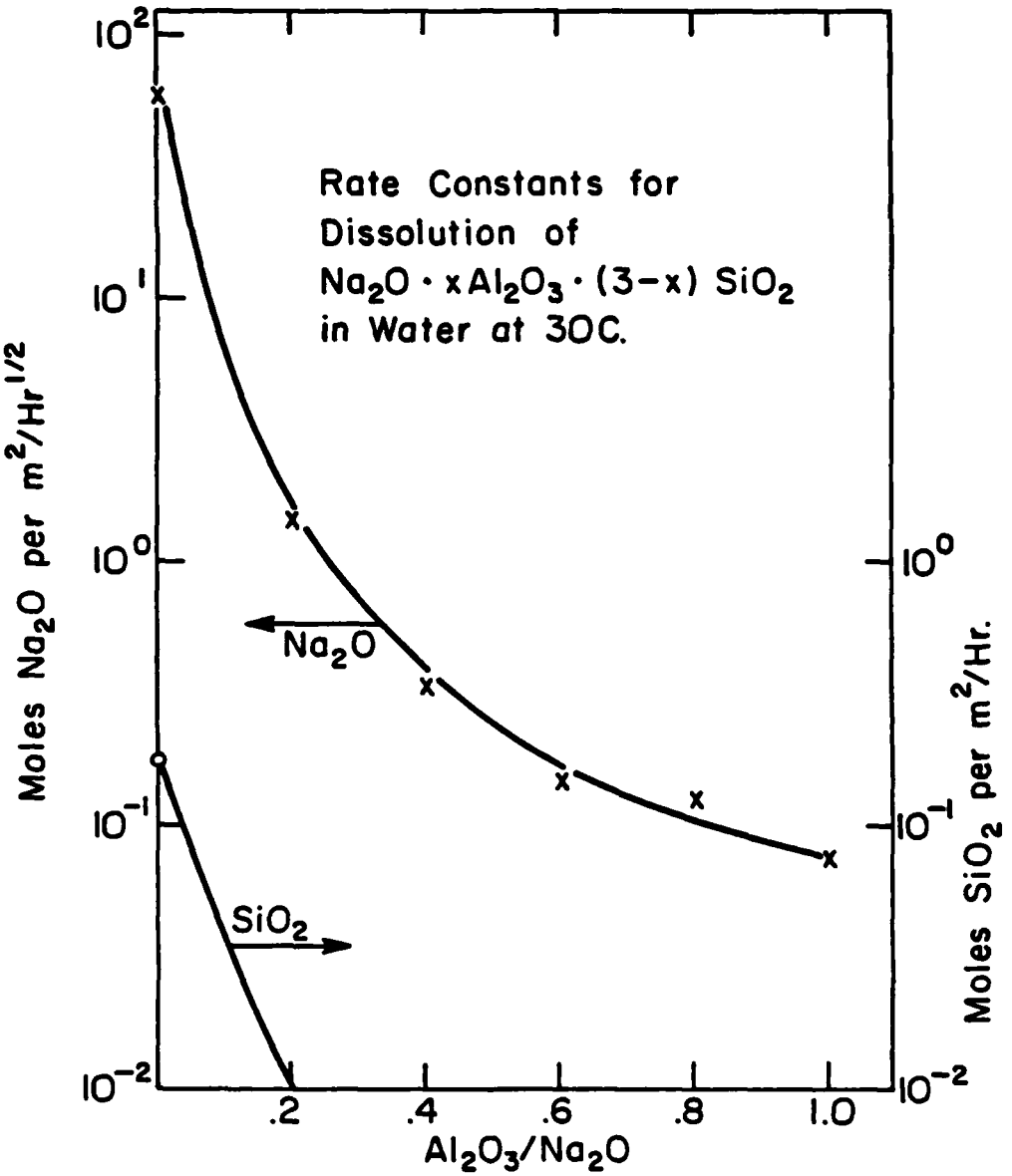

Figure 5. The rate constants for parabolic leaching of Na_2O and linear dissolution of SiO_2 from $Na_2O \cdot xAl_2O_3 \cdot (3-x)SiO_2$ glasses in water at 30°C.

and crack-growth susceptibility. Thus, concepts and theories which might attribute these properties to the concentration of sodium ions, per se, cannot be altogether correct. In the context of this study, though, the question is: can this wide variation in chemical corrosion properties be used to rationalize the crack-growth behavior?

At first glance, one notes the inverse correlation between the n-parameters (Fig. 3) and the chemical reactivity (Figures 4 and 5); i.e. the n-parameter increases - at least qualitatively - as the extent of pH change and glass dissolution decreases. A similar correlation was reported by Tummala (7), and Wiederhorn (15) attributed this to changes in crack-tip pH. That is, glasses with higher alkali leach rates would lead to a significant difference in pH between the localized crack-tip region and the bulk solution. This is a plausable suggestion which is clearly consistent with the data reported here. The 0.0 and 0.2 glasses exhibit higher equilibrium pH values, and thus, one would expect the solution near the crack-tip in these glasses to be alkaline relative to the bulk solution. And correspondingly, these two glasses exhibit the lowest n-values. Nevertheless, this apparent correlation is not consistent with the behavior of high Al/Na ratio glasses. The n-parameter for these glasses were found to be the same at pH 5 and pH 11. Yet, these glasses dissolve readily at pH 11. Similarly, the 0.0 and 0.2 glasses - whose crack tip pH values are expected to be controlled by the high leach rate rather than the bulk solution - showed differences in the low K_I region between pH 5 and pH 11. Altogether, these observations indicate that ion-exchange, leaching and dissolution are not the primary factors which control slow crack growth. These observations were made in a family of glasses whose compositions were systematicaly varied, and thus, the lack of complete consistency with the chemical corrosion model lends further validity to this conclusion.

Structure Effects

It is widely accepted that as Al_2O_3 is added to soda-silica glass, the non-bridging oxygen concentration decreases. There is some controversy concerning the range of Al/Na ratios over which this structural modification occurs, but one of these studies revealed a complete elimination of the non-bridging oxygens at an Al/Na ratio of .6-.7 (16).

Figure 6 shows the variation of Young's elastic modulus measured as a function of composition for the sodium-aluminosilicate glass series. Notice that the moduli increases in a linear manner with increased Al_2O_3 concentration for glasses with an Al/Na ratio less than about 0.5. The moduli remained constant for the glasses with an Al/Na ratio of 0.6 or greater. It is reasonable to expect that Young's elastic modulus will reflect structural trends within a compositional family of glasses. Since the network polymerizes as the concentration of non-bridging oxygen decreases, this cross-linking should render the glass more resistant to strain for a given amount of stress. Thus, the observed increase in Young's modulus with Al/Na is consistent with a corresponding decrease in non-bridging oxygen concentration. In this sense, the elastic moduli represent an indirect measure of the molecular structure of the glass network.

It is evident that the n-parameter (Figure 3) and Young's elastic modulus (Figure 6) exhibit a very similar dependence upon the Al_2O_3 concentration. This suggests that the slow crack growth behavior and elastic response of a material are closely related. Figure 7 plots the n-parameters as a function of Young's elastic modulus for this set of glasses, as well as, for soda-lime-silica and fused silica glass. Clearly, the n-parameter increases uniformly with Young's modulus.

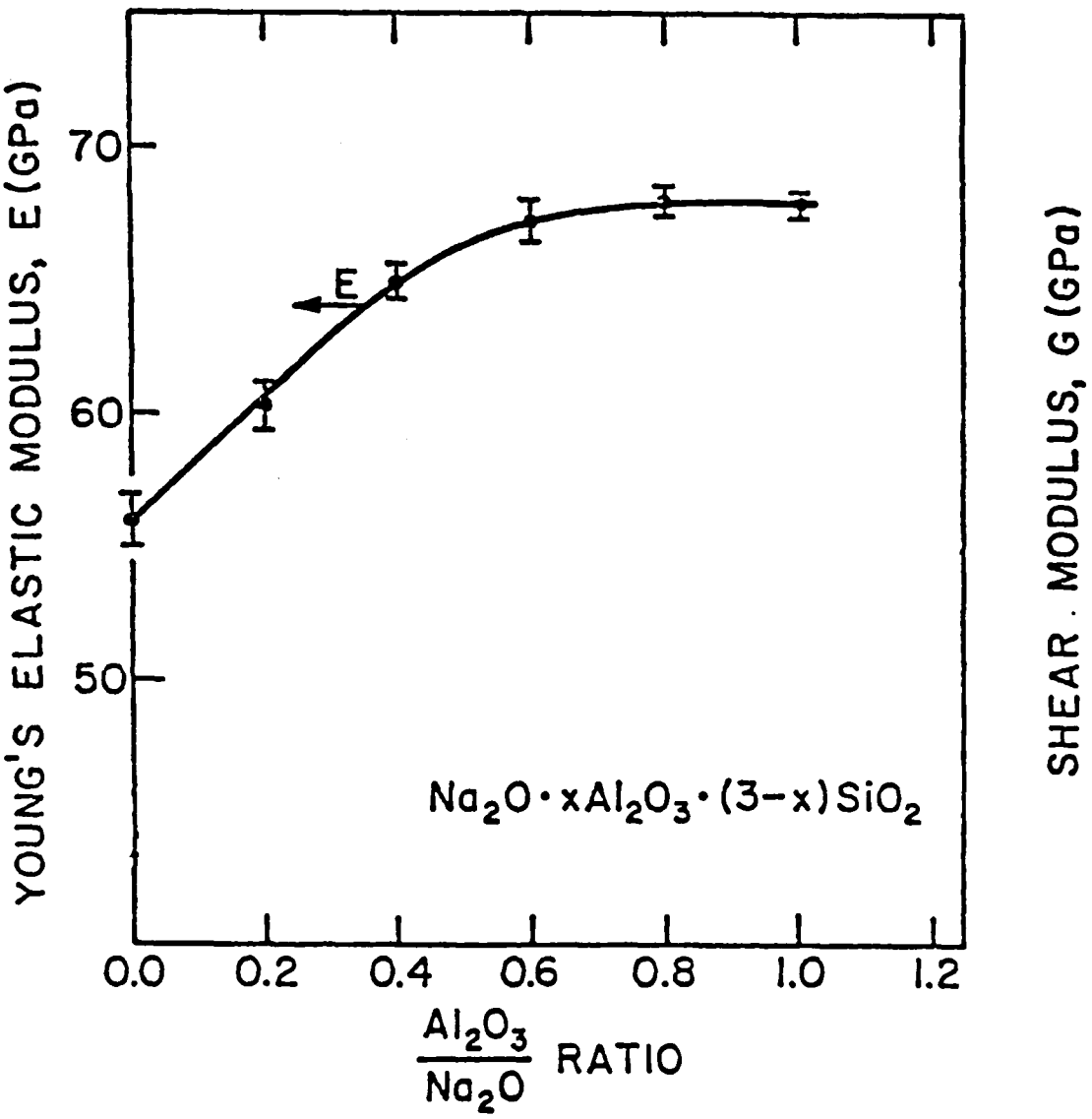

Figure 6. The variation of Young's elastic modulus with composition in $Na_2O \cdot xAl_2O_3 \cdot (3-x)SiO_2$ glasses.

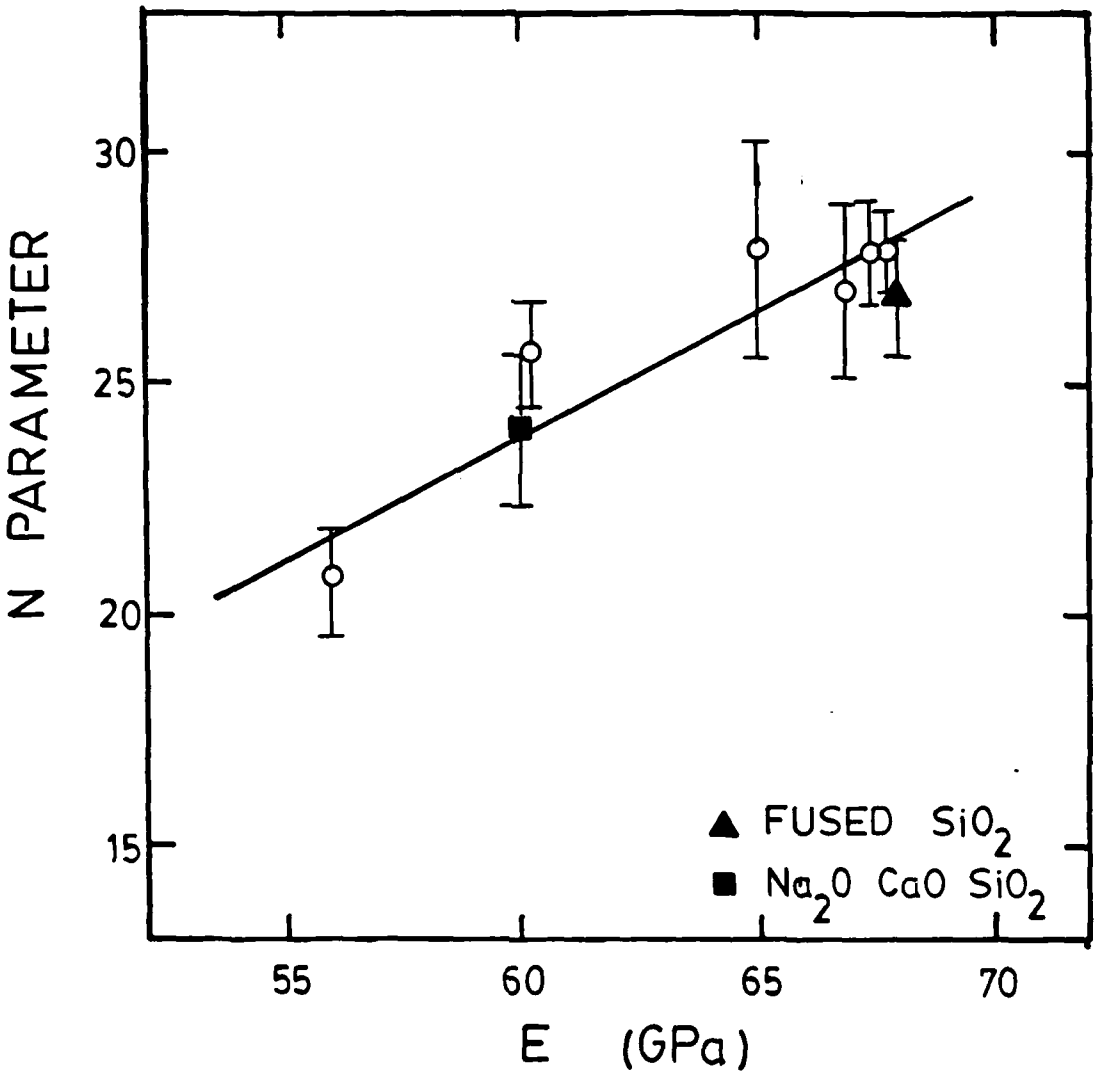

Figure 7. The relationship between the n-parameter and Young's elastic modulus in $Na_2O \cdot xAl_2O_3 \cdot (3-x)SiO_2$ glasses, as well as, in fused silica and soda-lime-silica.

Elastic Strain and Slow-Crack Growth Susceptability

Although the underlying mechanism of slow crack growth is a chemical reaction between environmental species and crack tip bonds, the correlations developed in the previous sections of this paper suggest that the rate of that chemical reaction is controlled through the elastic strain. In this section, the expected effect of strain upon the rate of chemical reaction is discussed, and the elastic properties are used to define the extent to which that rate can be altered under the action of an applied stress. In this manner, a relationship will be developed between the observed slow crack growth behavior and the stress-strain behavior.

The rate limiting chemical reaction in slow crack-growth is expected to occur between the aqueous environment and the highest strength bonds in the glass structure. Of course, this assumes the material to be homogeneous and isotropic with no easy fracture path. Sodium ions are bound to either a non-bridging oxygen or an $(AlO_4)^-$ aluminate tetrahedral unit. These bonds - especially those at the aluminate sites - are of relatively low strength. In contrast, the Al^{3+} and Si^{4+} ions are strongly bonded to oxygen to form the network or structural backbone of the glass. A simple estimate of the bond strength can be obtained from the charge/coordination ratio. Silicon ions exist only in fourfold coordination whereas aluminum ions may exist in either four-or sixfold coordination depending upon the composition. The bond strength can be estimated as:

silicon (CN=4) $4/4 = 1$ (12)

aluminum (CN=4) $3/4 = 0.75$ (13)

aluminum (CN=6) $3/6 = 0.50$ (14)

where CN = the coordination number. Therefore, it would be predicted that the rate limiting reaction would be between water and the silicon-oxygen bonds.

In silicate-based glasses, then, the crack-growth reaction of primary interest is:

$$(\equiv Si\text{-}O\text{-}Si\equiv) + H_2O \xrightarrow{E_{tot}} 2(\equiv Si\text{-}OH) \qquad (15)$$

where E_{tot} = activation energy. It is possible to express reaction 15 by the following series of sequential reactions:

$$\equiv Si\text{-}O\text{-}Si \equiv \xrightarrow{E_1} \equiv Si - O^- + Si^+, \qquad (16)$$

$$H_2O \xrightarrow{E_2} H^+ + OH^-, \qquad (17)$$

$$\equiv Si\text{-}O^- + H^+ \xrightarrow{E_3} \equiv Si\text{-}OH, \text{ and} \qquad (18)$$

$$\equiv Si^+ + OH^- \xrightarrow{E_4} \equiv Si\text{-}OH \qquad (19)$$

The energy necessary to break a silicon-oxygen bond is given by E_1, the dissociation energy of a water molecule is given by E_2, and the energy gains due to satiation of the dangling surface charges by the dissociated environment are given by E_3 and E_4. Since reaction 15 is equivalent to the sum of reactions 16 through 19, the activation energy, E_{tot}, can be represented by an analogous sum:

$$E_{tot} = E_1 + E_2 + E_3 + E_4 \qquad (20)$$

The reaction rate can be approximated by:

$$\exp[-E_{tot}/RT] \tag{21}$$

and then, substituting Equation 20 into Equation 21 yields:

$$\text{rate} \propto \exp\left[-(E_1 + E_2 + E_3 + E_4)/RT\right] \tag{22}$$

Assuming the velocity of crack extension to be limited by the rate at which the reaction can proceed, the crack velocity can be approximated by:

$$V = V_o \exp\left[-(E_1 + E_2 + E_3 + E_4)/RT\right] \tag{23}$$

The energy input to the crack tip system lowers the required activation energy. This energy may be input in the form of mechanical energy, thermal energy, etc. In the slow crack growth phenomenon, the effect of mechanical energy on the system is of most concern. Since the presence of H^+ and OH^- species can be expected to varying degrees under all conditions,the application of external stress is of little consequence in affecting the ability of the environment to dissociate or satiate the surface charges. Rather, it is the effect of an external stress on the energy necessary to break a silicon-oxygen bond, E_1, which is of primary interest. This concept is unique relative to recent suggestions (17), but is more consistent with all of the experimental observations. That is, in isostructural network glasses (e.g., SiO_2 and $Na_2O \cdot Al_2O_3 \cdot 2SiO_2$), as well as glasses with widely varying corrosion

susceptibilities (e.g., $Na_2O \cdot xAl_2O_3 \cdot (3-x)SiO_2$), the stress corrosion susceptibility is relatively insensitive to the H^+ or OH^- activity (except in the low K_I threshold/plateau regions).

Initially, consider an isolated silicon-oxygen bond where the strain is simply a change in the bond length, r, relative to the equilibrium position, r_o. The strain, ε, in this bond can be defined as:

$$\varepsilon = [r - r_o]/r_o = \Delta r/r_o \tag{24}$$

If the strain is tensile, Δr is greater than 0, and the bond length will increase.

The silicon-oxygen bond is predominantely ionic in nature, and so, the energy of the lone ion pair is given by the sum of the coulombic attractions, and the repulsion and ionization energies (18):

$$[(Z_1 Z_2 e^2)/(4\pi\varepsilon_o r)] + [B/r^n] + E_{ion} \tag{25}$$

where: Z_i = charge on ion i

e = electronic charge

ε_o = permittivity

r = ion-ion separation distance

B, n = constants

E_{ion} = ionization energy

This relationship is shown graphically in Figure 8. The equilibrium separation, r_o, is determined by the minimum in the energy function.

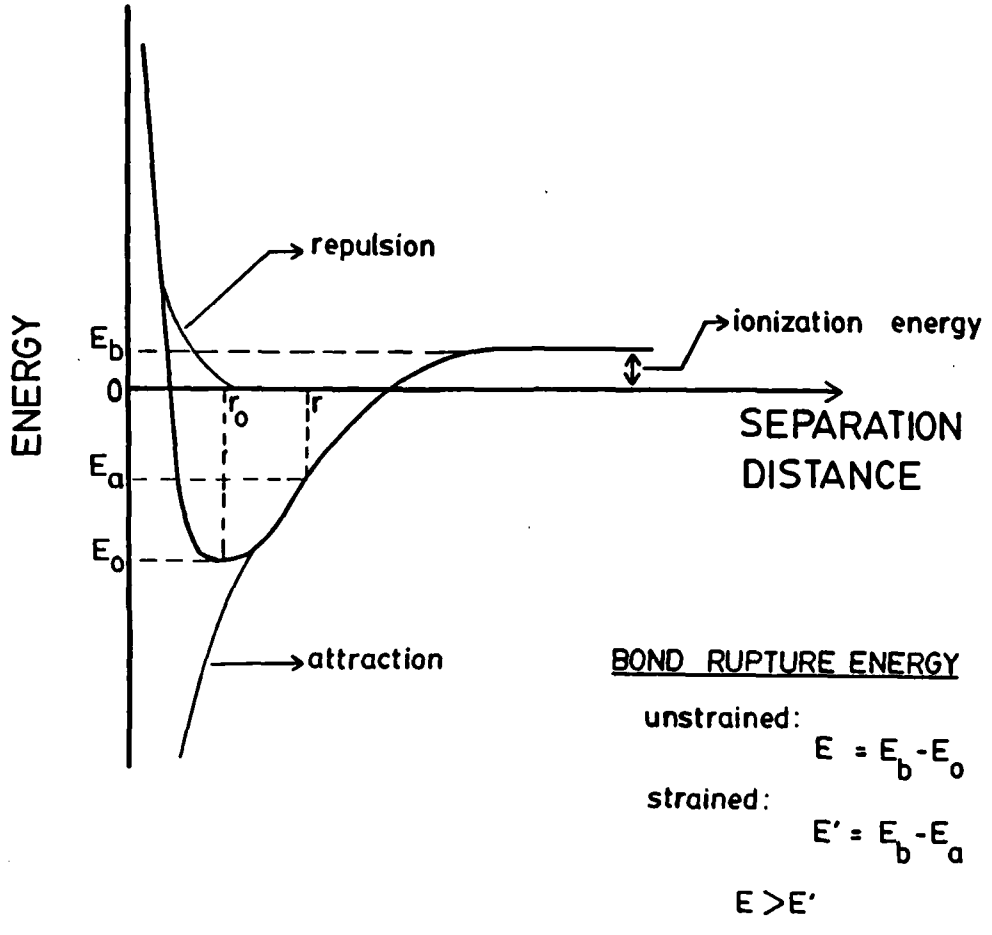

Figure 8. Energy-bond length relationship for an isolated ionic bond.

The energy to rupture a silicon-oxygen bond can be defined as:

$$E_l = E_b - E_o \tag{26}$$

(E_b and E_o are defined in Figure 8) whereas the energy required to rupture a strained bond can be defined by:

$$E_l' = E_b - E_a \tag{27}$$

After substituting Equation 26 into Equation 27:

$$E_l' = (E_l + E_o) - E_a \tag{28}$$

or,

$$E_l' = E_l - \Delta E_\sigma \tag{29}$$

where: ΔE_σ = change in rupture energy under the action of an applied stress. When the bond is strained from r_o to r, the repulsion term - which is proportional to r^{-n} - drops quickly to zero with respect to the attraction term. Therefore, this term can be ignored without imparting a significant error in the analysis. The change in energy, ΔE_σ, can now be defined as:

$$\Delta E_\sigma = [E_b - (k/r_o)] - [E_b - (kr)] \tag{30}$$

or,

$$\Delta E_\sigma = [k/r_o] - [k/r] \tag{31}$$

where: $k = [Z_1 Z_2 e^2]/[4\pi\varepsilon_o]$. Equation 31 can be rewritten as:

$$\Delta E_\sigma = k[(r-r_o)/rr_o], \tag{32}$$

and then substituting Equation 24 into Equation 32 yields:

$$\Delta E_\sigma = k[\varepsilon/r] \tag{33}$$

Equation 33 shows quantitatively that as the strain (or stress) is increased, the change in bond rupture energy increases. The magnitude of the increase is determined directly by the amount of strain.

This exercise is a simplified manner of showing that it is necessary to do work on a bond in order to strain it and that the work is stored in the bond and used to reduce the effective bond rupture energy. Elasticity theory defines the amount of work done on the bond by:

$$Y = \int_o^\varepsilon \sigma d\varepsilon \tag{34}$$

where Y = stored elastic strain energy. Thus, the next step in the derivation is to define the stored elastic strain energy at the crack-tip in terms of the elastic constants.

For the isolated ion pair, the stress necessary to strain a bond from 0 to ε is uniquely defined by the properties of the bond, whereas the bond of interest in slow crack-growth is bound within an infinite glass network. The amount of stress necessary to strain that bond from 0 to ε is no longer uniquely defined by the bond, but is determined by the material surrounding the bond. In other words, the amount of stored elastic strain energy available is determined by the

elastic properties of the surrounding material and not the properties of the bond itself.

It is reasonable to assume that the stored elastic strain energy in the vicinity of the crack tip is available to reduce the effective bond rupture energy. The work necessary to produce a strain ε_i can be expressed as (19):

$$Y = (1/2)c_{ij}\,\varepsilon_i\,\varepsilon_j \tag{35}$$

where: c_{ij} = stiffness matrix. Considering only the unidimensional strain, ε_2, Equation 35 becomes:

$$Y = c_{11}\,(\varepsilon_2)^2 \tag{36}$$

The magnitude of the stored energy is determined by the strain and stiffness.

Qualitatively, the n-parameter should be related to the magnitude of the stored energy since glass can support only small strains. Thus, assuming that the strain in the crack tip region does not vary significantly from glass to glass, the difference in stored energy would be determined primarily by differences in the stiffness. Therefore, the n-parameter should vary as c_{11}.

The elastic moduli can be used to express either the stiffness (s_{ij}) or the compliance (c_{ij}). For an isotropic material (19):

$$s_{11} = 1/E \tag{37}$$

$$s_{12} = -\nu/E \tag{38}$$

$$c_{11} = [s_{11} + s_{12}]/[(s_{11} - s_{12})(s_{11} + 2s_{12})] \tag{39}$$

where: ν = Poisson's ratio. Using these relationships, it is possible to express c_{11} as:

$$c_{11} = S \cdot E \tag{40}$$

where: $S = [1 - \nu]/[(1 + \nu)(1-2\nu)]$

Since the n-parameter is expected to vary as c_{11}, and $c_{11} = S \cdot E$, then a relationship between n and $S \cdot E$ exists. Figure 9 shows the relationship between the n-parameter and the predicted function (Eq 40) of the elastic modulus ($S \cdot E$). Given the fact that the prediction is semi-quantitative, the agreement is very good. Thus, one could re-write the expression for the crack velocity as:

$$V = V_o(K_I)^{\eta SE} \tag{41}$$

where V_o and η are constants and S and E are material parameters. Notice that silica and soda-lime-silica data also fit the correlation in Figure 9. Therefore, η may be a universal constant for oxide glasses in which case the material parameters S and E can be used to predict the composition dependence of slow crack growth via Eq (41). The analysis developed does provide insight as to why the stress-strain behavior of a material is intimately related to its slow crack growth behavior. It leads naturally to the conclusion that the composition dependence of the stress corrosion susceptibility is due to composition dependence of the elastic properties and not the chemical corrosion properties.

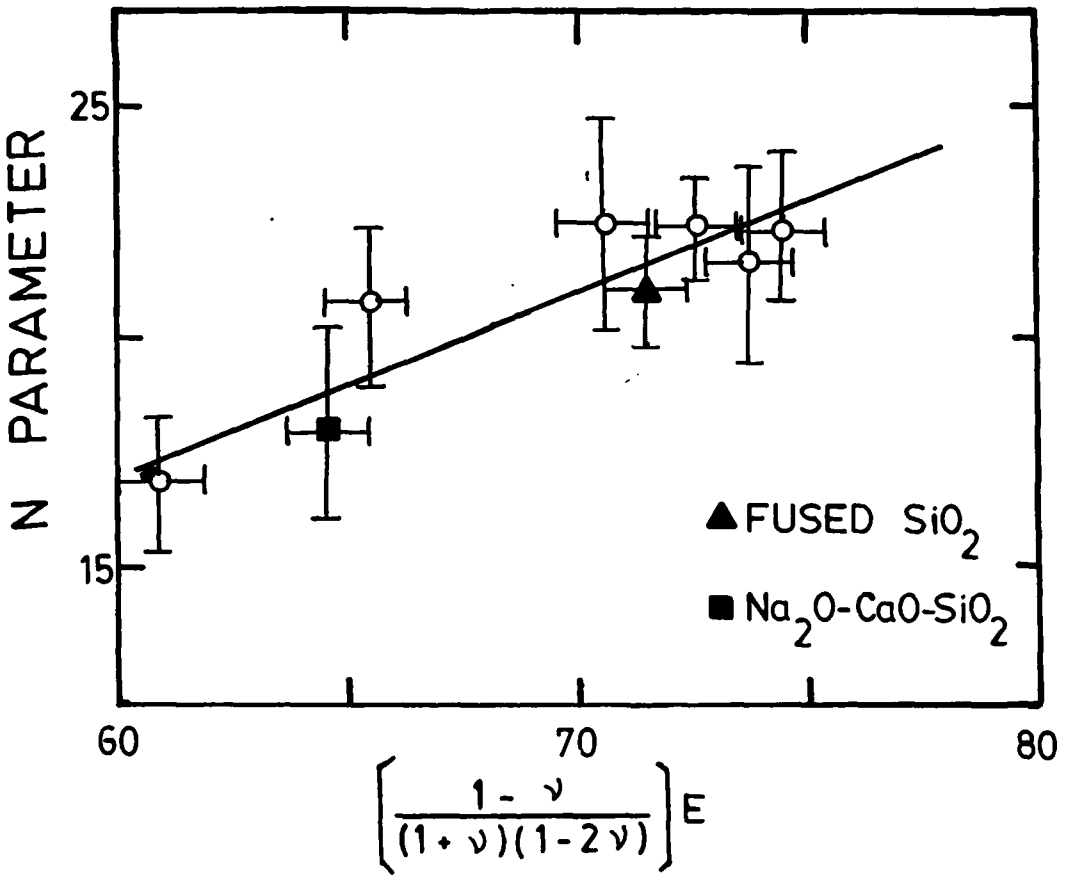

Figure 9. The relationship between n-parameter and the predicted function of the elastic moduli for $Na_2O \cdot xAl_2O_3 \cdot (3-x)SiO_2$ glasses, as well as, for fused silica and soda-lime-silica.

CONCLUSIONS

The region 1 slow crack growth behavior was characterized by the n-parameter which varied from 16 to 23 and varied linearly with alumina concentration for 0.0, 0.2, and 0.4 glasses. However, for 0.6, 0.8, and 1.0 glasses the n-parameter was independent of alumina concentration and equivalent to the n-parameter for the 0.4 glass. The invariance of the n-parameter with variations in the environmental pH suggest that corrosion plays only a minor role in determining the slow crack growth behavior. It was proposed that the elastic properties, and hence the glass structure, determines the n-parameter.

The fundamental mechanism of slow crack growth was assumed to be a chemical reaction between the glass and the aqueous environment in contact with it. It was proposed that the activation energy of such a reaction would be lowered by an amount equivalent to the strain energy stored in the crack tip vicinity. It was shown that the n-parameter is directly related to the magnitude of this stored strain energy which, in turn, is determined by the elastic properties. In this manner, the elastic properties were related directly to the slow crack growth behavior. A good correlation between the n-parameter and elastic properties was observed for sodium-aluminosilicate, soda-lime-silica, and fused silica glasses.

ACKNOWLEDGEMENT

The authors gratefully acknowledge the financial support of the Air Force Office of Scientific Research (AFOSR-82-0013).

Table I. The slope and n parameters determined by regression analysis of the stress intensity-crack velocity data sets.

Glass No.	slope	n
0.0	17.8 ± 1.3	16.9 ± 1.5
0.2	22.3 ± 2.0	20.7 ± 1.7
0.4	25.5 ± 3.0	22.5 ± 2.3
0.6	21.8 ± 2.0	21.6 ± 2.2
0.8	22.7 ± 1.0	22.4 ± 1.0
1.0	24.5 ± 1.5	22.4 ± 1.5

REFERENCES

1. R. E. Mould and R. D. Southwick, "Strength and Static Fatigue of Abraded Glass Under Ambient Conditions," J. Am. Ceram. Soc., 42 [12], 582 (1959).

2. S. M. Wiederhorn, "A Chemical Interpretation of Static Fatigue," J. Am. Ceram. Soci, 55 [2], 81 (1972).

3. W. B. Hillig and R. J. Charles, "Surfaces, Stress-Dependent Surface Reactions, and Strength," High Strength Materials, pp. 682-701, edited by W. F. Zackey, Wiley Publishing Co., New York, New York, 1965.

4. S. M. Wiederhorn and L. H. Bolz, "Stress Corrosion and Static Fatigue of Glass," J. Am. Ceram. Soc., 53 [10], 543 (1970).

5. S. M. Wiederhorn, "Crack Growth as an Interpretation of Static Fatigue," Journal of Non-Crystalline Solids, 19, 169 (1975).

6. S. W. Freiman, "Fracture Mechanics of Glass," Glass Science and Technology: Elasticity and Strength in Glasses, Vol. 15, pp. 21-78, Edited by D. R. Uhlman and N. J. Kreidl, Academic Press, New York, New York, 1980.

7. R. R. Tummala, "Stress Corrosion Resistance Compared with Thermal Expansion and Chemical Durability of Glasses," Glass Technology, 17 [4], 145 (1976).

8. H. M. Cekirge, W. R. Tyson and A. S. Krausz, "Static Corrosion and Static Fatigue of Glass," J. Am. Ceram. Soc., 59 [5-6], 265 (1976).

9. C. J. Simmons and S. W. Freiman, "Effect of Corrosion Processes on Subcritical Crack Growth in Glass," J. Am. Ceram. Soc., 64 [11], 683 (1981).

10. S. W. Freiman, D. R. Mulville and P. W. Mast, "Crack Propagation Studies in Brittle Materials," Journal of Materials Science, 8 [11], 1527 (1973).

11. W. Wasserman and J. Neter, Applied Linear Statistical Models, Richard D. Irwin, Inc., Honewood, Illinois, 1978.

12. D. N. Coon, J. J. Mecholsky and C. G. Pantano, "A Static Fatigue Limit due to Crack-Healing in $Na_2O \cdot 3SiO_2$ Glass," to appear.

13. Corrosion of Glass by D. E. Clark, C. G. Pantano and L. L. Hench (Books for Industry, New York, 1979).

14. T. M. El-Shamy, J. Lewis and R. W. Douglas, "Dependence on the pH of the Decomposition of Glasses by Aqueous Solutions," Glass Technology, B(3), 81 (1972).

15. S. M. Wiederhorn and H. Johnson, "Effect of Electrolyte pH on Crack Propagation in Glass," J. Am. Ceram. Soc., 56 [4], 192 (1973).

16. B.M.J. Smets and T.P.A. Lommen, "The Incorporation of Aluminum Oxide and Boron Oxide in Sodium Silicate Glasses, Studied by X-ray Photoelectron Spectroscopy," Physics and Chemistry of Glasses, 22 [6], 158 (1981).

17. T. A. Michalske and S. W. Freiman, "A Molecular Interpretation of Stress Corrosion in Silica," Nature, 295 [11], 511 (1982).

18. W. D. Kingery, H. K. Bowen and D. R. Uhlmann, Introduction to Ceramics, Wiley Co., New York, New York, 1976.

19. J. F. Nye, Physical Properties of Crystals, Oxford University Press, 1979.

AD-A170 243 SURFACE CHEMISTRY AND STRUCTURAL EFFECTS IN THE STRESS 2/3
CORROSION OF GLASS..(U) PENNSYLVANIA STATE UNIV
UNIVERSITY PARK DEPT OF MATERIALS SCI..
UNCLASSIFIED C G PANTANO ET AL. 31 MAR 86 F/G 11/2 NL

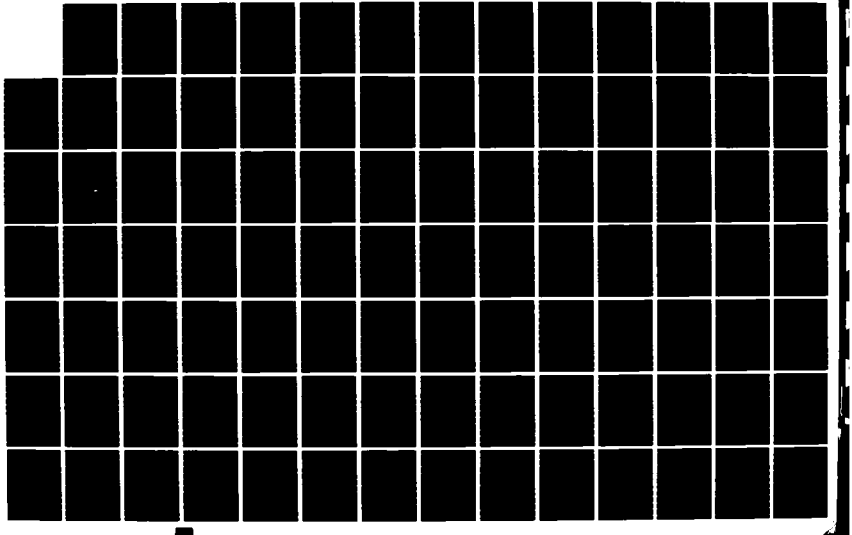

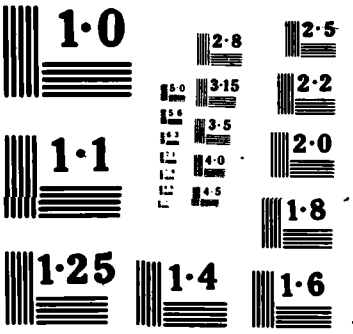
1·0
1·1
1·25
2·8
3·15
3·5
4·0
4·5
2·5
2·2
2·0
1·8
1·4
1·6

CHAPTER III

SLOW CRACK GROWTH BEHAVIOR IN THE THRESHOLD REGION

by

D. N. Coon, J. J. Mecholsky and C. G. Pantano

Department of Materials Science and Engineering

Pennsylvania State University

University Park, PA 16802

Submitted for publication to J. American Ceramic Society.

Slow Crack Growth Behavior in the Threshold Region

by

D. N. Coon,[+] J. J. Mecholsky and C. G. Pantano
Department of Materials Science and Engineering
Pennsylvania State University
University Park, PA 16802

ABSTRACT

Crack velocity was measured as a function of stress intensity for $Na_2O \cdot 3SiO_2$ glass in several solutions varying in pH from 1 to 11. At pH = 11, a velocity plateau was observed at $K_I < .35$ MPa$\cdot m^{1/2}$ and $v \cong 10^{-8}$ m/sec; in a solution of pH 5, the plateau shifted to $K < .30$ MPa$\cdot m^{1/2}$ and $v < 10^{-9}$ m/sec. When $AlCl_3$ was added to the solution, the plateau disappeared and a threshold was observed at $K \cong .40$-$.45$ MPa$\cdot m^{1/2}$. Similarly, sodium-aluminosilicate glasses exhibited a threshold rather than a velocity plateau.

This behavior is explained in terms of interactions between the fracture surfaces wherein ionized surface sites, specifically adsorbed aluminum cations, or hydrogen bonds create forces of repulsion and attraction. These observations represent the first experimental evidence that processes behind a propagating crack-tip can dramatically affect the crack extension rate. Since these effects are limited to the low velocity/low stress intensity regime, they are relevant to the practical strength and fatigue of glass.

[+] Now with EG&G Idaho, Idaho Falls, ID.

INTRODUCTION

Wiederhorn (1) has proposed that Region 1 slow crack growth can be explained by a stress enhanced chemical reaction between the environment and glass. These theories predict that the log of the crack velocity varies linearly with the applied stress intensity. However, it has also been reported that slope changes are observed at low stress intensities (2). The objective of this study was to examine the slow crack growth behavior of a simple $Na_2O \cdot 3SiO_2$ glass at low stress intensity, K_I, and to determine the effects of specific adsorbates - namely H^+ and Al^{3+} - upon the presence or absence of velocity plateaus and thresholds. The crack growth characteristics of the binary sodium-silicate glass in the environment containing aluminum was compared to the behavior of sodium-aluminosilicate glasses in water.

BACKGROUND

Simmons and Freiman (2) were the first to report the existence of low velocity plateaus in the $V-K_I$ diagram for glass. They observed these plateaus in binary soda-silica glasses at K_I levels which depended upon pH, although they were typically in the range .30-.40 $MPa \cdot m^{1/2}$. These investigators suggested that the velocity plateaus were due to corrosion; i.e., the crack grows at a velocity which approximates the rate of silica dissolution. Nevertheless, their data showed that the plateau shifted to lower velocity with increasing pH (whereas the corrosion rate increases with increasing pH). Moreover, the plateau occurred at the same velocity in both 25% Na_2O-75% SiO_2 and 33% Na_2-67% SiO_2 glasses even though the corrosion rates of these glasses are very different at any pH.

More recently, Lawn and co-workers (3,4) have attempted to explain slow crack growth on the basis of mechanisms occurring behind, and not at, the crack

tip. They argue that environmental-fracture surface interactions can cause the neutralization of charged surfaces, or conversely, the charging of neutral surfaces. Electrostatic interactions result when two charged surfaces are in close proximity to one another. Surfaces of like charge would repel, whereas surfaces in the presence of electrolyte species could form adsorbed double layers whose overlap or cationic/anionic bridging could lead to attractive forces. Since crack surfaces are separated by only a small distance at low K_I, the authors suggested the existence of large electrostatic interactions between the crack walls. They have predicted three distinct types of stress intensity-crack velocity behavior depending on the electrical nature of the crack surfaces (Figure 1). There are two features of their model which are relevant here. First, at low K_I levels, constant velocity plateaus can be explained by electrostatic interactions. Second, above some K_I level, shown as K_A in Figure 1, the slow crack growth behavior becomes independent of the electrical nature of the crack surfaces. This behavior at higher K_I is in agreement with the work of Wiederhorn and Johnson (5). They measured the Region I slow crack growth behavior of soda-lime-silica glass in various aqueous environments which produced surfaces of known - but varying - zeta potential. The zeta potential was assumed to be a measure of the electrical charge at the glass surface. They observed no effect of zeta potential on slow crack growth behavior. This suggests that at velocities in excess of 10^{-7} m/s, the slow crack growth behavior of glass is independent of electrostatic crack wall interactions. However, electrostatic effects may be important at lower velocities than were considered by Wiederhorn and Johnson (5).

The possibility of estimating the relative surface charge due to ionized hydroxyls on a silicate glass surface has been reported (6). The ionization process is represented by:

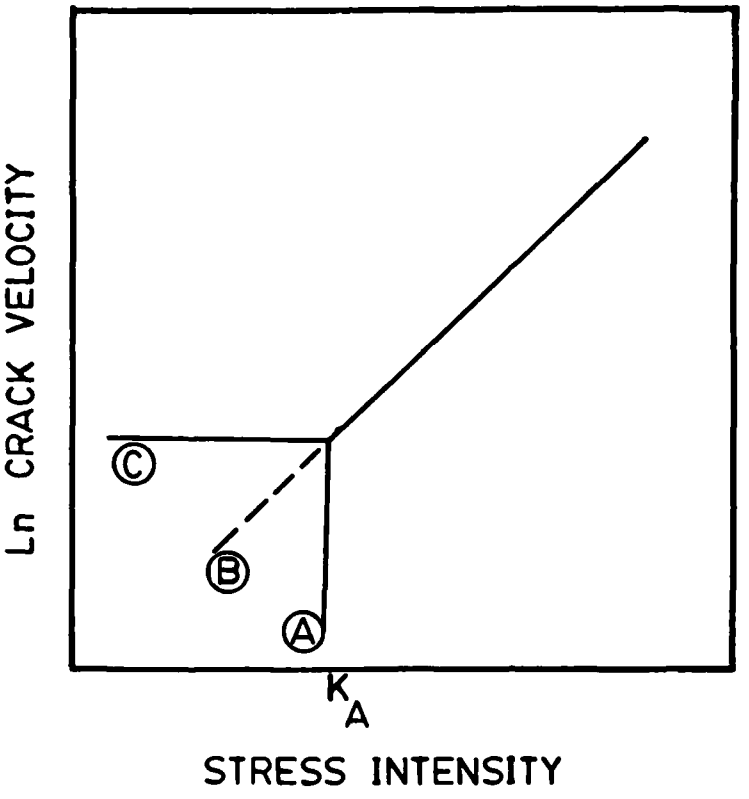

Figure 1. Schematic of crack velocity as a function of stress intensity for cracks with interacting surfaces. The threshold behavior (A) represents fracture surfaces with an attractive interaction, whereas the plateau (C) is due to a repulsive interaction. The extension of Region I - (B) - occurs when surface forces are insufficient to influence the crack growth.

$$SiOH \rightleftarrows SiO^- + H^+, \quad (1)$$

in which case the fraction of hydroxyls ionized as a function of pH is given by:

$$\frac{[SiO^-]}{[SiOH]} = 10^{-9.8 + pH} \quad (2)$$

These calculations are given in Table I. A high pH environment produces a surface of high net negative charge. It is in this sense that the surface charge of a silicate glass is pH dependent. Of more interest here is the fact that, in principle, the surface charge in a crack can be varied through control of the solution pH and/or the solution composition during a crack-growth experiment.

The existence of negatively charged silica surfaces in solutions of high pH has been experimentally verified using streaming potential and other methods (7). These studies also showed that the presence of multivalent cations in solution, for example trivalent aluminum (Al^{+3}), can neutralize or even reverse the charges.

EXPERIMENTAL PROCEDURE

Specimens of $Na_2O \cdot 3SiO_2$ glass, as well as a series of sodium aluminosilicate glasses ($Na_2O \cdot xAl_2O_3 \cdot (3-x)SiO_2$), were cut into plates approximately 7.5 cm x 1.27 cm x 0.25 cm with a groove down the center of the plate. The groove depth was approximately one-half of the plate thickness and the groove width was 0.00075 to 0.001 cm. Slow crack growth behavior was determined by the constant moment double cantilever beam technique as described by Freiman, Mullville, and Mast (8). The slow crack growth behavior of these specimens was examined in water (pH 5), HCl solution (pH 1), NaOH solution (pH 11), and a NaOH solution to which 0.4 g/l of $AlCl_3 \cdot 6H_2O$ had been added.

Table I. Fraction of hydroxyls ionized on a silicate glass surface as a function of pH.

pH	$[SiO^-]/[SiOH]$
<5	0.0
5	0.0
6	0.0
7	0.0
8	0.02
9	0.14
10	0.61
11	0.94
12	0.99
13	1.0

RESULTS

Figure 2 shows the crack velocity data sets of the $Na_2O \cdot 3SiO_2$ glass tested in solutions of pH 1, 5, and 11. Above stress intensities of 0.35 $MPa \cdot m^{1/2}$ and velocities of 10^{-8} m/s, no difference in the slow crack growth behavior was observed. All measurements simply scatter about the line predicted by the data obtained in water. At low velocity, a stress independent plateau was observed in solutions of pH 5 and 11. The plateau was observed at a velocity of 10^{-8} m/s in the pH 11 solution and 10^{-9} m/s in the pH 5 solution. No plateau was observed at pH 1. The pH dependence of the $V-K_I$ diagrams obtained here contradict those reported by Simmons and Freiman (2), but interestingly, these data are quite consistent with their corrosion model.

Figure 3 shows two sets of $V-K_I$ data. One was observed for $Na_2O \cdot 3SiO_2$ tested in pH 11 solution while the other was observed in a pH 11 solution to which $AlCl_3 \cdot 6H_2O$ had been added prior to testing. In the solution containing Al^{+3} ions, no plateau was observed.

The series of sodium-aluminosilicate glasses [$Na_2O \cdot xAl_2O_3 \cdot (3-x)SiO_2$ with x=0.2, 0.4, 0.6, 0.8, and 1.0], as well as commercial borosilicate and soda-lime glasses [which contain a fraction or up to 2 percent Al_2O_3] do not exhibit low velocity plateaus under any conditions (2,9). Figure 4 presents the crack velocity sets for the $Na_2O \cdot .2Al_2O_3 \cdot 2.8SiO_2$ and $Na_2O \cdot Al_2O_3 \cdot 2SiO_2$ glasses at pH 11. These should be compared with the $V-K_I$ diagrams in Figure 3.

DISCUSSION

The surface charge of silicate glasses is known to be pH dependent. It has already been pointed-out that the surface is predominantly negative in solutions of high pH, but that the presence of Al^{+3} ions in solution can alter the surface

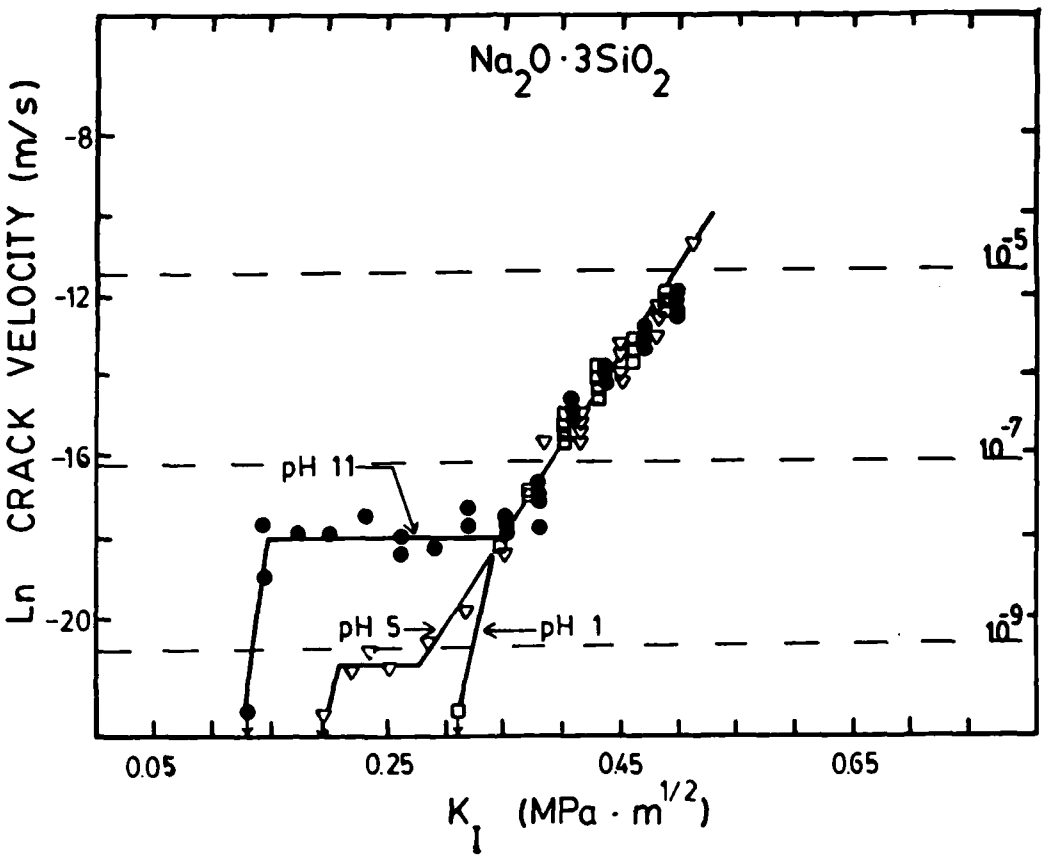

Figure 2. Crack velocity as a function of stress intensity, K_I, for $Na_2O \cdot 3SiO_2$ glass in solutions of pH 1, pH 5 and pH 11.[2] The $V-K_I$ data was measured using the constant moment double cantilever beam (CMDCB) technique.

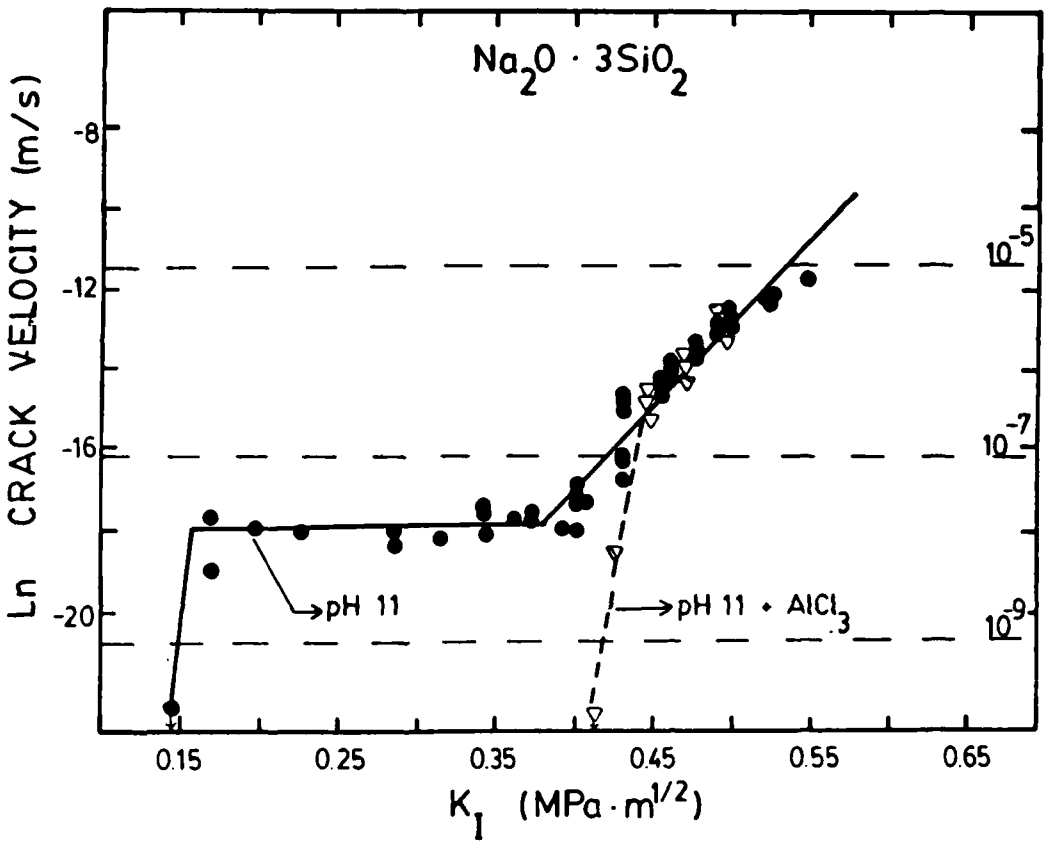

Figure 3. Crack velocity as a function of stress intensity for $Na_2O \cdot 3SiO_2$ glass in a pH 11 NaOH solution and in a pH 11 NaOH solution to which .4 g/l $AlCl_3 \cdot 6H_2O$ has been added (pH ≈5 after the addition).

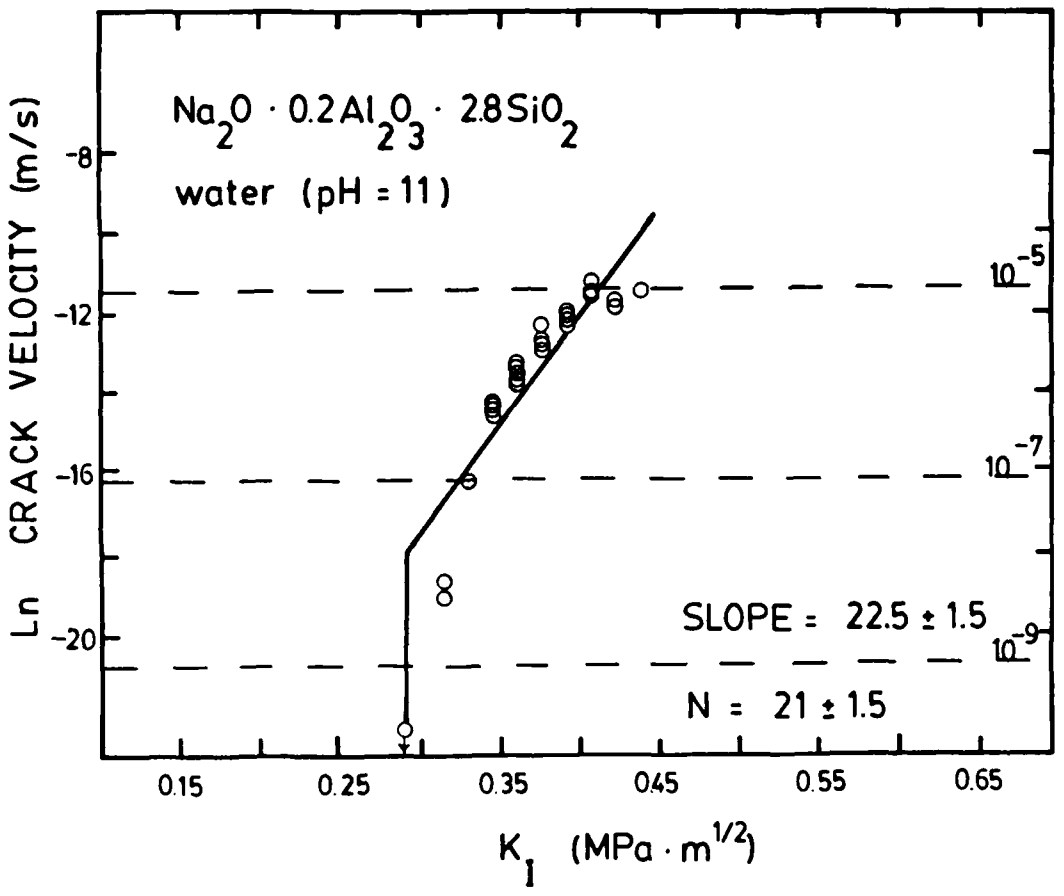

Figure 4a. Crack velocity as a function of stress intensity for sodium-aluminosilicate glass in pH 11 NaOH solution; $Na_2O \cdot 2Al_2O_3 \cdot 2.8SiO_2$.

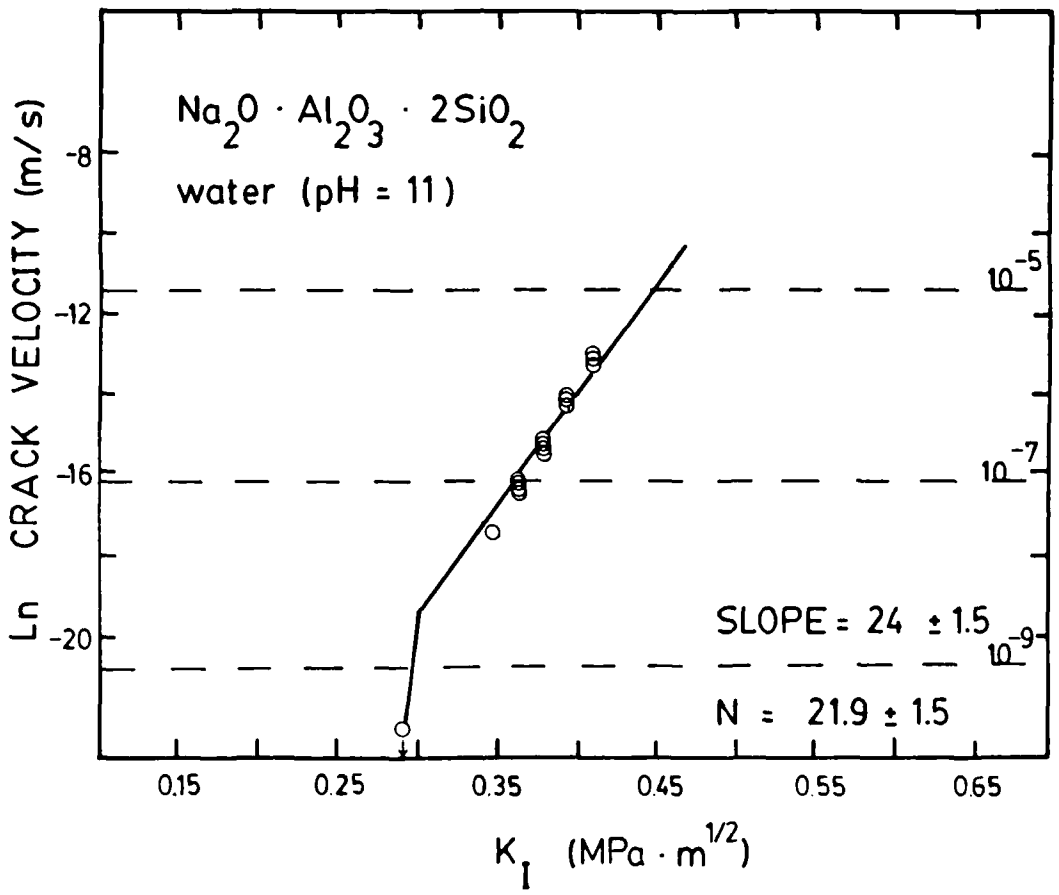

Figure 4b. Crack velocity as a function of stress intensity for sodium-aluminosilicate glass in pH 11 NaOH solution; $Na_2O \cdot Al_2O_3 \cdot 2SiO_2$.

charge. First, the effect of solution pH upon the low velocity plateaus will be discussed, and then the effects of Al^{+3} ions in solution are considered.

The slow crack growth behavior of $Na_2O \cdot 3SiO_2$ glass was determined in solutions of pH 1, 5, and 11 (Figure 2). Above stress intensities of approximately 0.35 $MPa \cdot m^{1/2}$, no effect of solution pH on crack growth was observed. However, at stress intensities below 0.35 $MPa \cdot m^{1/2}$, the behavior of the material changed dramatically with pH. A constant velocity plateau was observed when the experiments were performed in pH 5 and pH 11. The plateau occurred over a larger stress intensity range and was observed at a higher velocity in the pH 11 solution. The plateau occurred over a smaller range of stress intensities and was observed at lower velocities in water. When the solution pH was lowered to 1, the plateau was not observed.

The $Na_2O \cdot 3SiO_2$ glass is known to chemically alter the aqueous solution in contact with it (6). That is, the alkali is released into solution and thereby increases the pH. The pH usually increases up to a point termed 'the equilibrium pH' (pH_{eq}), but the pH_{eq} value depends upon the glass composition and surface-area of glass to solution-volume ratio. Obviously, the pH_{eq} will be achieved quite rapidly within the confines of the crack-tip, especially in the low velocity regions. The equilibrium pH of $Na_2O \cdot 3SiO_2$ has been reported (9), and using that data, one can predict that the crack tip solution will increase in pH by at least 4 units for pH_o = 1 and pH_o = 5 (where pH_o is the initial or 'bulk' solution pH). Since pH_o = 11 is well above the equilibrium pH, however, no significant change in the crack tip pH was anticipated under these alkaline conditions. Using these predictions of the crack-tip pH (5, 9 and 11 for solution pH_o values of 1, 5 and 11, respectively), one can estimate the fraction of ionized surface sites at the crack-tip. A crack tip solution of pH 11 would result in a surface whose silanol species are completely ionized. In

this case, both fracture surfaces would be highly negative and, there would be a 'strong' electrostatic repulsion (although the force is clearly insufficient to propagate the crack at $K_I < .15$ MPa.m$^{1/2}$). A crack tip solution of pH 9 (pH 5 bulk solution) would result in a surface where the silanols are only partially ionized. In this case, the fracture surfaces would possess a small negative charge. There would be a 'weaker' electrostatic repulsion and thus, the plateau shifts to lower velocity and the threshold moves to higher K_I. A crack tip solution of pH 5 would result in a surface which is almost completely hydroxylated. Both fracture surfaces would be neutrally charged and no repulsive forces will exist. Nevertheless, there may be an interaction between these neutrally-charged, but fully hydroxylated surfaces. In fact, it is possible that the threshold observed here, as well as in the other glasses, is due to hydrogen bonding and/or double-layer overlap behind the crack-tip which creates an attractive force between the fracture surfaces. These thresholds are usually observed in glasses containing modifier species where surface silanol densities and/or double-layer formations are expected to be most extensive. It is likely that the attractive force due to hydrogen bonding, in particular, is significant only when ionic forces are minimized or when very low K_I conditions bring the fracture surfaces into close proximity. In this sense, the thresholds observed at low K_I may be due - in general - to hydrogen-bonding between surface silanols. The fact that a threshold (or plateau) has not been reported for silica can be attributed to the low surface silanol density of the fully cross-linked SiO_2 glass; thus, Region I crack growth extends to very low K_I. Any plateaus and thresholds for silica glass, if they exist, would occur at a crack velocity below the detection limit of most experimental measurements.

The low velocity plateau was not observed when the $Na_2O \cdot 3SiO_2$ glass was tested in a solution containing 10^{-4} moles/l $AlCl_3 \cdot 6H_2O$; the aluminum chloride

was added directly to the pH 11 solution in order to keep the alkali ionic strength a constant. The pH of this solution dropped to 5 due to addition of the aluminum chloride species. Nevertheless, according to Horn and Onoda (7), the presence of this aluminum species at 10^{-4} M/l and pH 5 changes the zeta potential from -100 mV to 125 mV; alone, the pH change from 11 to 5 would reduce the value of the zeta potential slightly (~20 mV), but could not reverse the sign. The elimination of the low velocity plateau with $AlCl_3 \cdot 6H_2O$ addition - and the consequent threshold behavior - is consistent with the concept that the plateaus result from negatively-charged fracture surfaces; i.e., Al^{+3} can neutralize and/or reverse the charge by specific adsorption upon the fracture surfaces at and behind the crack-tip. It is likely that the presence of a threshold under these conditions is due to Al^{+3} 'cation bridging' across the crack and/or overlap of the double-layers associated with the adsorbed aluminum species; in a sense, there is little fundamental difference between these two effects. These data, and their interpretation, are clearly consistent with the recent models put forth by Lawn and co-workers (3,4).

It is especially noteworthy that the sodium aluminosilicate glasses - at pH 11 - do not exhibit the low velocity plateaus expected under these conditions. Thus, it seems likely that the aluminum in the glass plays a dynamic role during the crack growth process in the threshold regime. The absence of low velocity plateaus in the sodium-aluminosilicate glasses (Figure 4), as well as in commercial glasses containing alumina and probably in any glasses containing multivalent cations, may be due to 'steady-state' dissolution/adsorption phenomena at and behind the crack-tip. There is always some dissolution of the glass within the crack, and thus the presence of Al^{+3} or other multivalent ions, can be expected even when they are not intentionally

introduced into the crack-growth environment. This represents, perhaps, the only practical approach to chemical passivation of slow crack growth in glass.

CONCLUSIONS

The occurrence of low velocity plateaus and/or thresholds in sodium silicate glasses was shown to be dependent upon environmental pH and the presence of Al^{3+} ions in solution. This behavior was shown to be consistent with an interaction between the fracture surfaces. Such behavior represents the first experimental evidence that processes behind a propagating crack tip can dramatically affect the crack extension rate.

ACKNOWLEDGEMENT

The authors gratefully acknowledge the financial support of the Air Force Office of Scientific Research (AFOSR-82-0013).

REFERENCES

1. S. M. Wiederhorn, "Influence of Water Vapor on Crack Propagation in Soda-Lime Glass" J. Am. Ceram. Soc., 50[8], 401 (1967).

2. C. J. Simmons and S. W. Freiman, "Effect of Corrosion Processes on Subcritical Crack Growth in Glass" J. Am. Ceram. Soc., 64[11], 683-6 (1981).

3. B. R. Lawn, S. M. Wiederhorn and D. R. Clarke, "Subcritical Crack Growth: The Role of Surface Forces" Presented at the Annual Meeting of the American Ceramic Society Annual Meeting, Cincinnati, OH, May, 1985.

4. B. R. Lawn, "Interfacial Forces and the Fundamental Nature of Brittle Cracks" Appl. Phys. Ltrs., 47, 809 (1985).

5. S. M. Wiederhorn and H. Johnson, "Effect of Zeta Potential on Crack Propagation in Glass in Aqueous Solutions" J. Am. Ceram. Soc., 58[7-8], 342 (1975).

6. R. W. Douglas and T. M. El-Shamy, "Reactions of Glasses with Aqueous Solutions," J. Am. Ceram. Soc., 50(1), 1 (1967).

7. J. M. Horn, Jr. and G. Y. Onoda, Jr., "Surface Charge of Vitreous Silica and Silicate Glasses in Aqueous Electrolyte Solutions" J. Am. Ceram. Soc., 61[11-12], 523 (1978).

8. S. W. Freiman, D. R. Mulville and P. W. Mast, "Crack Propagation Studies in Brittle Material" J. Mater. Sci., 8[11], 1527 (1973).

9. D. Coon, J. J. Mecholsky, C. G. Pantano, "Relationship between Elastic Properties and Slow Crack Growth in Sodium-Aluminosilicate Glasses" to be published.

CHAPTER IV

STATIC FATIGUE LIMIIT DUE TO CRACK HEALING IN $Na_2O \cdot 3SiO_2$ GLASS

by

D. N. Coon, J. J. Mecholsky and C. G. Pantano

Department of Materials Science and Engineering

Pennsylvania State University

University Park, PA 16802

To be submitted.

STATIC FATIGUE LIMIT DUE TO CRACK HEALING IN $Na_2O \cdot 3SiO_2$ GLASS

by

D. N. Coon,[+] J. J. Mecholsky and C. G. Pantano
Department of Materials Science and Engineering
Pennsylvania State University
University Park, PA 16802

ABSTRACT

A model is developed which can explain the static fatigue limit in terms of a crack healing mechanism. The model assumes that a high water-content material can form at the crack-tip due to healing when $K_I < K_{Io}$ (the static fatigue limit). This 'healed' region is resistant to crack propagation not because it is blunted, but rather, because it is deformable. In this study, the model was tested by aging $Na_2O \cdot 3SiO_2$ glass at $K_I > K_{Io}$, and then measuring the time delay to crack extension upon reloading at $K_I > K_{Io}$. The time delays could be predicted as a function of reload stress intensity by modeling the strain rate in terms of a viscous deformation and by assuming the existence of some critical strain for crack re-propagation.

[+] Now with EG&G Idaho, Idaho Falls, ID

INTRODUCTION

Originally, crack extension studies were envisioned as a route to the prediction of service lifetimes of structural materials. The existence of a static fatigue limit, which is a stress level below which cracks do not extend, would be of fundamental importance in the design of these materials. Typically, a static fatigue limit is observed in crack extension studies of glass at stress levels approximately one-third the fracture toughness. Clearly, the determination of the mechanism by which this fatigue limit occurs has been the stimulus for much experimental activity.

BACKGROUND

The two theories which are most widely accepted for explaining the static fatigue limit in glass involve crack-tip blunting (1,2) and crack healing (3,4). More recently, it has been suggested that interactions between the fracture surfaces behind the crack tip may contribute to the fatigue limit, or 'threshold,' for crack growth (5,6). The blunting and healing models are most pertinent to the arguments presented in this study.

Charles and Hillig (1) suggested that the driving force for blunting could be envisioned as being composed of two contributing factors. First, as the crack-tip radius of curvature increases (i.e., the tip becomes more blunt), the driving force for blunting decreases. Secondly, as the corrosiveness of the environment increases (i.e., the tendency of the environment to attack the material increases), the driving force for blunting increases. They modeled these trends as:

$$E_{blunt} = [V_m \gamma]/\rho \qquad (1)$$

where E_{blunt} = driving force for blunting

ρ = crack tip radius

V_m = molar volume of the material being corroded

γ = surface energy of the material with respect to the environment.

An externally applied stress would provide a driving force for crack extension which would act in opposition to the crack tip blunting force. This driving force would be high for large values of applied stress and small crack tip radii.

A simple energy balance of the driving forces determines whether the tip will blunt or extend. When the two driving forces are exactly equal, the crack tip will neither extend nor blunt. This is traditionally termed the static fatigue limit, K_{Io}. For all values of K_I greater than K_{Io}, the driving force for extension is greater than the driving force for blunting, and the crack tip extends at some finite rate maintaining a constant tip radius. In contrast, for values of K_I less than K_{Io}, the driving force for blunting is greater than the driving force for extension, and the crack tip blunts. However, this blunting will not continue indefinitely to produce a crack-tip of infinite radius. Both driving forces are dependent upon the tip radius. As the crack-tip radius increases, the driving force for blunting decreases by ρ^{-1} while the crack extension driving force decreases by $\rho^{-1/2}$. The two driving forces will become equal at some ρ' (which is greater than the original radius) and then, the crack extension ceases.

Michalske (2) used the model described above to explain the delay in crack extension which is observed after aging a crack-tip under load. He showed that double cantilever beam specimens of soda-lime-silica glass aged at stress levels below the fatigue limit exhibited a hysteresis upon reloading to levels above the fatigue limit. He hypothesized that aging specimens at a K_I of 0.225

$MPa \cdot m^{1/2}$, which is less than the observed static fatigue limit of approximately 0.3 $MPa \cdot m^{1/2}$, would result in crack tip blunting. He then showed that when this specimen was reloaded to K_I levels where measurable crack extension had been observed before aging, the cracks did not extend without an appreciable time delay. This time delay was attributed to the time necessary to sharpen a crack tip which had blunted during aging. He further supported his model through fractographic examination of the aged fracture surfaces. To date, the work of Michalske represents the strongest evidence of crack tip blunting in glass at room temperature.

Fuller and Thomson (3) have developed an atomistic model for crack extension. They assume a two-dimensional lattice of two parallel infinite chains of atoms. The separation of these two chains of atomically bonded atoms is used to describe crack growth. Their derivation of the cohesive energy is an expression containing three terms:

$$U_{cohesive} = 2nc\gamma_7 + 2\gamma u_n c + 2\alpha \sum_{j=n+1}^{\infty} uj^2 \qquad (2)$$

where n = the number of bonds in the chain

c = the interatomic distance

γ = the surface energy or fracture surface energy

u = the displacement distance of a given atom from its equilibrium position

α = constant.

The first term simply accounts for the energy of formation of two new surfaces where γ_f is the fracture surface energy per unit length and nc is the crack length. The second term accounts for the strain energy stored in the crack-tip bond, which is the only bond considered to undergo a non-linear deformation. The third term accounts for the strain energy in all the bonds ahead of the

crack tip bond. These bonds support linear deformation only. After performing an energy balance, Fuller and Thomson showed that:

$$\text{crack extension force} = \sum \text{restoring forces} \qquad (3)$$

The crack extension force was taken to be proportional to K_I. Thus, at K_I's greater than K_+ (where K_+ is analogous to K_{Ic}), the crack propagates catastrophically since crack extension would result in a lowered crack driving force. For K_I's between K_+ and K_-, the crack can exist at two possible lengths corresponding to equivalent driving forces. In this region, stable crack growth is predicted. For K_I's less than K_- (where K_- is analagous to K_{Io}), the only means for lowering the driving force is a reduction in crack length. Hence, Fuller and Thomson proposed crack healing to be a viable mechanism to explain the fatigue limit. Cekirge, Tyson, and Krausz (4) used the concept of crack healing to predict a fatigue limit.

The objective of this study was to examine the crack extension behavior of aged $Na_2O \cdot 3SiO_2$ specimens and to analyze those observations based upon a crack healing mechanism.

EXPERIMENTAL PROCEDURE

The methods of specimen preparation and crack-velocity measurement (using the constant moment double cantilever beam technique) have been previously reported (7). Since the fatigue limit in this material occurs at approximately 0.2 $MPa \cdot m^{1/2}$, the specimens were aged at K_I = .142 $MPa \cdot m^{1/2}$ for two hours in deionized water. The specimen was then reloaded to stress intensities which produced an observable crack velocity. The crack extension after aging was recorded as a function of K_I and time.

RESULTS AND DISCUSSION

The crack extension behavior of the aged $Na_2O \cdot 3SiO_2$ glass specimens is given in Figure 1. After aging, time delays to crack elongation of 0 to 1700 seconds were observed. The corresponding stress intensities were between .43 and .38 $MPa \cdot m^{1/2}$, respectively.

The possibility that crack healing had caused the observed time delays - rather than crack blunting - was considered. In the case of crack healing, no geometrical alteration of the crack tip is expected. Consequently, one would expect the cracks to extend at the same velocity before and after aging. The magnitude of that velocity would be determined by the stress intensity applied to the crack. Figure 2 shows the velocity of the crack after reloading plotted against the velocity before aging. The 1:1 correlation line is also plotted to show that the cracks did extend at the expected velocity. Another indication that crack blunting was not responsible for the effect was the comparable delay times observed for a series of sodium-aluminosilicate glasses (7), whose corrosion resistance (and hence resistance to blunting) should greatly exceed the $Na_2O \cdot 3SiO_2$ glass.

The mechanism by which crack healing could produce the observed time delays was envisioned as follows. During the aging process, the crack heals some small amount. Since the aqueous environment chemically reacts with the crack surfaces, it is only reasonable to anticipate that the aqueous species will be incorporated within the healed region. Although the nature of this healed region is unknown, this model considers the healed crack-tip to be a region of high water content. It has been reported that glasses of high water content (12 wt%) can deform plastically (8). It has also been shown that the viscosity of a glass is lowered by the incorporation of water (9). Assuming that the

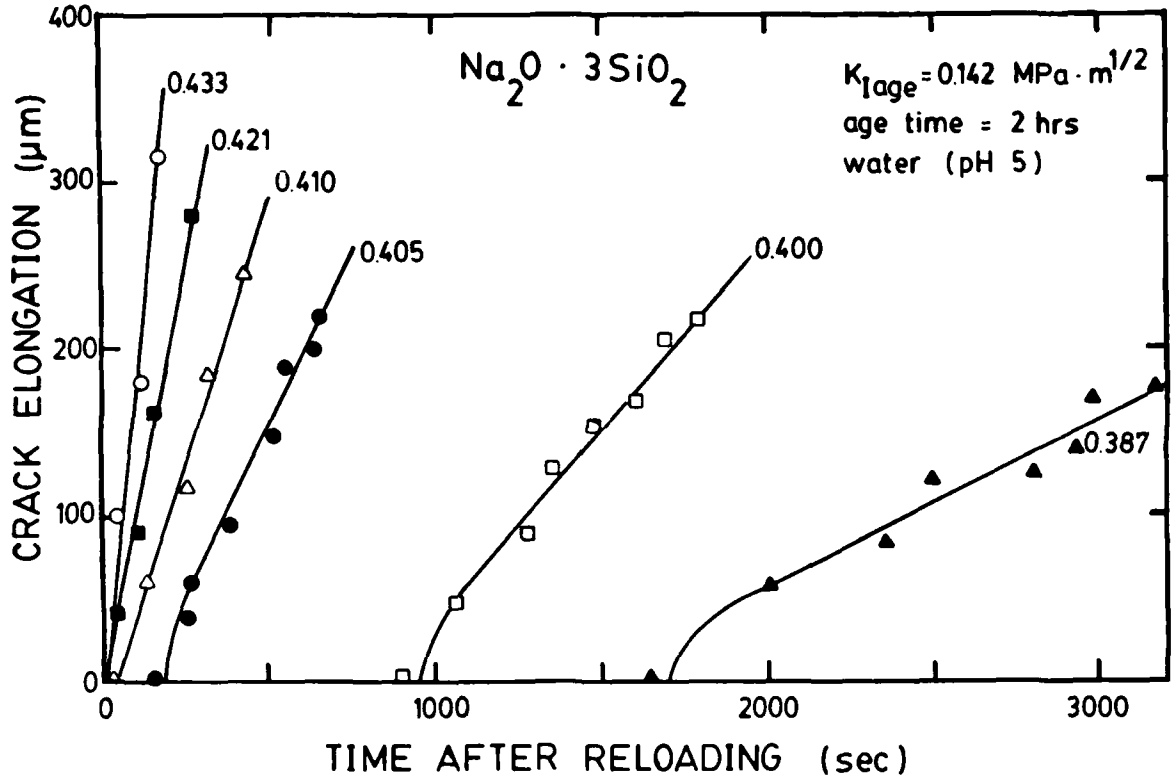

Figure 1. The crack elongation behavior of $Na_2O \cdot 3SiO_2$ glass after aging under load in deionized water.

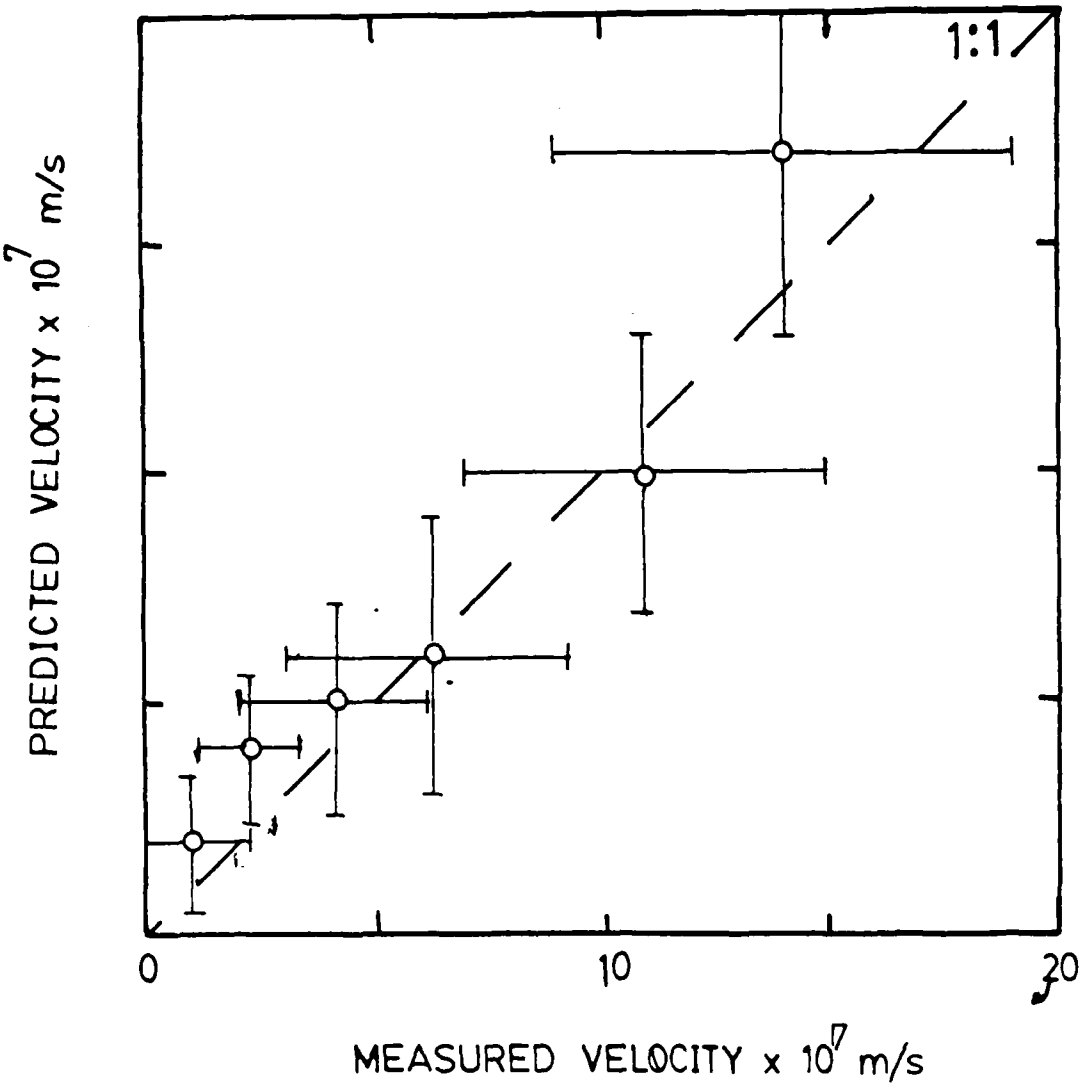

Figure 2. The correlation between the crack velocity measured before and after aging under load.

healed material is deformable, and thus can exhibit some finite viscosity, a permanent deformation or 'strain' can account for the time delay.

The strain rate can be evaluated if we assume the material deforms in a viscous nature

$$\frac{d\varepsilon}{dt} = \begin{bmatrix} \frac{1}{3\eta} & -\frac{1}{6\eta} & -\frac{1}{6\eta} & 0 & 0 & 0 \\ -\frac{1}{6\eta} & \frac{1}{3\eta} & -\frac{1}{6\eta} & 0 & 0 & 0 \\ -\frac{1}{6\eta} & -\frac{1}{6\eta} & \frac{1}{3\eta} & 0 & 0 & 0 \\ 0 & 0 & 0 & \frac{1}{\eta} & 0 & 0 \\ 0 & 0 & 0 & 0 & \frac{1}{\eta} & 0 \\ 0 & 0 & 0 & 0 & 0 & \frac{1}{\eta} \end{bmatrix} \qquad (4)$$

where $d\varepsilon/dt$ = strain rate, and

η = viscosity.

The process which is expected to occur at the crack-tip if a deformable material is present is shown in Figure 3. It is assumed that the healed region begins to deform immediately after reloading. This deformation continued until enough strain is developed to stretch the bonds in the virgin materials. Once the strain in these bonds reaches some limit, the crack begins to re-propagate. The experimetal variables which can be controlled are aging stress intensity, aging time, and aging environment. The aging stress intensity determines the driving force for crack extension during the aging process. According to the Fuller and Thomson lattice fracture model (3), less healing would be expected with an increase in the aging stress intensity. In these experiments, the aging stress intensity, aging time and aging environment were held constant. Thus, an invariant amount of healing would be expected, and thereby, the critical amount of strain in the healed region would be constant. However, the strain rate is

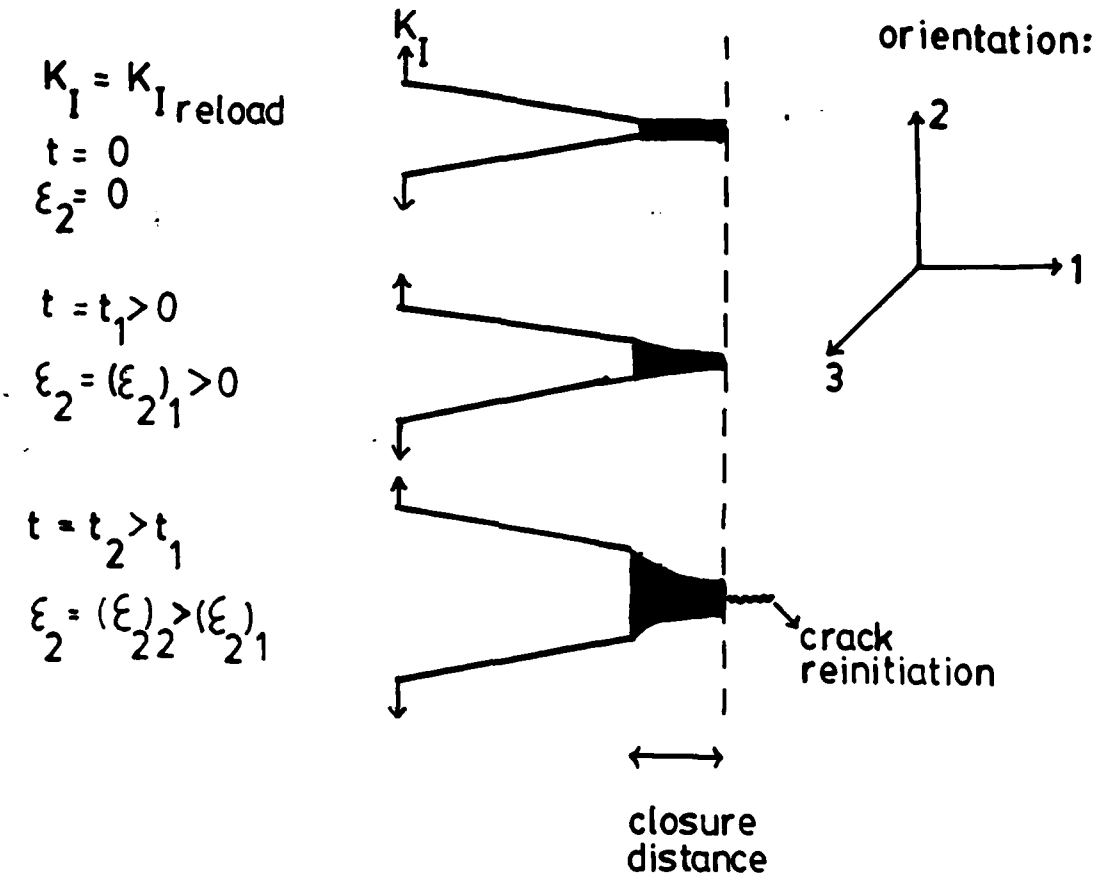

Figure 3. Schematic representation of a crack tip which has healed to form a deformable, high-water content material (the blackened areas), and its evolution upon reloading; the times, t, correspond to 'time after reloading.'

predicted to be dependent upon the 'reloading' stress intensity. In this manner, the delay time would vary with reloading stress intensity.

In order to quantify this effect, Equation 1 can be used by assuming a crack orientation such as shown in Figure 3:

$$\dot{\varepsilon}_2 = d\varepsilon_2/dt = [\sigma_1/(-6n)] + [\sigma_2/3n] + [\sigma_3/-6n] \tag{5}$$

Principal stresses can be expressed as a simple multiple of σ_2 such that:

$$\sigma_i = Q_i \sigma_2 \tag{6}$$

where Q_i is a scaling factor. Substituting this into Equation 5 yields:

$$d\varepsilon_2/dt = \sigma_2[(1/3n) - (Q_1/6n) - (Q_3/6n)] \tag{7}$$

The stresses can be expressed as a function of the applied stress intensity such that:

$$\sigma_i = A_i K_1 \tag{8}$$

Combining Equations 7 and 8 yields the desired result:

$$d\varepsilon_2/dt = K_I(A[(1/3n) - (Q_1/6n) - (Q_3/6n)]) \tag{9}$$

$$= B\, K_I \tag{10}$$

B is the accumulation of parameters relating to viscosity, crack orientation, and crack length. These parameters will be constant for any particular material and crack system.

This model shows that some critical amount of strain (ε_{crit}) is necessary for crack repropagation. This strain is attained at some critical time (t_{crit}) which depends upon the reloading stress intensity (assuming the other parameters such as glass composition, aging time, aging stress intensity and environment are constant). This results in the following boundary conditions:

$$\text{at } t = 0,\ \varepsilon_2 = 0$$

$$\text{at } t = t_{crit},\ \varepsilon_2 = \varepsilon_{crit}$$

Using these conditions to evaluate Equation 10 yields:

$$\int_0^{\varepsilon_{crit}} d\varepsilon_2 = B \cdot K_I \cdot \int_0^{t_{crit}} dt \tag{11}$$

Since $(K_I)_{reload}$ is a constant for each individual aging experiment, Equation 11 can be integrated to yield:

$$(K_{I\ reload})^{-1} = [B/\varepsilon_{crit}]\ t_{crit} \tag{12}$$

Figure 4 shows the aging data for the $Na_2O \cdot 3SiO_2$ glass plotted as predicted in Equation 12. The data reflects the expected trends reasonably well. A linear relationship existed for the $(K_I)_{reload}$ values where a finite delay time could be observed.

Figure 5 presents the data reported by Michalske (2), but plotted according to the expression derived in Equation (12). The trends are analagous to the

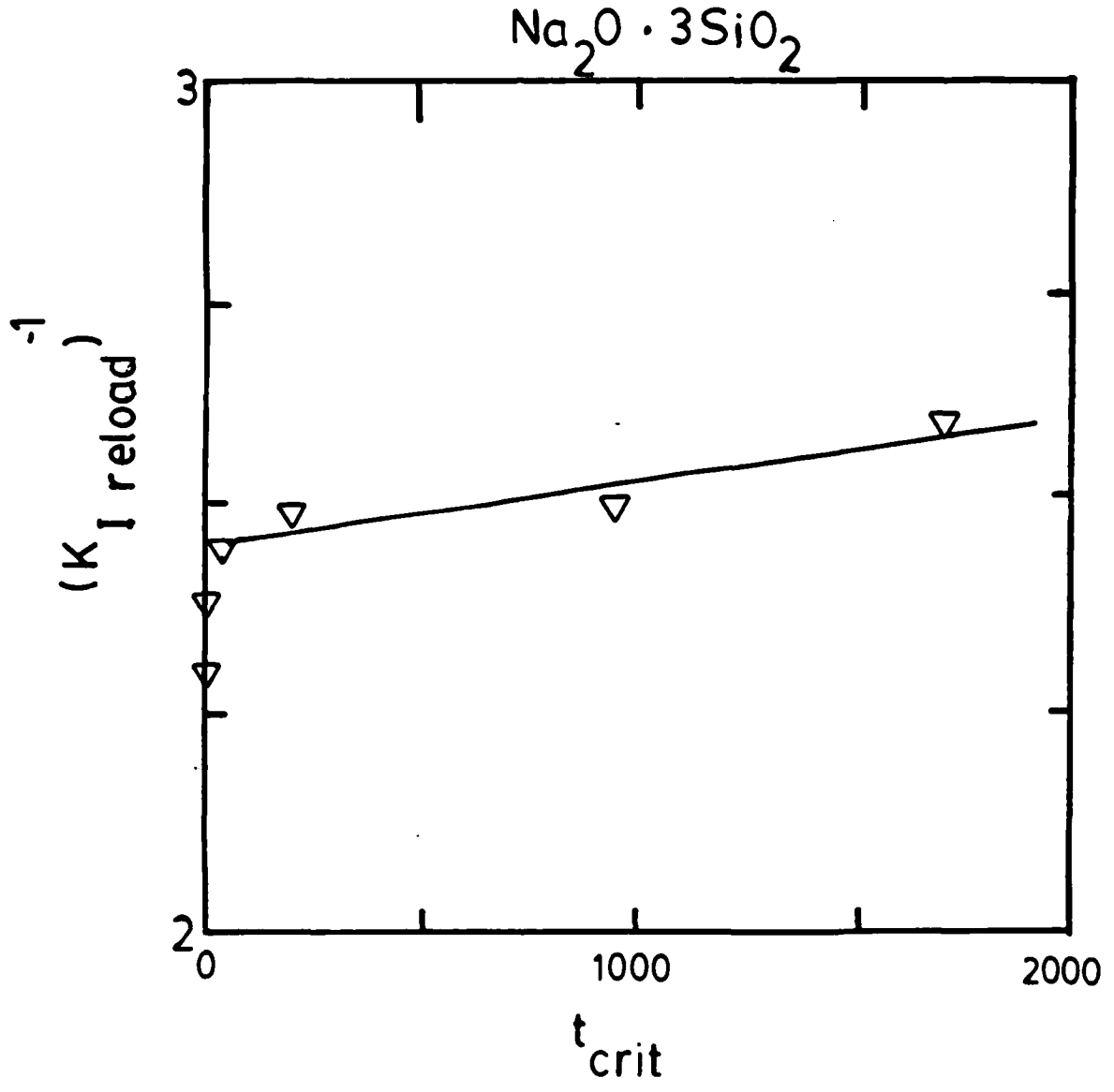

Figure 4. The measured delay time to crack elongation (see figure 1) plotted as a function of inverse reloading stress intensity (equation 12) for $Na_2O \cdot 3SiO_2$ glass aged in deionized water for two hours.

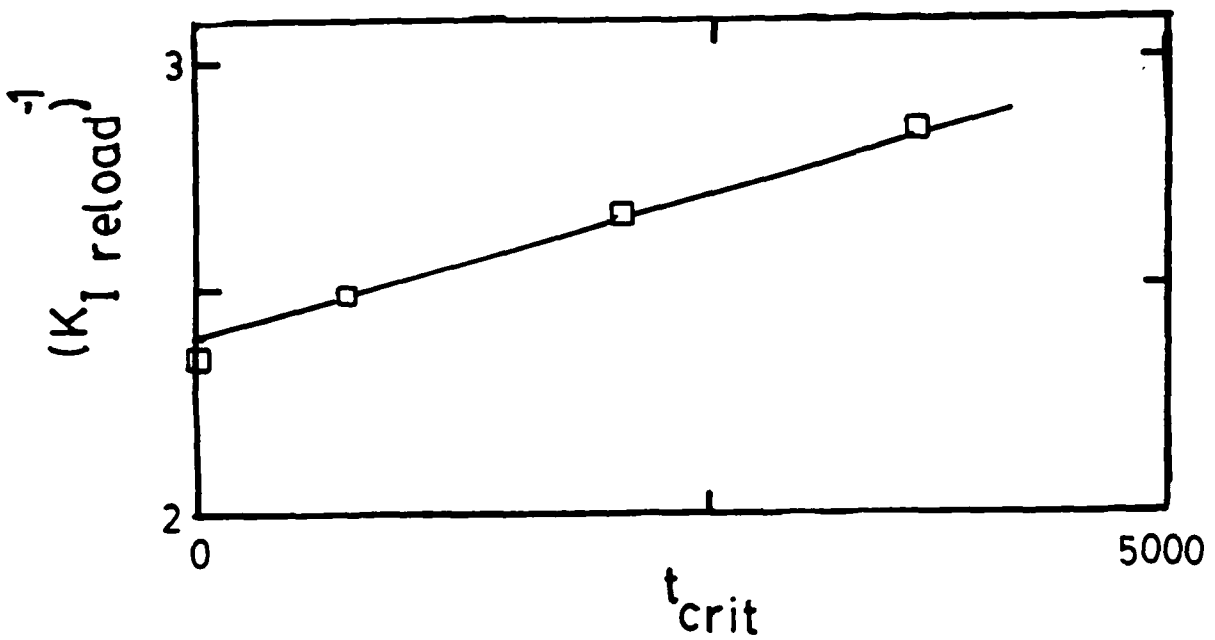

Figure 5. The delay time to crack elongation reported by Michalske (2) for soda-lime-silica glass; here, it is plotted according to equation 12.

ones obtained in this study. It should be mentioned that the slopes (B/ε_{crit}) of the linear portions in Michalske's data and the data obtained in this study are different. This is to be expected since experimental variables (aging time and aging stress intensity) and composition (viscosity and restoring force) were not the same for the two studies.

CONCLUSIONS

This paper suggests that alternatives are available to explain the sort of crack growth behavior previously attributed to crack tip blunting. The aging experiments presented here are consistent with a crack healing mechanism where the healed material is modified. This healed material is more resistant to crack-propagation upon reloading because it can undergo a plastic deformation. The presence of crack healing during aging supports models of a static fatigue limit resulting from crack healing. It is suggested that the static fatigue limits observed in crack extension studies can be attributed to comparable healing mechanisms thereby eliminating the necessity of considering crack tip geometry changes.

ACKNOWLEDGEMENT

The authors gratefully acknowledge the financial support of the Air Force Office of Scientific Research (AFOSR-82-0013).

REFERENCES

1. W. B. Hillig and R. J. Charles, "Surfaces, Stress-Dependent Surface Reactions, and Strength," High Strength Materials, pgs. 682-701, edited by W. F. Zackey, Wiley Publishing Co., New York, 1965.

2. T. A. Michalske, "The Stress Corrosion Limit and Its Measurement," Fracture Mechanics of Ceramics, Vol. 5, pgs. 277-289, edited by R. C. Bradt, A. G. Evans, D.P.H. Hasselman and F. F. Lange, Plenum Press, New York, 1983.

3. E. R. Fuller and R. M. Thomson, "Lattice Theories of Fracture," Fracture Mechanics of Ceramics, Vol. 4, pgs. 507-548, edited by R. C. Bradt, D.P.H. Hasselman and F. F. Lange, Plenum Press, New York, 1978.

4. H. M. Cekirge, W. R. Tyson and A. S. Krausz, "Static Corrosion and Static Fatigue of Glass," J. Am. Ceram. Soc., 59[5-6], 265 (1976).

5. B. R. Lawn, S. M. Wiederhorn and D. R. Clarke, "Sub-critical Crack Growth: The Role of Surface Forces," Presented at the Annual Meeting of the American Ceramic Society, May 6, 1985.

6. D. N. Coon, J. J. Mecholsky and C. G. Pantano, "Slow Crack Growth Behavior in the Threshold Region," to appear.

7. D. N. Coon, J. J. Mecholsky and C. G. Pantano, "The Relationship Between Elastic Properties and Slow Crack Growth in Sodium-Aluminosilicate Glasses," to appear.

8. M. Takata, M. Tomazawa and E. B. Wataon, "Effect of Water Content on Mechanical Properties of Na_2O-SiO_2 Glasses," J. Am. Ceram. Soc., 65[9], c156 (1982).

9. K. Kitazawa, A. Hishi, and K. Fueki, "Influence of Atmospheric Water on Surface Viscosity of Some Silicate Glasses," Yogyo Kyokai Shi, 88[12], 741 (1980).

CHAPTER V

STRESS CORROSION OF SODIUM-ALUMINOSILICATE GLASSES: A COMPARISON OF SMALL AND LARGE CRACKS

by

D. Coon, J. J. Mecholsky and C. G. Pantano

Department of Materials Science and Engineering

Pennsylvania State University

University Park, PA 16802

To be sumbitted to J. Fracture Mechanics.

STRESS CORROSION OF SODIUM-ALUMINOSILICATE GLASSES: A COMPARISON OF SMALL AND LARGE CRACKS

D. Coon,[+] J. J. Mecholsky and C. G. Pantano
Department of Materials Science and Engineering
The Pennsylvania State University

Abstract

The double cantilever beam and dynamic fatigue techniques were used to measure slow crack growth effects in a series of sodium-aluminosilicate glasses $Na_2O \cdot x\ Al_2O_3 \cdot (3-x)\ SiO_2$ with x varying between 0 and 1. The constant moment double cantilever beam (CM-DCB) technique with a large crack measures the threshold Region 0, and Regions I, II and III separately while the dynamic fatigue, or stressing rate, technique integrates the effect of Regions 0, I, II and III using small indentation cracks. Thus, although there exists, in principle, a direct correspondence between slow-crack growth measurements and fatigue tests, the measured n values are not always the same. The present study shows that dynamic fatigue and CM-DCB analyses yield different n-values; and, there were larger errors in n values in the dynamic fatigue analysis. The pH had little effect on the measured n values in either case, but surprisingly, the strength in the dynamic fatigue tests increased at low stressing rates in a pH 11 solution. This increase was shown to be due to a relief of residual stress and not crack blunting, and to be consistent with the low velocity plateaus observed in pH 11 solutions with the CM-DCB measurements. Thus, the absolute differences between n-values are due to multiregion crack growth.

[+] Now with EG&G Idaho, Idaho Falls, Idaho

INTRODUCTION

Several investigators[1-4] have attempted to experimentally show a direct correlation between the stress corrosion susceptibility parameter, n, as determined by techniques that involve large cracks such as the constant moment double cantilever beam (CM-DCB) technique and those that involve small cracks such as static fatigue (delayed failure) or dynamic fatigue (stressing rate) for soda-lime-silica glass. In the case of static fatigue, Fuller[5] showed a one-to-one mathematical correspondence between the velocity-stress intensity relationship and the slope of the time to failure-applied stress curve. However, the mathematical correspondence between dynamic fatigue and the $V-K_I$ relationship is much more difficult to evaluate.

Wiederhorn et al.[6] suggested that differences between large crack techniques and small crack techniques could result from differences in (1) residual stresses at the origin of fracture, (2) crack-tip blunting, and (3) geometry differences between large and small cracks. Residual stresses would be expected to affect the measurements to a greater degree on small cracks than large cracks. If crack blunting exists, i.e. crack tip rounding due to corrosion processes, then it would be expected to affect large cracks more than small cracks. Finally, the geometry factor in crack propagation would be different for a straight crack as in CM-DCB than for the small flaws or semi-elliptical indentation cracks in fatigue tests.

The present study uses CM-DCB and dynamic fatigue to examine the effect of small and large cracks on crack propagation in a series of $Na_2O \cdot x\ Al_2O \cdot (3-x)\ SiO_2$ glasses with x = 0, .2, .4, .6, .8 and 1.0 as a function of environment. Thus, it is possible to compare crack propagation in glasses that are quite susceptible to corrosion (x=0) with glasses that are not very susceptible to

corrosion ($x \geq 0.6$). In order to further investigate the effect of varying corrosion behavior, the crack propagation is evaluated in solutions of pH=5 and pH=11.

It is shown that different n values are obtained for the CM-DCB and stressing rate techniques even after accounting for residual stress effects. The absolute values of n determined by the dynamic fatigue were generally lower than those determined by the CM-DCB technique. Crack blunting is eliminated as a reason for the difference. However, the strength behavior for x=0 glass at slow loading rates was shown to be completely consistent with the CM-DCB V-K_I results at low velocity-low stress intensity region. Thus, although the mathematical formulism to account for multiregion crack-growth does not yet exist, it is possible - in principle - to translate V-K_I results to dynamic fatigue, and vice-versa.

BACKGROUND

The relationship between crack velocity V and (Mode I) stress intensity, K_I, is often represented by a power law function:[6,7]

$$V = A(K_I)^n \tag{1}$$

Although there is no fundamental reason for using this relationship, it is mathematically convenient and is considered a valid indication of stress corrosion behavior. The slope, n, of the log v-log K_I plot* is considered a

*Although the slope of the log crack velocity-stress intensity has more fundamental meaning, i.e., it is related to the activation energy and activation volume, it is more common for the slope of the log velocity-log stress intensity to be represented as a measure of the resistance to slow crack growth.

characteristic of stress corrosion and a measure of the resistance to slow crack growth:

$$\log V = \log A + n[\log K_I] \qquad (2)$$

where: V = crack velocity

A = constant

K_I = applied stress intensity

Direct measurement of crack velocity at known applied stress intensities permits the determination of n. However, difficulties in observing a moving crack tip generally limit the usefulness of this 'direct measurement' method to room temperature studies.

Evans[7] has proposed a method by which n can be obtained from strength measurements. Assuming the rate of crack extension is described by Equation 1, the following relationship can be derived:

$$\log \sigma_f = \log A + [1/n+1] \log \dot{\sigma} \qquad (3)$$

where σ_f = fracture stress

A = constant

$\dot{\sigma}$ = stressing rate

By experimentally determining the variation of fracture stress with stressing rate, n is easily obtained. This is known as the dynamic fatigue technique. Such an 'indirect method' eliminates the need for direct crack velocity measurement. The dynamic fatigue method assumes that the applied stress is the only stress acting on the strength controlling flaw. Typically, the strength controlling flaw is introduced by indentation. Since it is well known that residual stresses remain after the indentation process, these stresses must be removed in order to apply the Evan's analysis.[7]

Recently Fuller, Lawn and Cook[8] have reported a mathematical correction for the residual stresses which can be introduced after the test. They derived the following expression:

$$\log \sigma_f = \log B + [1/n'+1] \log \dot{\sigma} \qquad (4)$$

where B = constant

n' = apparent n

The apparent n' (i.e., the slope of the dynamic fatigue curve) is related to the "true" n by:

$$n = 4/3\ n' - 2/3 \qquad (5)$$

The analysis of Fuller, Lawn, and Cook[8] has refined the original concepts of Evans [7] such that removal of residual stress prior to testing is unnecessary.

EXPERIMENTAL PROCEDURE

Glasses in the family:

$$Na_2O \cdot xAl_2O_3 \cdot (3-x)SiO_2 \qquad (6)$$

were prepared with values of x = 0.0, 0.2, 0.4, 0.6, 0.8 and 1.0. In this series the molar concentration of Na_2O was held constant while Al_2O_3 was substituted for an equimolar amount of SiO_2. These glasses are herein identified by their Al_2O_3/Na_2O molar ratios or x-values. In this manner, $Na_2O \cdot 3SiO_2$ was labeled 0.0 glass and $Na_2O \cdot Al_2O_3 \cdot 2\ SiO_2$ was labeled 1.0 glass.

The specimen preparation and testing procedures for the constant moment double cantilever beam analysis have been previously reported[9]. The glasses for dynamic fatigue analysis were cut into rectangular bars approximately 2.5 cm x 0.25 cm x 0.25 cm. The bars were ground with 600 grit SiC paper such that opposite sides were parallel, and adjoining sides perpendicular. One face was polished with 15 μm diamond paste. All specimens were annealed after polishing.

The dynamic fatigue specimens were indented in the center of the polished face using a Vicker's indenter. The indentation load was constant (8.73 N) for all compositions investigated. A surface flaw approximately 100 μm in depth resulted. Consistent with the analysis of Fuller, Lawn and Cook[8], no attempt to remove the residual stress around the indentation was attempted.

Five specimens of each composition were broken immediately after indentation in four point bending at constant crosshead speeds of 1.61×10^{-6} m/s, 7.2×10^{-7} m/s, 1.69×10^{-7} m/s, and 4.23×10^{-8} m/s on an Instron tensile testing machine. The polished face was the tensile surface in each case. All compositions were tested in deionized water (pH 5). In addition, specimens of 0.0, 0.6 and 1.0 glass were tested in NaOH solution (pH 11). The size of the fracture initiating cracks were obtained by direct measurement with an optical microscope.

RESULTS

The results of the constant moment double cantilever beam (CM-DCB) analysis have been reported[9]. The reader is referred to that study for the experimental stress intensity - crack velocity data which will not be reproduced here. Figure 1 summarizes the slopes of the log v-log K_I plots determined from that CM-DCB data.

The results of dynamic fatigue experiments on the 0.0, 0.2, 0.4, 0.6, 0.8, and 1.0 glasses are shown in Figures 2, 3, 4, 5, 6 and 7 respectively. The n-values calculated from these data are also given in Figure 1. Figure 8 shows the variation in the critical flaw size for the 0.0 glass tested in water and NaOH solution as a function of stressing rate. Table I lists the fracture stresses and critical flaw sizes for the 0.0 glass tested in water and NaOH solutions at a crosshead speed of 4.23×10^{-8} m/s.

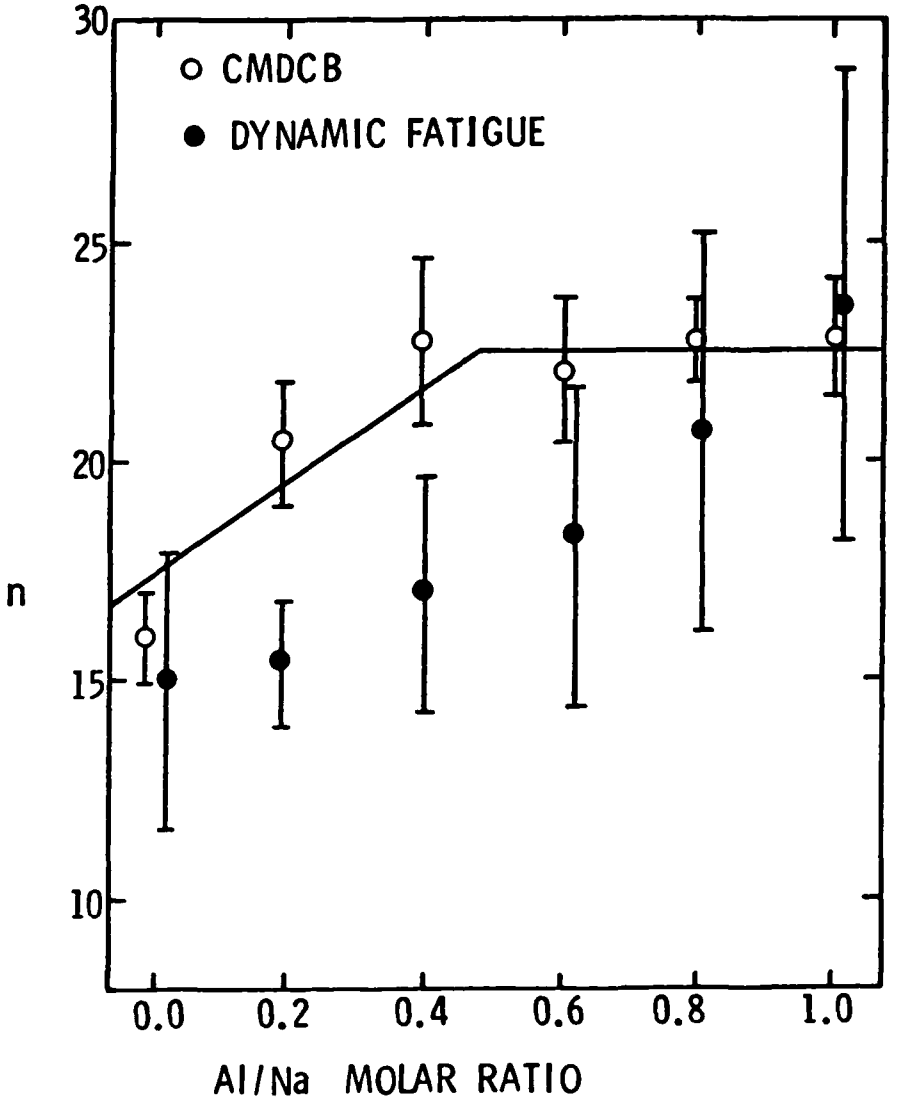

Figure 1. The n-parameters for a systematic series of sodium-aluminosilicate glasses [$Na_2O \cdot xAl_2O_3 \cdot (3-x)SiO_2$]; obtained by dynamic fatigue (using controlled microflaws) and the constant moment double cantilever beam technique.

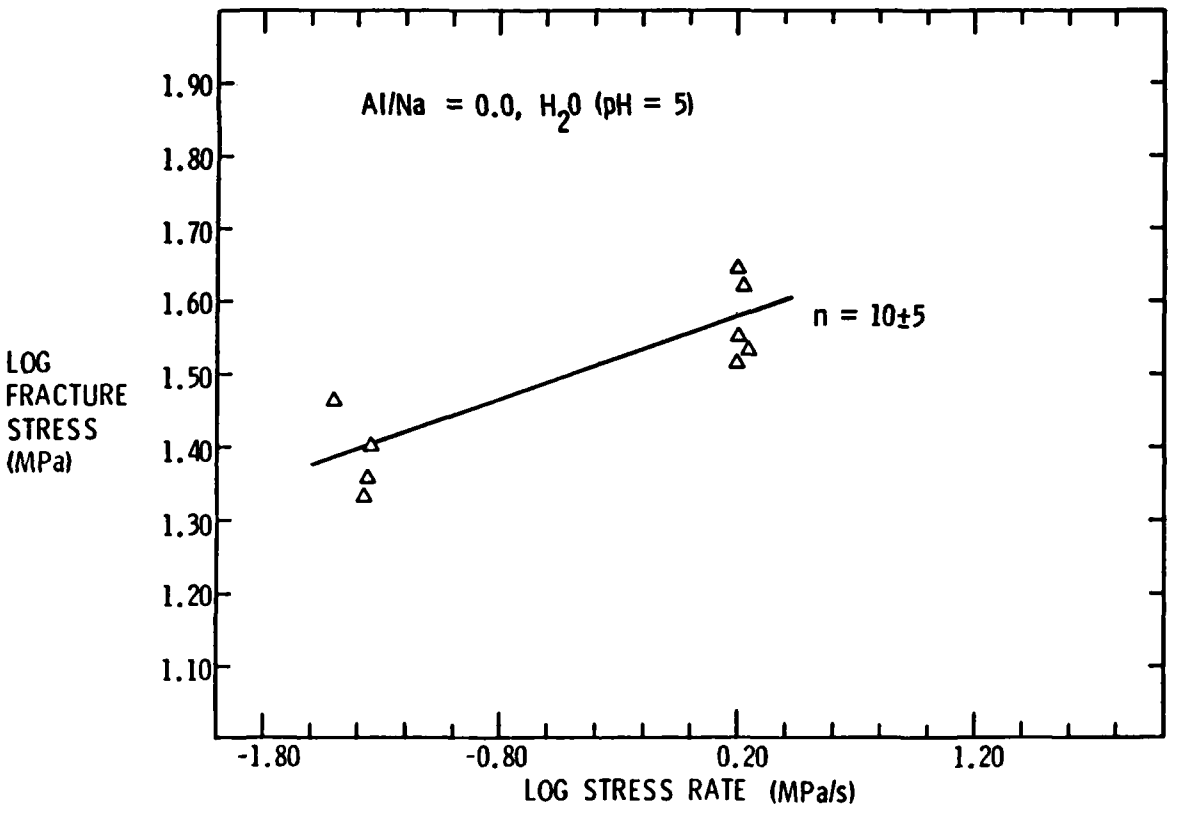

Figure 2a. Dynamic fatigue plot for $Na_2O \cdot 3SiO_2$ in deionized water.

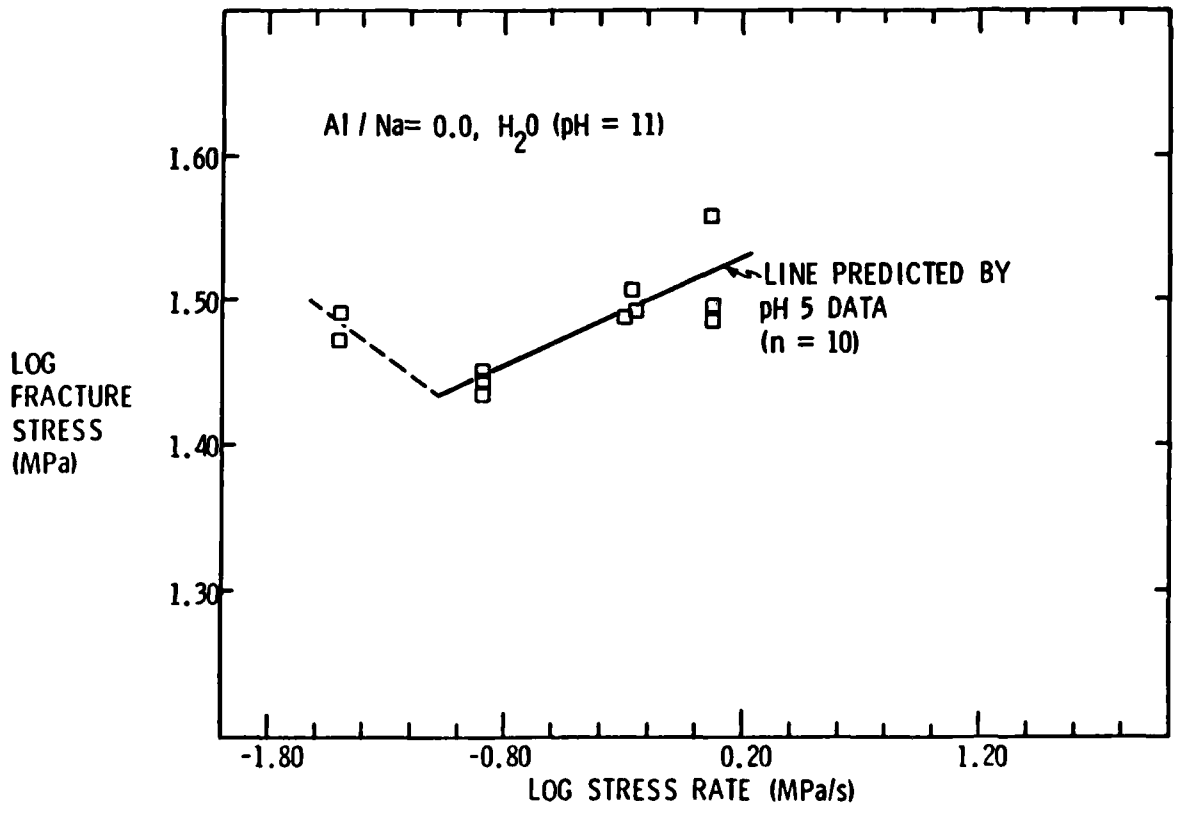

Figure 2b. Dynamic fatigue plot for $Na_2O \cdot 3SiO_2$ in pH 11 NaOH solution.

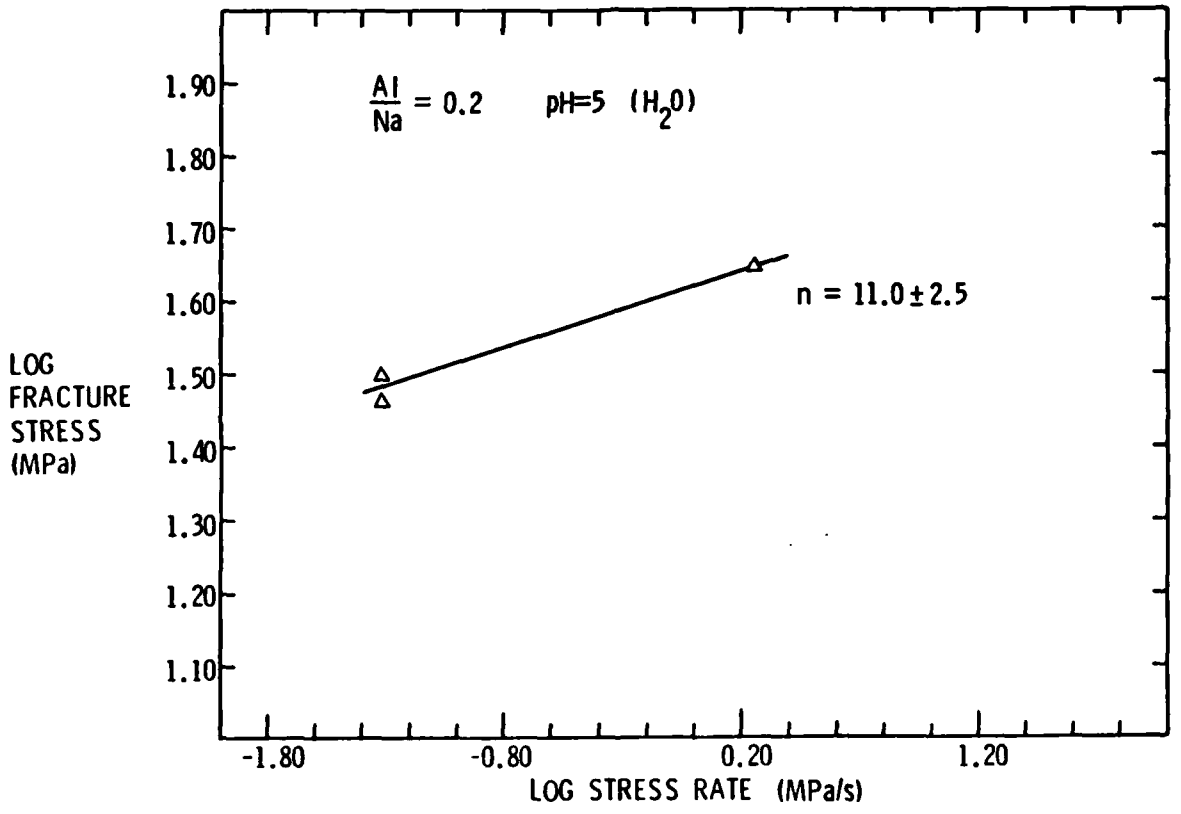

Figure 3. Dynamic fatigue data for $Na_2O \cdot 2Al_2O_3 \cdot 2.8SiO_2$ in deionized water.

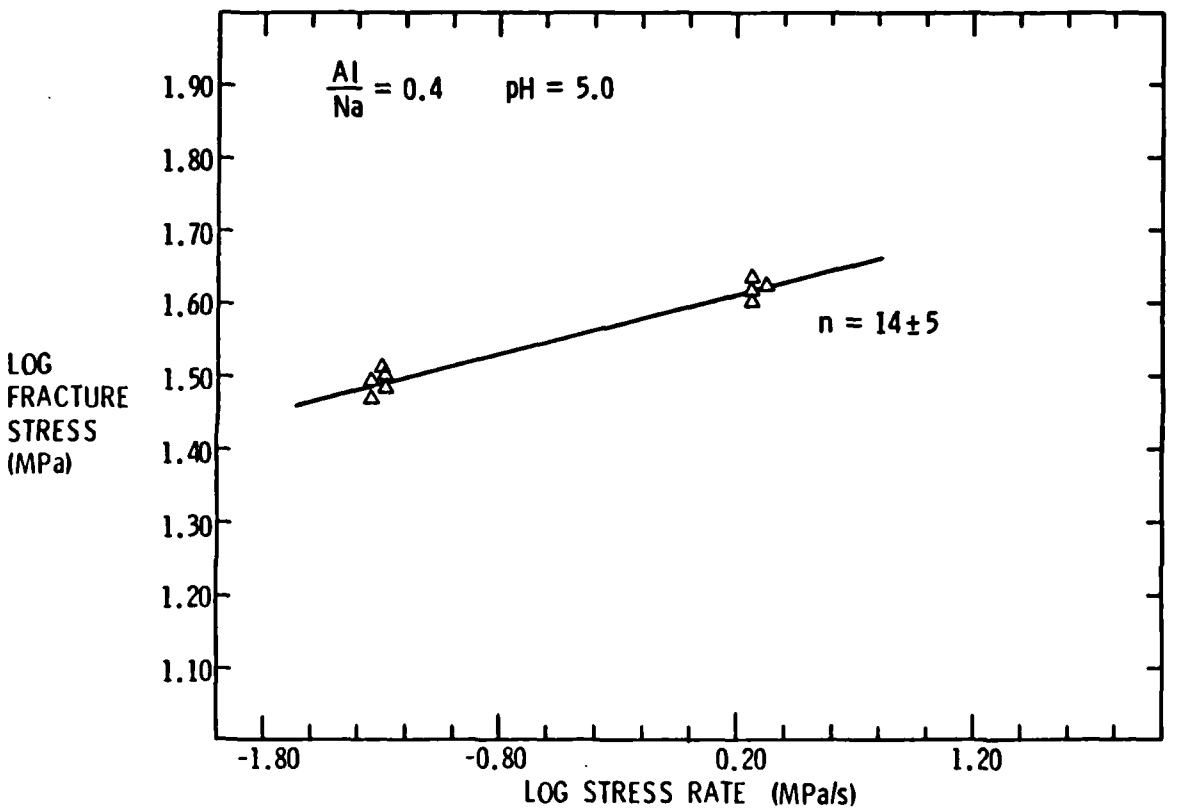

Figure 4. Dynamic fatigue data for $Na_2O \cdot 4Al_2O_3 \cdot 2.6SiO_2$ in deionized water.

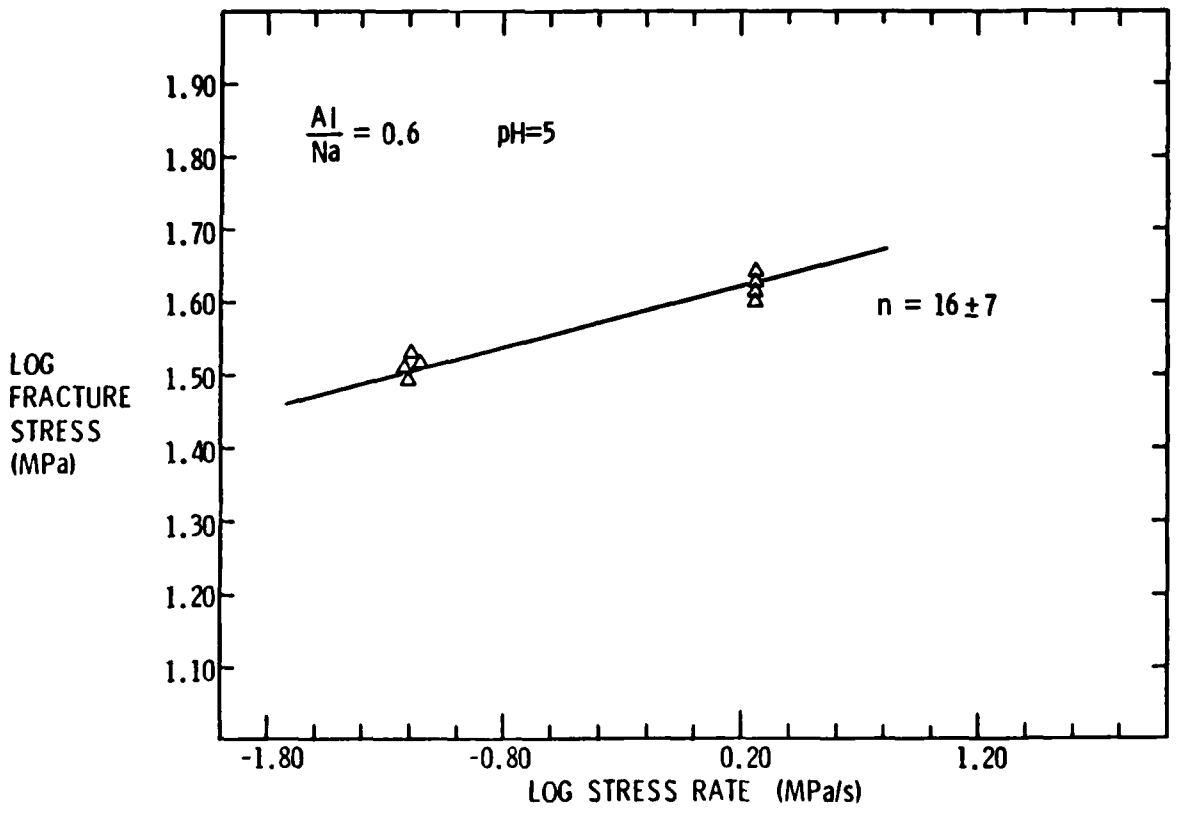

Figure 5. Dynamic fatigue data for $Na_2O \cdot 6Al_2O_3 \cdot 2.4SiO_2$ in deionized water.

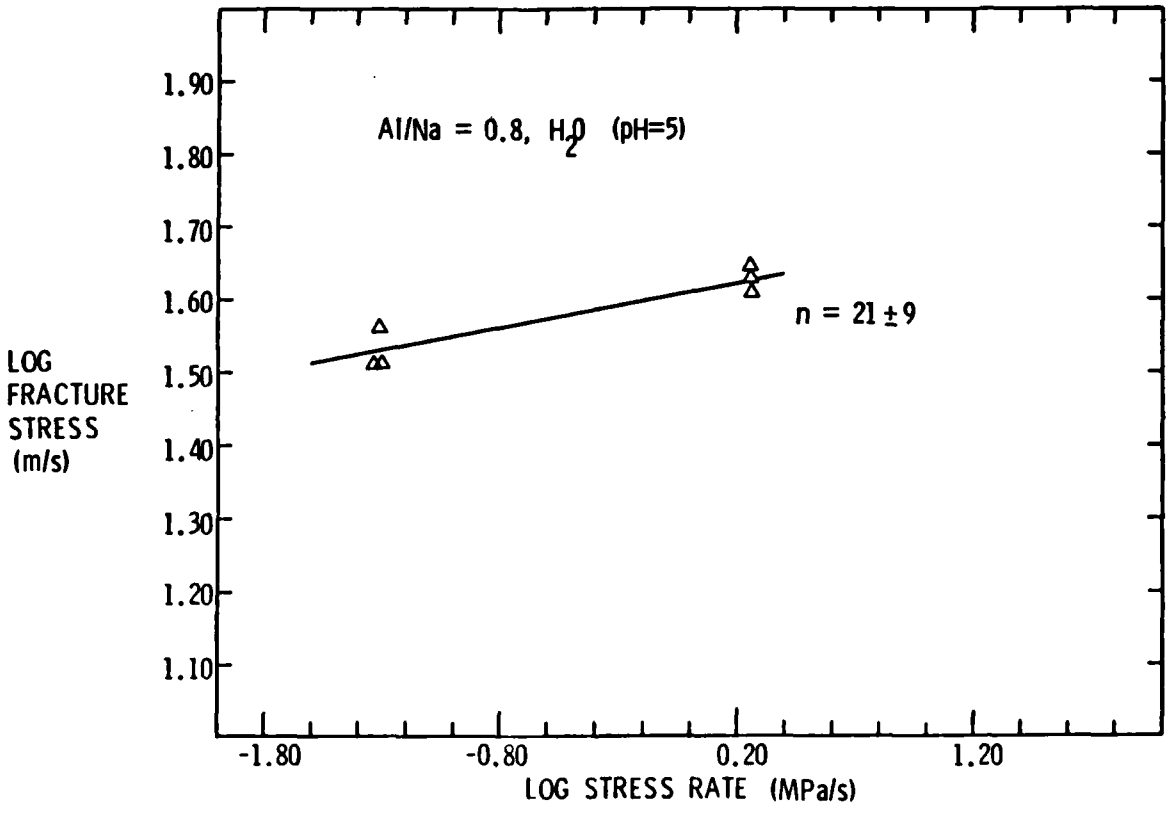

Figure 6. Dynamic fatigue data for $Na_2O \cdot 8Al_2O_3 \cdot 2.2SiO_2$ in deionized water.

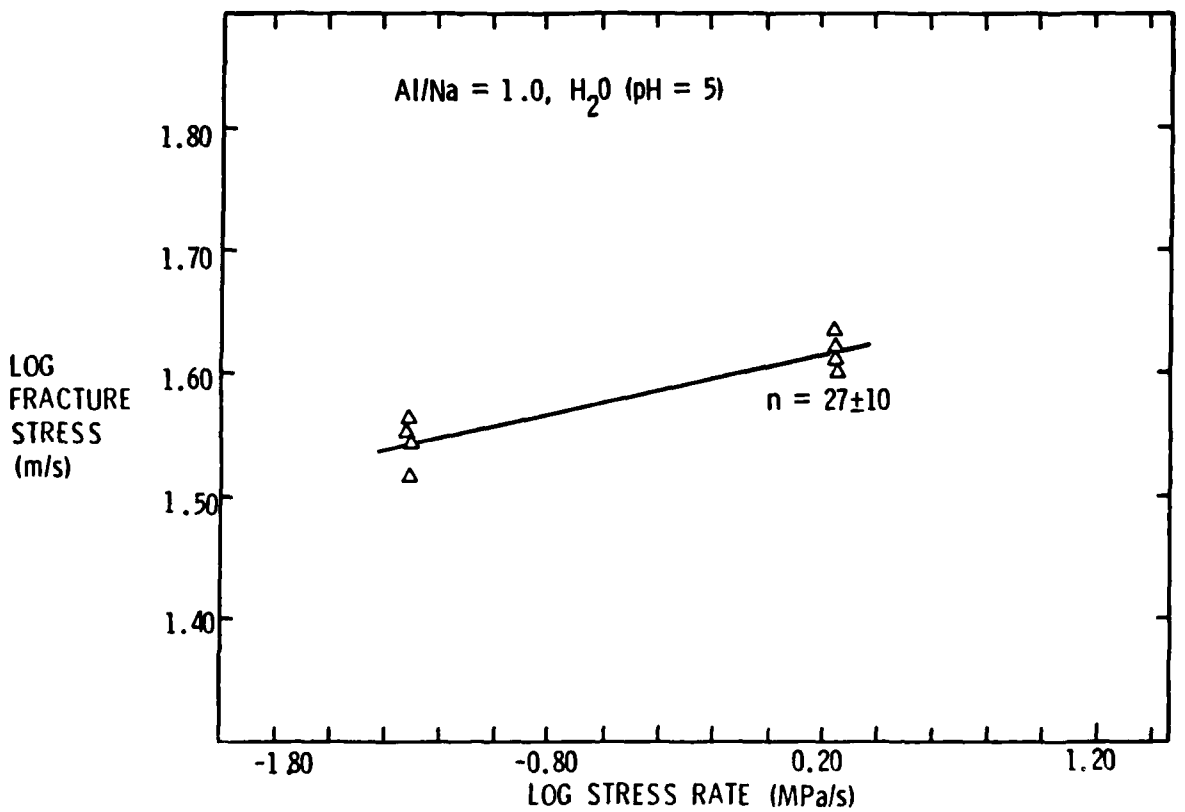

Figure 7. Dynamic fatigue data for $Na_2O \cdot Al_2O_3 \cdot 2SiO_2$ in deionized water.

DISCUSSION

The slope, n, as determined by the CM-DCB technique ranged from 16 to 23 which is typical of silicate glasses.[10] Figure 1 shows that n increased linearly with Al_2O_3 concentration for 0.0, 0.2, and 0.4 glasses. However, n for 0.6, 0.8 and 1.0 glasses was invariant and equivalent to that of the 0.4 glass. These trends were determined by 'direct' observation of crack tip extension for large cracks and, was reported to be readily explained by the elastic properties.[9]

The Fuller, Lawn and Cook[8] method of dynamic fatigue resulted in the variation of n with composition as shown in Figure 1. The n-value increased in a non-linear manner with alumina concentration over a range of 10 to 27. Clearly, the n-values obtained by the two techniques are not identical over the compositional range.

It is also noteworthy that the error observed in the dynamic fatigue analysis is approximately 300% greater than that observed for the CM-DCB analysis. This results from the manner in which the dynamic fatigue data must be statistically analyzed. In dynamic fatigue analysis:

$$n' = \frac{1}{\text{slope}} - 1 \tag{7}$$

The error in n' is defined by:

$$\text{error } (n') = \frac{\text{error(slope)}}{(\text{slope})^2} \tag{8}$$

Since the n' value is typically much greater than one, the slope is much less than one. Equation 8 results in a large error in n'. Subsequently, the error in the "true" n value is defined by:

$$\text{error}(n) = 1.33[\text{error}(n')] \tag{9}$$

Thus the dynamic fatigue technique utilizing indentation analysis is inherently less sensitive to measuring n than the CM-DCB technique. Nevertheless, the

difference in n-values between the two measurement techniques are outside the range of experimental error.

Multi-Region Crack Growth

In addition to the larger error in the indentation-dynamic fatigue analysis, there is an inherent difference between dynamic fatigue data and CM-DCB data. Dynamic fatigue data is taken over a range of stress intensity levels from 0 up to a critical value, K_{Ic}. Thus the crack spends time in the various $V\text{-}K_I$ regimes for different periods of time. Depending on the initial crack size the jump from zero to the initial stress intensity is abrupt and continues at a different rate depending on the stressing rate and the initial crack size. Thus the final failure condition is an integrated effect over almost the entire $V\text{-}K_I$ curve including Regions I, II and III and 0 (threshold). The process is more complicated with the residual stress present due to the indentation, but in principle the same conclusion holds. The slope one measures in dynamic fatigue, then, is really a combination of Regions 0, I, II, and III. However, the slope reported for the $V\text{-}K_I$ data obtained with the CM-DCB technique is only Region I!

Fuller[5] showed that for static fatigue experiments, the individual points in the time-to-failure plots could be related to specific points on the $V\text{-}K_I$ curve (many of which were actually in the threshold region). However, the sum total of the points on the static fatigue curve did not result in a slope corresponding to the n value of Region I in the $V\text{-}K_I$ data. A comparable effect is expected in dynamic fatigue data, but with the important difference that the stress is varying along with the stress intensity. This is a complication that renders a detailed mathematical analysis difficult, but the phenomenology is essentially identical. In general, then, one cannot expect to derive the same n value from the two types of experiments in glasses which exhibit multiregion crack growth.

Residual Stress Effects

In general, the n-values were insensitive to pH, but the 0.0 glass tested in 10^{-3} M NaOH solution exhibited anomalous behavior at low stressing rates (Figure 2b). The fracture stress increased with decreasing stressing rate as opposed to the decrease observed when this composition was tested in water. This type of upturn in fracture stress at low stressing rates has been observed by Yavuz, Tressler, and Minford[11] for SiC tested at high temperatures. They hypothesized the behavior to result from crack tip blunting.

Other work[12] with these glasses has shown that the time to repropagate the crack on a CM-DCB specimen after aging under water is approximately the same for the x = 0, x = 0.6 and x = 1.0 glasses. Since these glasses have enormously different corrosion behaviors, these results suggest that crack blunting during aging cannot explain the delay time before crack propagation; i.e., one would expect different amounts of blunting due to the large differences in corrosion behavior for these glasses. Thus, an alternate explanation is required for the upturn in strength at low stressing rates. This alternate explanation can be the relief of residual stress.

Anstis and co-workers[13] have shown that an indentation crack system consists of two crack systems: radial and lateral. Extension of the lateral cracks was shown to be responsible for residual stress relaxation whereas extension of radial cracks was shown to be responsible for the strength decrease in bend bars. Since the total stress intensity, $K_{I_{tot}}$, experienced by a specimen consists of two components:

$$K_{I_{tot}} = K_{I_{applied}} + K_{I_{residual}}, \qquad (10)$$

the critical condition is met when $K_{I_{tot}}$ reaches the fracture toughness, K_{Ic}. If $K_{I_{residual}}$ is reduced due to lateral crack extension prior to failure, $K_{I_{applied}}$ must necessarily increase. In this manner, the applied stress at failure is larger if the residual stress is relaxed before failure.

A more distinct low velocity plateau was observed for the 0.0 glass tested at pH 11 than when tested in water (Figure 2b). Moreover, the threshold decreased to a lower value in pH 11 solution (NaOH). The change in residual stress intensity is determined by the change in lateral crack size:

$$K_{I_{residual}} = \frac{\chi_R}{C_i^{3/2}} - \frac{\chi_R}{C_f^{3/2}} \qquad (11)$$

where: χ_R = constant = 0.016

P = indentation load

C_i = initial crack size

C_f = final crack size

The extension of the lateral cracks would be expected to progress at a much faster rate in a pH 11 solution relative to water because dissolution, and hence corrosion, occurs much more rapidly in this solution. Also, lateral crack extension is expected at lower levels of $K_{I_{residual}}$. Therefore, greater reductions in residual stress, and larger lateral cracks at failure, are anticipated in the 0.0 glass tested in pH 11 relative to water. This is a rate dependent phenomenon since a certain amount of time is required for crack extension, and hence, residual stress relaxation. Thus, it is reasonable that it is only observed at the low stressing rates.

The applied stress intensity is determined by both the crack length, c, and applied stress, σ_{app}:

$$K_I = Y\sigma_{app}\sqrt{c} \qquad (12)$$

where Y = geometric and location constant.

It is apparent that for a given level of applied stress, a larger (or longer) crack results in a larger stress intensity. It is hypothesized that the long lateral cracks at pH 11 grow along with the radial cracks during strength testing. In contrast, the 'short' lateral cracks obtained in water are stable while the radial cracks grow. Thus, we predict higher fracture stresses and lower critical flaw sizes in pH 11. The higher fracture stresses have already been demonstrated. The critical flaw sizes are shown in Figure 8. Although the flaw sizes are comparable for the three higher stressing rates, the flaw sizes are indeed smaller at the low stressing rate for pH 11 compared to water. This supports the concept that the observed upturn in fracture stress in pH 11 is due solely to residual indentation stress effects and is not caused by blunting.

Additional evidence that residual stress was responsible for the upturn was obtained by removing the residual stress prior to testing via a post-indentation anneal cycle. Table I shows that both the fracture stress and flaw size were comparable for pH 5 and 11 when tested after annealing. Wiederhorn et al.[6] argue that it is unlikely that the behavior of large cracks differ significantly from small cracks when only Region I or Region III crack growth is involved in degrading the strength. Recall that Region I is environmentally dependent and Region III is environmentally independent crack growth. Region II, however, is the combined effect of Region I and Region III crack growth behavior, and will influence crack growth differently for small and large cracks. In Regon II, the portion of the crack away from the surface moves slower than the portion nearer the surface because of water depletion. Thus, the shape of cracks are changed due to the water content near the crack boundary. Because of the difference in

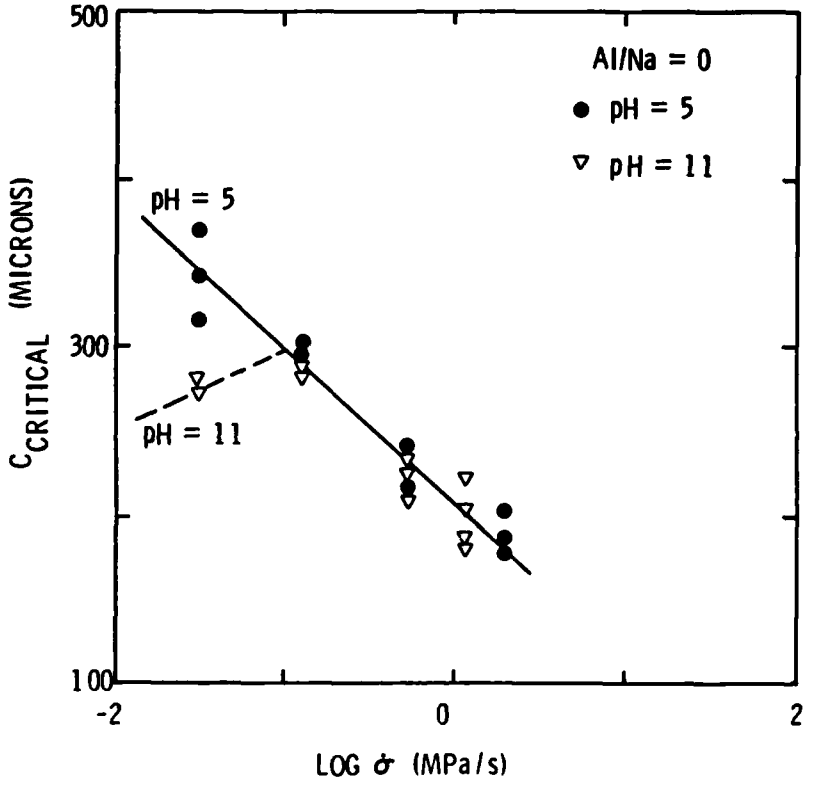

Figure 8. The flaw sizes measured after strength testing the indented $Na_2O \cdot 3SiO_2$ glasses at various rates; note the decrease in flaw size at low stressing rates in alkaline solution.

TABLE I

4-Point Flexure Test of $Na_2O\ 3SiO_2$ Glass

Annealed (480°C for 1 hr)

pH	Fracture Stress (MPa)	Flaw Size (μm)
5	45 ± 9	92 ± 29
11	44 ± 4	104 ± 5

Crosshead speed ~4 x 10^{-8} m/s

the crack shapes between large (flat) and small (elliptical) cracks in the two tests, respectively, physical constraints on the crack front would be expected to be different for the two types of cracks; i.e., crack growth in Region II is not expected to be the same for the two type of cracks. Although we cannot demonstrate unequivocally the validity of our hypothesis, it seems reasonable that the two cracks will behave differently. Elliptical cracks can vary by as much as 50% in K_I along the perimeter while K_I at flat cracks is expected to be nearly constant except near the sides.

CONCLUSIONS

The absolute values of n determined by dynamic fatigue were generally lower than those determined by the CM-DCB technique. This is because the CM-DCB test measures the velocity of a crack at a given stress intensity, whereas the dynamic fatigue test measures velocities along various parts of the $V-K_I$ curve depending on the initial crack size and loading rate. The dynamic fatigue n parameters were consistent with the double cantilever beam analyses in showing that pH had little effect on n, while the observed 'upturn' in fracture stress at low stressing rate observed for the 0.0 glass was related to the low velocity plateaus observed in the stress intensity - crack velocity curves through corrosion and residual stress. In the threshold region and in Region II, the geometry difference between dynamic fatigue tests with semi-elliptical small cracks and the CM-DCB test with large straight cracks further accounts for some of the apparent difference in slow crack growth behavior. Finally, it was shown that dynamic fatigue analysis produced n parameters exhibiting larger errors when compared with n parameters obtained by the constant moment double cantilever beam technique. This difference is due to the inherent error for the indentation-dynamic fatigue technique.

Thus, the major differences in n values for the CM-DCB and dynamic fatigue techniques for the sodium-aluminosilicate glasses is due to residual stress in the small cracks, the integrating effect of multiregion crack growth upon dynamic fatigue tests, and to a lesser extent, the consequential larger inherent error in the indentation-dynamic fatigue technique.

ACKNOWLEDGEMENT

The authors gratefully acknowledge the financial support of the Air Force Office of Scientific Research (AFOSR-82-0013).

REFERENCES

1. K. Jakus, D. C. Coyne and J. E. Ritter, Jr., "Analysis of Fatigue Data for Lifetime Predictions for Ceramic Materials," J. Mater. Sci., 13, 2071-2081 (1978).

2. J. E. Ritter and C. L. Shellburne, "Dynamic and Static Fatigue of Silicate Glasses," J. Am. Ceram. Soc., 54, 601-605 (1971).

3. J. E. Ritter and S. M. Wiederhorn, "Application of Fracture Mechanics in Assessing Against Fatigue Failure in Ceramic Compounds" in Ceramics For High Performance Applications III: Reliability (Lenz, Katz and Burke, Eds., AMMRC Technical Conference VI, Plenum Press, 1981).

4. J. E. Ritter, P. B. Oates, E. Fuller and S. M. Wiederhorn, "Proof Testing of Ceramics: I Experiments, J. Mater. Sci., 15, 2275-2281 (1980).

5. E. R. Fuller, Jr., "Determining Crack Growth Behavior From Delayed Failure Tests" Bull. Am. Ceram. Soc., Abstr. 5B80 (1980).

6. S. M. Wiederhorn, S. W. Freiman, E. R. Fuller, Jr. and H. Richter, "Effect of Multiregion Crack Growth on Proof Testing" in Methods for Assessing the Structural Reliability of Brittle Materials, ASTM STP 844, (S. W. Freiman and C. M. Hudson Eds, American Society for Testing and Materials, Phila. PA, 1984) pp. 95-116.

7. A. G. Evans, "Slow Crack Growth in Brittle Materials Under Dynamics Loading Conditions," Int. J. Fracture, 10, 251-59 (1974).

8. E. R. Fuller, Jr., B. R. Lawn and R. F. Cook, "Theory of Fatigue for Brittle Flaws Originating From Residual Stress Concentrations," 66(5), 314-321 (1983).

9. D. N. Coon, J. J. Mecholsky, C. G. Pantano, "Relationship Between Elastic Properties and Slow Crack Growth Behavior in Sodium-Aluminosilicate Glasses" J. Am. Ceram. Soc., to be published.

10. S. W. Freiman, "Fracture Mechanics of Glass" in Glass Science and Technology: Elasticity and Strength in Glasses - Vol. 15 (D. R. Uhlmann and N. J. Kreidl, Eds., Academic Press, New York, 1980) pp. 21-78.

11. B. Yavuz, R. E. Tressler and E. Minford, "Simulation of Dynamic Fatigue Test of Silicon Carbide at Elevated Temperature," to appear in J. Am. Ceram. Soc., 1986.

12. D. N. Coon, J. J. Mecholsky and C. G. Pantano, "Effect of Aging of Na_2O xAl_2O_3 $(3-x)SiO_2$ Glasses on Crack Propagation," J. Am. Ceram. Soc. to be published.

13. G. R. Anstis, P. Chantikul, B. R. Lawn and D. B. Marshall, "A Critical Evaluation of Indentation Techniques for Measuring Fracture Toughness: I. Direct Crack Measurements," J. Am. Ceram. Soc., 64, 533-38 (1981).

CHAPTER VI

SURFACE CHEMISTRY AND SLOW CRACK GROWTH BEHAVIOR OF FLUOROZIRCONATE GLASSES

by

Carlo G. Pantano

Department of Materials Science and Engineering

Pennsylvania State University

University Park, PA 16802

To appear in Infrared Fiberoptics (Proceedings of a NATO Advanced Research Workshop, 1986).

SURFACE CHEMISTRY AND SLOW CRACK GROWTH BEHAVIOR OF FLUOROZIRCONATE GLASSES

Carlo G. Pantano
Department of Materials Science and Engineering
Pennsylvania State University
University Park, PA, USA, 16802

ABSTRACT

The surface chemical reactions which might contribute to stress corrosion in fluorozirconate glasses have been investigated and the results are related to the slow crack growth behavior of these glasses. The surface studies indicate that aqueous environments are especially aggressive. It is found that the penetration and bulk diffusion of molecular water precedes any hydrolysis or dissolution of the glass structure. The chemisorption of water to produce oxide or hydroxide species is not prevalent except in the case of the basic aqueous environments. The most notable feature of the stress intensity-crack velocity diagrams is a distinct and reproducible stress-intensity threshold at K_I = .15-.20 MPa-$m^{1/2}$ in the environments which contain water. This threshold is observed for both gaseous and liquid environments even though the surface chemistry and corrosion in water vapor and liquid water are very different. The wet nitrogen atmospheres exhibit a velocity plateau whose magnitude increases systematically with the water activity; it approaches the plateau observed in pure liquid water at ~10^{-3} m/s. Altogether, it appears that the crack growth mechanism may be independent of any chemisorption reactions at the crack-tip. Perhaps, the formation of a coordinate bond between molecular water and the barium or zirconium cations weakens the coulombic forces of attraction with the fluorine anions, and thereby, influences the energy necessary for crack propagation. This interaction also appears to be the first step in the corrosion reaction. It is further suggested that the stress-intensity thresholds and velocity plateaus may be related to stress-enhanced water diffusion ahead of the crack tip where it modifies both the material and stress distribution.

1. INTRODUCTION

It has already been shown that both fluorozirconate and barium-thorium fluoride glasses exhibit a susceptibility to dynamic fatigue and slow-crack growth (1). These data indicate that water is an especially active environment, but the stress intensity-crack velocity (KV) diagrams have unique characteristics relative to those observed in silicate glasses. Otherwise, very little has been reported on the fracture and stress corrosion behavior of these glasses.

In a more general sense, the stress corrosion mechanisms in ionic materials, whether glassy or crystalline, have not been clarified. In a study of slow crack growth in single-crystalline alkaline earth fluorides (CaF_2, SrF_2 and BaF_2), both H_2O and HF were found to enhance the crack-growth rate (2). The delayed failure of polycrystalline MgF_2 (3) and ZnSe (4) were also reported, and here too, water-enhanced slow crack growth was observed. Although these studies described the importance of dislocation motion and microstructure in the fracture process, they did not lead to the establishment of a stress corrosion mechanism.

In the most definitive studies of stress corrosion mechanisms in silicate glasses (5-7), the availability of an extensive data base concerning their surface chemistry (adsorption, hydration/dehydration, chemical reactivity, etc.) and corrosion behaviors was of great benefit. A comparable data base for fluoride glasses does not exist. A number of papers have appeared recently concerning the corrosion of fluoride glasses (8-15), but the reaction mechanisms are still not well understood. The adsorption and other surface chemical reactions have yet to be reported for these glasses, although some adsorption studies of water vapor on crystalline alkaline-earth fluorides have been reported (16-21).

There is no question that these fluoride glasses are susceptible to stress corrosion, and this will certainly limit many of their potential applications for infrared fiber optics. In this paper we report further on the surface chemistry and slow crack growth behavior of fluorozirconate glasses. The study of chemical effects at fracture surfaces is emphasized where methods including low-energy ion scattering (ISS), Auger electron spectroscopy (AES) and secondary ion mass spectroscopy (SIMS) are used for characterization. The constant moment double cantilever beam technique was employed to determine the slow crack growth behavior in a wide variety of liquid and gaseous environments including water, water vapor, methanol,

methanol vapor, ammonia, formamide and water-methanol mixtures. These data are used to discuss the mechanism of stress corrosion in fluoride glasses.

2. EXPERIMENTAL PROCEDURE

All of the double cantilever beam specimens were cut from a single billet of glass. The glass - whose composition is $.57ZrF_4 \cdot .36BaF_2 \cdot .03LaF_3 \cdot 04AlF_3$ (ZBLA) - was fabricated by Le Verre Fluore. The beams - appproximately 6mm x 30mm x 3mm - were cut and oriented so that the crack followed a path of constant thermal history through the glass. A 2mm wide groove - approximately 2mm deep - was machined down the center of the beam to guide the crack. The groove and faces of the glass plates were polished to eliminate residual stresses due to the machining operations. The cracks were initiated by thermal shock with a hot nichrome wire. The crack was then extended under load into the middle two-thirds of the specimen where the crack velocities were recorded. The constant moment double cantilever beam technique (22) was used with the crack elongation being monitored through a 40X traveling microscope. The specimens were enclosed in a sealed chamber which could be purged with a gaseous environment before and/or during the test. The controlled humidity environments were produced by mixing measured amounts of dry nitrogen and water-saturated nitrogen gas. The humidity was measured with a dew point hygrometer.

The clean surfaces used for adsorption studies were created by fracturing pre-notched rods of the glass in an ultra-high vacuum analytical chamber. The chamber could be baked and ion-pumped to a base pressure of less than 1×10^{-9} torr before the fracture to eliminate water vapor and other residual gases. The species present in the vacuum environment were monitored with a quadrupole residual gas analyzer. The chamber incorporated a low-energy ion scattering spectrometer (ISS) and an Auger electron spectrometer (AES) for analysis of the 'clean' surfaces before and after controlled-amounts of water vapor were introduced through a leak valve. This system was also used for the chemical analysis of fracture surfaces created externally in air and liquid environments. It is important to point out that a careful evaluation of the electron beam effects which occur during Auger analysis of these glasses was carried out; this evaluation showed that the electron beam current density must be maintained at or below 6 $\mu A/cm^2$ to prevent beam damage to the specimen.

The glasses were hydrated at elevated temperatures in a tube furnace under flowing Ar or O_2 gases which were first saturated with water vapor at 30C or 75C. These glasses, as well as those hydrated at room temperature in water-methanol liquid mixtures, were depth profiled with secondary ion mass spectroscopy (SIMS).

3. CRACK-GROWTH STUDIES

The K-V diagrams measured for ZBLA in a wide variety of environments are summarized in Figures 1 and 2. In Figure 1, the presence of a well-defined threshold - followed by a velocity plateau - appears to characterize the behavior in humid gas and in liquid water. The velocity plateau shifts to higher values with increasing water activity and reaches its maximum value in liquid water. The K-V diagrams in Figure 2 show that ammonia vapor behaves very much like a humid gas, whereas the methanol liquid, methanol vapor and formamide extend the region of slow crack growth to lower stress-intensity. The absence of a threshold or velocity plateau for the nonaqueous environments indicates that they are each active in promoting crack growth.

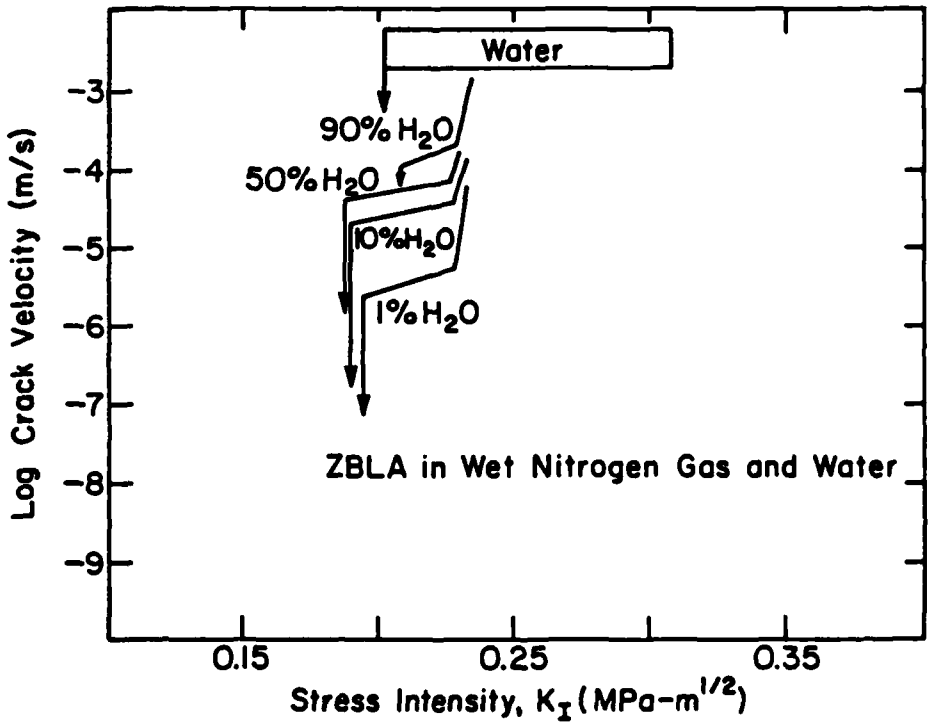

Figure 1. The stress intensity - crack velocity diagrams for a fluorozirconate glass in aqueous environments; the crack velocity in water varies over the range represented by the box.

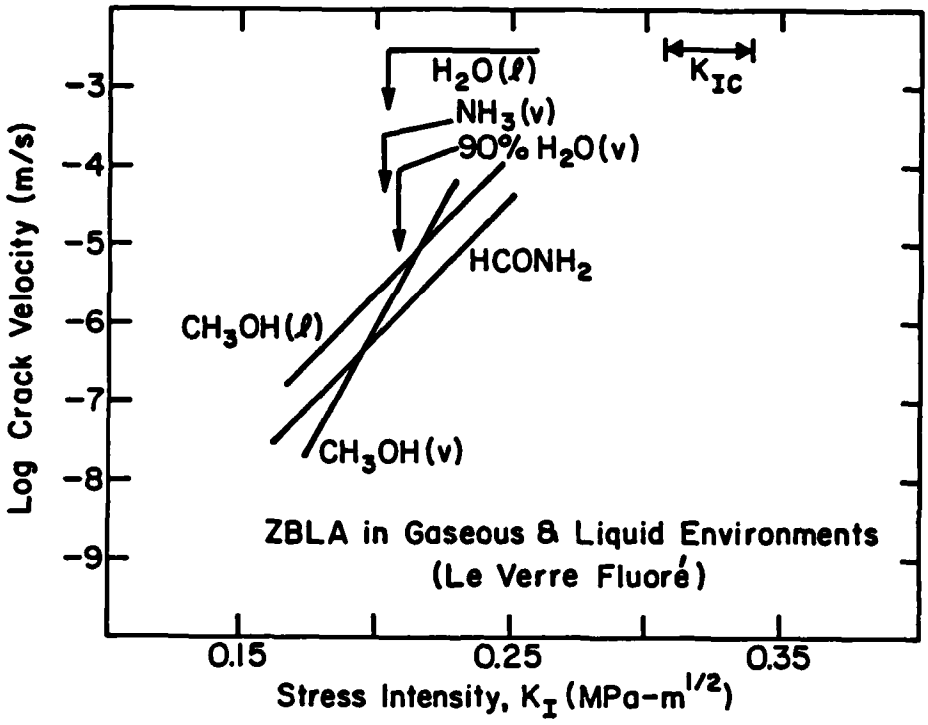

Figure 2. The stress intensity - crack velocity diagrams for a fluorozirconate glass in aqueous and non-aqueous environments.

It is interesting to note that decreasing the activity of water vapor in the inert nitrogen gas phase systematically lowers the velocity plateau, whereas decreasing the activity of liquid water by dilution with methanol yields a straight line whose slope depends upon the water activity (1). The slope of this line can be used to define the stress corrosion susceptibility (n) which is ~77 in pure methanol and is ~40 in methanol containing 1-5% water. The absence of thresholds and plateaus in the water-methanol mixtures suggests that these features may be related to the formation of a surface reaction product between adsorbed or liquid water and the glass. The reaction products can be neutralized or carried away by the methanol 'solvent' in the liquid mixtures but not in the humid gas. In pure water, these reaction products probably accumulate in the crack, whereas in the pure methanol vapor and formamide they may not form. Later, it is suggested that HF may be a surface reaction product which is unique to the environments which exhibit thresholds and velocity plateaus.

It is quite clear that water is an aggressive crack growth agent. This is consistent with the aqueous corrosion behavior of fluorozirconate

glasses where rapid and extensive surface hydration, dissolution and crystalline reaction product formation are evident (8-15). This corrosion reaction is greatly accelerated in acidic solutions, but is practically non-existent in basic solutions. For this reason, additional crack growth measurements were made in a pH 11 ammonium hydroxide solution. The K-V diagram in this solution was comparable to the curve for liquid water. Nonetheless, these fracture surfaces were free of any visible degradation whereas in the pure water environments a highly corroded surface is typically observed.

Additional crack growth measurements were made in mixtures of methanol and either acid or base. The pH of the mixtures was systematically varied between 1 and 12. These data are shown in Figure 3 and they, too, indicate an insensitivity of the crack velocity to pH. The data points are scattered about a line whose slope gives an n value of about 40. In view of the obvious pH dependence of the corrosion and dissolution reactions (15), these observations suggest that the stress corrosion mechanism in fluorozirconate glasses may be distinct relative to the corrosion mechanism.

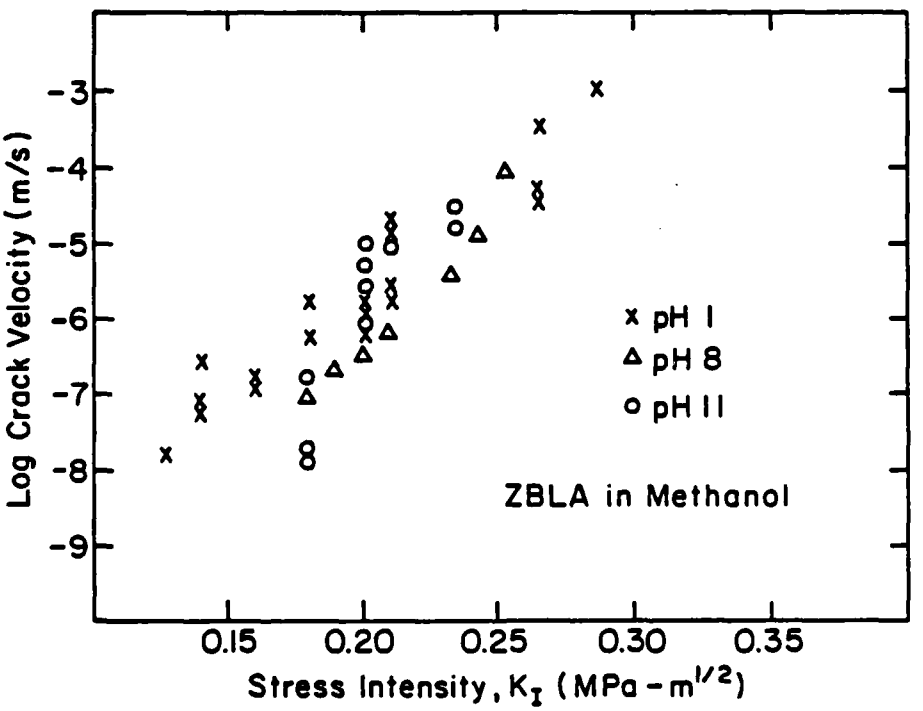

Figure 3. The sub-critical crack velocities measured in mixtures of methanol and either water, acid or base; in all cases, the water content is less than 1%.

4. SURFACE STUDIES

The reaction of clean fracture surfaces exposed to water vapor, as well as the composition of fracture surfaces created in various environments, have been investigated with ion-scattering spectrometry (ISS) Auger electron spectroscopy (AES) and secondary ion mass spectroscopy (SIMS).

The ISS technique is sensitive to the elemental composition of the outermost atomic layer of a solid. It has been used here to determine whether oxidation and/or the chemisorption of water are prevalent reactions in the surface monolayer of clean fracture surfaces. The upper spectra in Figure 4 represents a clean surface created by fracturing a rod of ZBLA glass under ultra-high vacuum conditions. The peaks due to F and Al are clearly evident, whereas the peaks due to Zr, Ba and La exhibit some overlap. The fact that the fluorine signal is strong - in spite of its lower scattering cross-section relation to zirconium and barium - indicates that the fluorine ions shield the cations at the surface, and thereby, dominant the sites in the surface monolayer. Clean fracture surfaces of this type have been exposed in-situ to air and water vapor, and in both cases, no oxygen signal due to oxide, hydroxide or water adsorption was detected. In contrast, creation of the fracture surface in air leads to the adsorption of some oxygen (or hydroxyl) as shown in the second spectra of Figure 4. This suggests that active surface adsorption sites may be generated by the stress which is present during the fracture event. In general, though, the extent of oxygen chemisorption in the outermost monolayer of the fracture surfaces is minimal.

A similar ISS analysis of water adsorption was reported by Strecker (21) for clean surfaces of single-crystal CaF_2. He found that water adsorption was practically non-existent until the temperature was lowered to the point where an epitaxial condensation of water was observed. His data also provided an indication of the monolayer sensitivity of this method; i.e., condensation of a single monolayer of water was sufficient to completely extinguish the Ca and F peaks in the ISS spectra, and correspondingly, to generate a strong oxygen signal. Thus, the oxygen or water coverage represented in the middle spectra of Figure 4 is small indeed.

The lower spectra in Figure 4 represents a surface created by fracture in water. Due to the aggressive reaction between fluorozirconate glass and water, though, one must recognize that the surfaces have been corroded

in the water after the fracture. Nonetheless, the absence of an oxygen signal indicates that oxide and/or hydroxide reactions products are not abundant at the glass/solution-interface, nor within any associated surface layer. Rather, the spectra reveals the presence of only Zr and F. This is probably due to the local precipitation and accumulation of ZrF_2 in the surface. Others have shown the eventual formation of ZrF_4 crystals at the surface of ZBLA after an extended exposure to water (12).

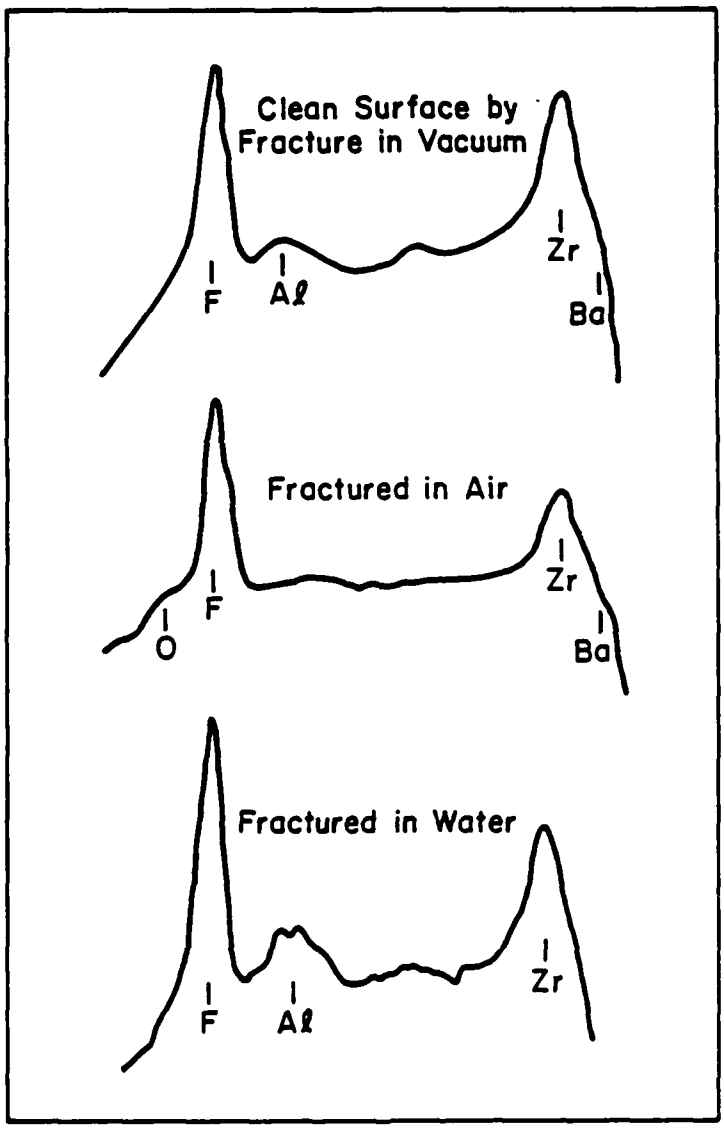

Figure 4. Low-energy ion scattering spectra (^4He at 1.5 KeV) for fracture surfaces of ZBLA.

The ISS studies have shown that neither the chemisorption of water, nor the formation of oxides and hydroxides, are prevalent reactions at the surface of ZBLA. However, the heavy Zr and Ba cations are responsible for the high background in the low energy region of the ISS spectra, and for this reason, the sensitivity to oxygen is less than ideal. And since the low energy ion scattering occurs almost exclusively in the outermost atomic layer, it is also possible that ion scattering by oxygen, hydroxyl or water species is physically shielded at the surface by the heavier cations. Thus, a corresponding set of surface analytical studies were attempted with Auger electron spectroscopy (AES). The AES technique averages the elemental composition in the outermost 3.0-5.0 nm of the surface; moreover, the AES method is exceedingly sensitive to oxygen.

The Auger spectra in Figure 5 show that oxygen can be detected by AES even on the fracture surfaces created in vacuum, but it is not yet known whether this oxygen is intrinsic to the glass or was adsorbed from the residual vacuum via electron-beam stimulated adsorption (23). In any event, it corresponds to a relatively low concentration (~5-6 atomic percent). After in-situ exposure to ~1800 Langmuirs of water vapor, the Auger spectra showed no substantial increase in oxygen, but the zirconium signal was eliminated and some increase in the fluorine signal was observed. The attenuation of the zirconium signal could be due to shielding by some adsorbed species, but it is unlikely that this species is water because it would have produced a significant increase in the oxygen signal. The fact that hydrogen is undetectable by AES suggests that a hydrogen species may be involved. The observed increase in fluorine concentration leads one to consider HF surface reaction products. The HF could form due to a reaction between ZBLA and H_2O with the resulting hydroxyl specie diffusing further into the glass.

The other spectra in Figure 5 was obtained on a fracture surface created in air. One notes again that little oxygen is present on the surface, but a carbon signal-presumably an adsorbed hydrocarbon-is observed. After the analysis of six fracture surfaces created in air, it became apparent that the oxygen content could vary between 5% and 10%. The C and O ratio was not constant, and so, hydrocarbons, rather than CO or CO_2, may be involved. In general, though, the spectra in Figure 5 further support the contention that these fracture surfaces are not especially reactive in humid atmospheres. The oxygen species - whatever

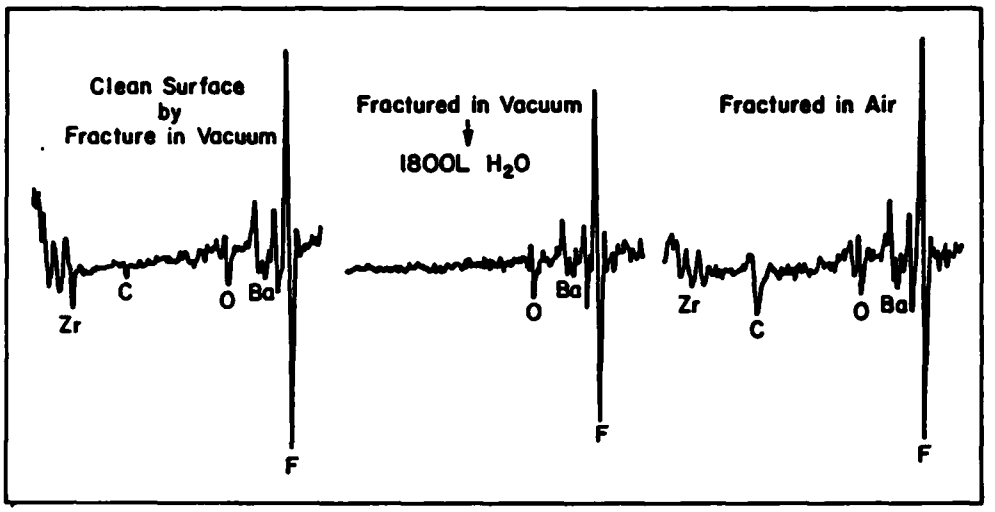

Figure 5. Auger spectra for fracture surfaces of ZBLA; the center spectra represents the clean vacuum-fractured surface after exposure to 1800 Langmuirs of water.

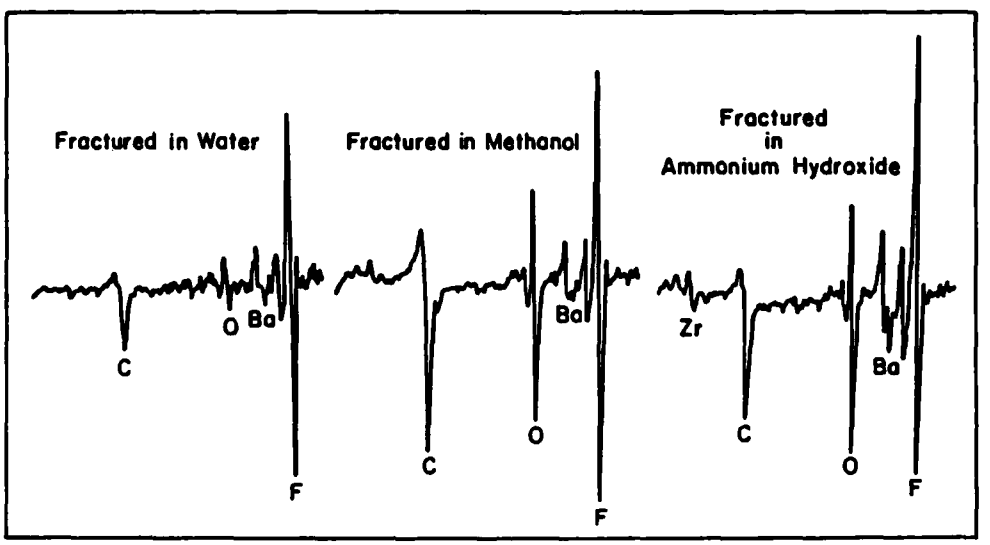

Figure 6. Auger spectra for surfaces of ZBLA which were created by fracture in liquid environments; the spectra in Figures 5 and 6 were obtained using a 3KeV electron beam at ~6uA/cm^2.

they are - do not cover the surface, but rather, are present at a relatively low concentration (at least relative to the anion content of the ZBLA glass).

The Auger spectra in Figure 6 represent the influence of some liquid environments upon the surface composition. In all cases, the glasses were fractured under the liquid, and then, were immediately extracted and dried in a stream of dry nitrogen. The specimen fractured under water shows a significant attenuation of the barium and zirconium signals, some carbon, and background levels of oxygen; the obvious decrease in the [Ba,Zr]-to-[F] ratio, again, points to the possible formation of HF reaction products on the surface. In contrast, the glasses fractured in methanol and ammonium hydroxide show substantial increases in oxygen content. The oxygen concentration represented in these two spectra is approximately 20 atomic percent. The fact that nitrogen is not detected at the surface created in the ammonium hydroxide indicates that specific adsorption of oxygen or hydroxyl has occurred. The presence of these oxygen levels at the surface has not attenuated the fluorine signal, and so, the exchange of F and OH seems unlikely even in the highly basic hydroxide solution. A noticeable increase in carbon content was always observed on fracture surfaces created in the ammonium hyroxide which may be due to enhanced adsorption of hydrocarbon, or possibly CO/CO_2 adsorption, at oxidized or hydroxylated surface sites. The surfaces created under methanol consistently showed increases in both the oxygen and carbon, and in general, the C to O ratio was usually larger than that observed for all other surface conditions. This suggests a strong physical adsorption of the methanol species, especially since the exposure to ultra-high vacuum has not triggered their desorption. In the case of alkali-chlorides, bromides and iodides, the physical adsorption of methanol has been observed and attributed to hydrogen bonding with the surface anions (24).

The SIMS technique has been used to depth profile a wide variety of ZBLA glass surfaces after exposure to humid and aqueous environments. In contrast to AES and SIMS, this method is relatively insensitive to the outermost atomic layer(s) of the solid, but is ideally suited for profiling .1 to 10.0 μm into the surface. The fact that these glasses do corrode in aqueous environments, but show little reaction at the glass/solution interface, suggests that the reactants penetrate the material and breakdown the structure from within. Since it was already

known that the hydration of ZBLA is very slow at ambient temperatures - even when the relative humidity is as high as 95% - hydration experiments were carried out at 200C and 275C in water-saturated Ar or O_2.

Figure 7 shows that both oxygen and hydrogen are found to penetrate nearly 5,000.0 nm into the surface within 4 hours at 200C. It is especially noteworthy that the distribution of glass constituents has not been influenced by the water penetration. In multicomponent silicate glasses, hydration in water vapor usually leads to a redistribution of modifier species and the growth of a distinct surface layer. The temperature, time and carrier gas (Ar vs O_2) were varied, and in all cases, only the apparent penetration of H, O and in some instances C, were revealed in the profiles. This is clearly consistent with the ISS and AES surface studies in air and water vapor which showed only minimal surface reactions. A quantitative analysis of the SIMS data has not yet been completed, but the surface concentrations of water appear to be quite low after the exposure to humid gases (or dilute water-methanol mixtures - see below); thus, the oxygen associated with the molecular water observed in SIMS is probably at, or below, the detection limit in AES and ISS(~100 ppm).

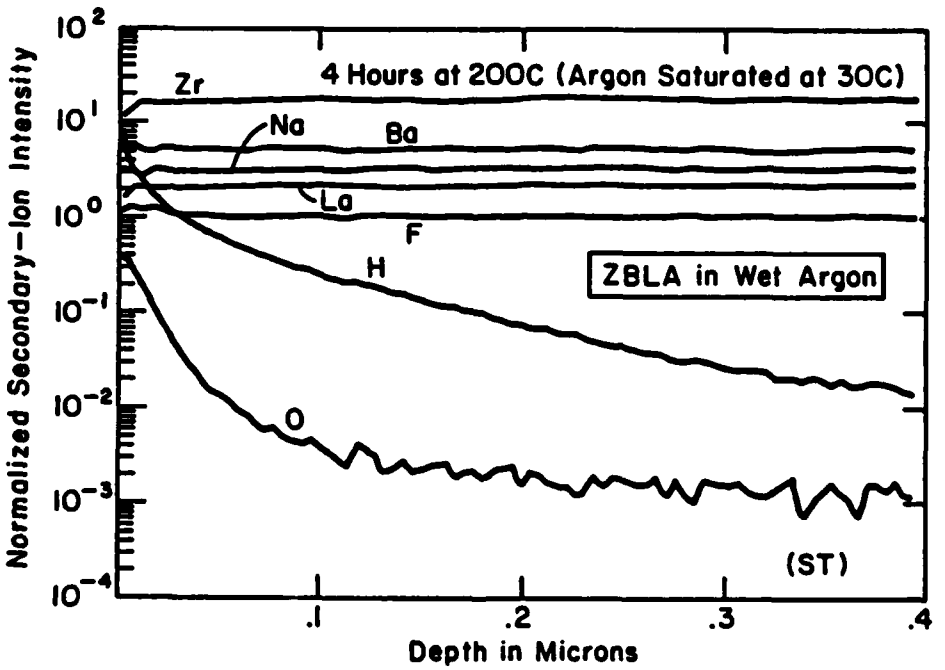

Figure 7. The in-depth concentration profiles observed after an elevated temperature (200C) exposure of a fluorozirconate glass to argon-which was first saturated with water at 30C; profiles were obtained using secondary ion mass spectroscopy.

SIMS was also used to examine ZBLA surfaces after exposure to liquid environments. Figure 8 summarizes the hydrogen profiles obtained after ten minute exposures at 30C to acid, water and base. The absence of any in-depth hydration (or any other in-depth effect) in ammonium hydroxide is clearly evident and is consistent with dissolution studies that show the relative inertness of these glasses to high pH environments. In contrast, the acid solution - within only ten minutes - generated a visible film on the surface, and the hydrogen profile in Figure 8 indicates that this layer is about 4 μm thick. The uniform hydrogen content, and the corresponding profiles for other constituents of the glass, reveal that this is a layer or film of surface reaction products. The scanning electron microscope (SEM) was also used to examine this surface; a layer containing dense agglomerates and clumps of fluoride crystals were observed. The glass which was exposed to water also exhibited a visible

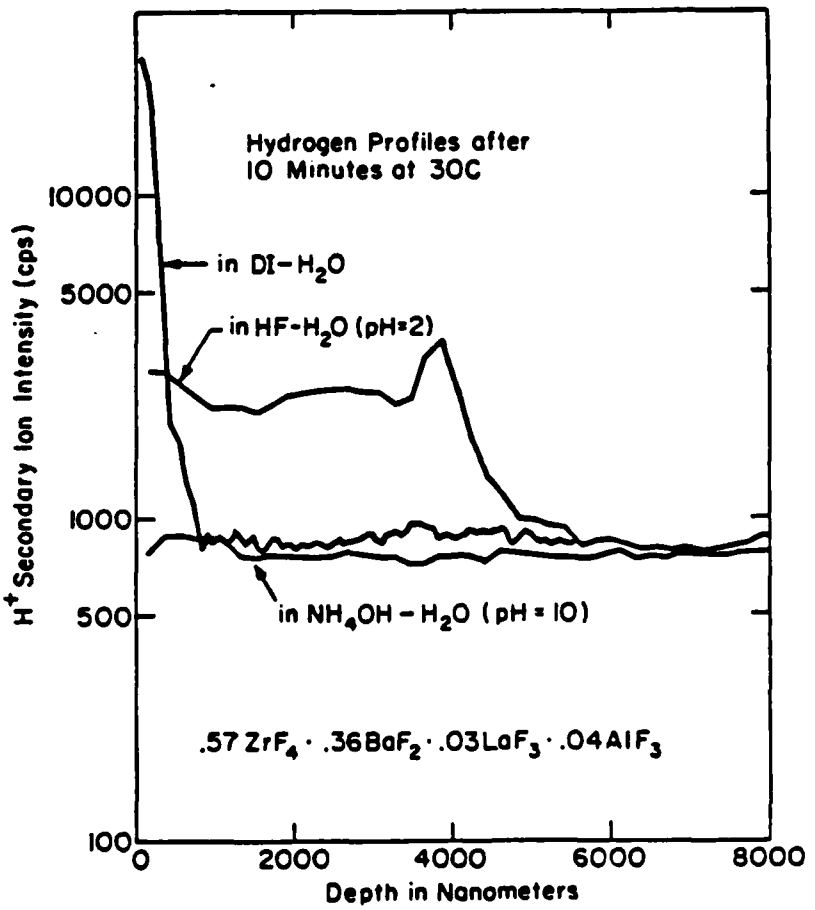

Figure 8. The in-depth concentration profiles for hydrogen in the surface layer of fluorozirconate glasses after exposure to water, acid and base; the profiles were obtained with secondary ion mass spectroscopy.

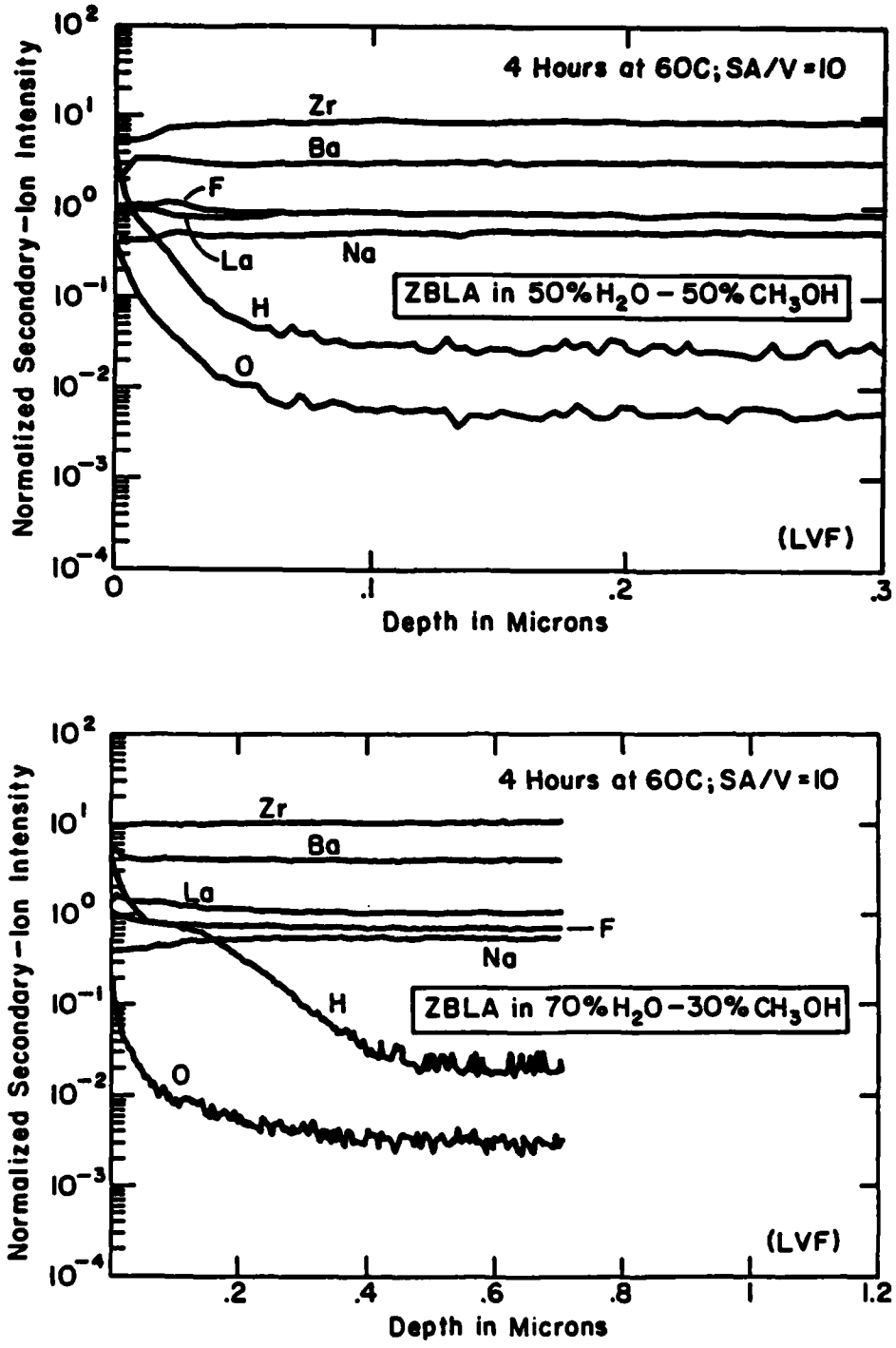

Figure 9. The in-depth concentration profiles for a fluorozirconate glass after exposure to water-methanol mixtures; the profiles were obtained with secondary ion mass spectroscopy.

film on the surface. The corresponding hydrogen-profile in Figure 8 shows that this layer is about .5-1.0 μm in thickness. Although the profile suggests that the hydrogen content is greater after the water corrosion, than after the acid exposure, this is more likely due to a density difference between the films produced in water versus acid. The 'acid-generated' surface layer is loosely adherent and often flakes-off during drying of the sample, whereas the 'water-generated' surface layer is usually more tenacious.

Since the mechanism of aqueous attack - rather than the formation of surface layers - is of primary relevance to stress corrosion, it again became necessary to lower the water activity by dilution with methanol so that the earliest stages of the reaction could be investigated. Figure 9 shows two sets of SIMS depth profiles; one set was obtained after a 4 hour hydration of ZBLA in 50% H_2O - 50% CH_3OH and the other after a 4 hour hydration in 70%H_2O-30%CH_3OH. Although other mixtures and conditions were examined, these two samples bracket the critical range of water activity. In addition to profiling the hydrated surfaces, the solutions were analyzed spectrochemically for dissolved constituents of the glass after the hydration.

The profiles in Figure 9 look very much like those due to water vapor hydration at elevated temperatures (Figure 7). Namely, there has been little or no attack of the glass structure - only penetration of hydrogen and oxygen; the corresponding infrared spectra obtained here, as well as those reported elsewhere (13), indicate that these species are associated with molecular water. The solution analyses showed negligible quantities of dissolved fluorine in the 50% H_2O - 50% CH_3OH mixture. This situation changes dramatically once the water concentration reaches 70% (at least for a 4 hour exposure). In this case, a twenty-fold increase in dissolved fluorine is observed, and the profiles show the initial stages of a distinct 'surface layer' formation due to this dissolution of the glass structure. This layer contains substantial levels of hydrogen and fluorine, but the oxygen profile is still reminiscent of an underlying diffusion process.

It seems clear that the ISS and AES analyses of water or acid corroded glasses detected surface reaction products, but these were fluorides rather than oxyfluorides, oxides or hydroxides. They are probably precursors to the ZrF_4 and $BaZrF_6$ crystals observed at the surface after

more extensive corrosion in water and acid (12). The SIMS analyses show that these fluoride reaction products will form layers at the surface whose rate of formation increases with decreasing pH. In addition, though, the SIMS mass spectra (not presented here) show peaks at m/e = 20, 40 and 60 whenever the surface has been exposed to gaseous or liquid water environments. These peaks can only be attributed to HF^+, $(HF)_2^+$ and $(HF)_3^+$, and so it is likely that these surface layers contain hydrogen fluoride (hydrogen cannot be detected with AES or ISS). The important point, though, is that these surface layers are not relics of the original glass structure, but rather, are the reaction products of its hydrolytic decomposition, dissolution and local precipitation. Due to the non-uniform nature of these surface layers, it is not possible to sputter-profile through to the underlying 'glass' and clearly define the interaction that occurs at the interface. But, if the layer formation is limited by lowering the water activity (e.g., in the water vapor or water - methanol mixtures), the penetration of molecular water into the glass can be seen.

These data show that in the case of both water vapor (at 200-300C) and liquid water the in-depth penetration of molecular water is more prevalent than hydrolysis or chemisorption at the glass surface. Tregoat, et al (25) exposed a barium-ytterbium-zinc-thorium fluoride glass to water vapor at 344°C, and in contrast to the behavior of this ZBLA glass, they observed HF gas evolution due to this interaction. Their infrared spectroscopic analyses showed the absence of molecular water vibrations in the hydrated surface, and thus, they proposed an interdiffusion reaction between F and OH. Loehr, et al. (13), also using infrared spectroscopy, did find molecular water - and little or no hydroxide species - in the surfaces of glasses hydrated in liquid water. The origin of these apparent discrepancies is not known, but may be related to temperature and composition differences.

5. DISCUSSION

Altogether, the surface studies indicate that the penetration and bulk diffusion of molecular water precedes any chemisorption, hydrolysis or breakdown of the glass structure. This appears to be true in humid

atmospheres as well as in liquid environments. Once the water reaches some critical concentration in the glass surface, the glass structure begins to disintegrate. It is likely that the molecular water - being somewhat nucleophilic - forms coordinate bonds with the Ba and Zr cations. This weakens the coulombic forces of attraction with the fluorine anions, and thereby, 'loosens' the structure. In the case of pure zirconium fluoride, mono-hydrates and tri-hydrates can be generated by exposure of ZrF_4 (ρ = 4.65 g/cc) to steam at 100°C-450°C. These hydrates are lower in density than the original ZrF_4 (ρ= 3.54 g/cc and 2.81 g/cc, respectively), and perhaps of greater significance, they form with little or no HF evolution (26). Since there is little or no evidence for ion-exchange or preferential leaching of any components in the fluorozirconate glasses, it seems certain that in-depth hydration by molecular water is fundamental to their hydrolytic decomposition and dissolution; i.e. it is the first step in the corrosion reaction.

In H_2O-CH_3OH mixtures and humid atmospheres, the water activity at the surface is low, and thus, the rate at which molecular water concentrates in the surface is limited by its diffusion into the bulk of the glass. Here, the penetration of water occurs with little or no hydrolysis, dissolution or surface layer formation (see Figures 7 and 9). In liquid water, the water activity at the glass/solution boundary is high. Thus, breakdown and dissolution of the glass commences rapidly, and as a result, the reaction products can accumulate and form surface layers. The pH determines the solubility of the glass constituents - once they are released from the glass structure - and so pH is critical to the overall dissolution rate and extent of surface layer formation. At low pH, for example, the dissolution rate is greatly enhanced because the solubility of fluorine increases. The extensive surface layer in this case is due to the insolubiliy of ZrF_4 at fluorine concentration greater than 10-100ppm; this condition is easily achieved in acid near the glass surface, and so the local precipitation of ZrF_4 is extensive. In contrast, the dissolution rate at pH 10 is 100-1000 times less than at pH 2 (15), and under these conditions the penetration of water is not observed. The fact that oxidation and/or hydroxylation of ZBLA was observed in the surface monolayer only for the pH 11 ammonium hydroxide solution suggests that these surface reaction products may 'block' the penetration of water and/or are exceedingly insoluble.

Some additional - albeit qualitative - evidence for a base-catalyzed 'passivation' of the ZBLA surface was provided by examining the corrosion of fracture surfaces which were pre-treated in the base. The fracture surfaces were created and aged in pH 10 ammonium hydroxide solution and were then placed in water. A set of control samples were fractured in air, as well as under the water, for comparison. There was no question that the fracture surfaces created and aged at pH 10 are more resistant to visible surface film formation than the glasses fractured in air or under water; i.e., a reproducible 'incubation time' can be observed before the glasses treated at pH10 begin to haze in the water.

The surface studies have provided considerable insight to the stress corrosion mechanism in ZBLA. The fact that the crack-growth behavior is relatively insensitive to pH is consistent with the idea that molecular water is primarily responsible for breakdown of the glass structure in aqueous environments. It is also clear that the crack velocities in acid, base, water and water vapor, and water-methanol mixtures depend in a consistent way upon the water activity. But since the extent of surface film formation and dissolution varies considerably amongst these environments, it can be concluded that surface film formation and/or dissolution are not important features of the stress corrosion reaction.

In the case of silicate glasses, the mechanism of stress corrosion has been attributed to a stress-enhanced dissociative chemisorption at the crack tip (7). This interaction occurs at the crack-tip between strained bonds and chemical species in the environment. The theory and experimental data support the idea that chemical species which possess both electron donor and proton donor sites are a prerequisite for this reaction. This property of chemical species has been characterized by Gutman (27) in terms of so-called donor numbers and acceptor numbers. Thus, chemical environments with high values for both of these numbers would be expected to enhance the crack-growth rate to the greatest extent. In the case of these fluoride glasses the crack-velocity at ~.2 MPa-$m^{1/2}$ (above the threshold for aqueous environments) shows an excellent correlation with the sum of those two numbers in all of the environments (28). This suggests that dissociative chemisorption may also be responsible for stress corrosion in these fluoride glasses. However, the surface studies of adsorption on clean fracture surfaces provided little evidence for the chemisorption of water. This indicates that the presence of strained-bonds may be required for the chemisorption reaction in this

system. Although the ISS data in Figure 4 supports this idea, many of the other surfaces prepared by fracture in gaseous and liquid environments did not show chemisorbed oxide a hydroxide species at the surface. It is to be emphasized, though, that these were all 'fast-fractured' in the environment, and so, these surfaces may not be representative of those prepared under sub-critical crack growth conditions. Clearly, the in-situ analysis of fracture surfaces created at low velocities would be a worthwhile endeavor.

On the other hand, the surface studies have indicated that the penetration of molecular water is the most prevalent interaction between aqueous environments and the fluorozirconate glasses. If a weakening of the ionic bonds due to the coordination of molecular water with the Zr and Ba cations is responsible for the sub-critical crack growth, then the crack velocity should scale with the dielectric constant or polarizibility of the environment. The relationship between crack velocity at K_I = .2 MPa-$m^{1/2}$, and the dielectric constant of the various environments, does not support this concept though. Thus, while hydration by molecular water may be fundamental to the corrosion and dissolution reactions, it may not be responsible for the bond-breaking event in stress corrosion.

Of particular significance are the thresholds (or stress-corrosion limits) - at about .20 MPa-$m^{1/2}$ - which are exhibited by the H_2O environments and the NH_3. These environments also exhibit velocity plateaus whose magnitude scales with the water activity. Since the rapid penetration and diffusion of molecular water is prevalent in these environments, one is led to consider the possible effects of 'stress-enhanced' water diffusion ahead of the crack-tip. This phenomena could influence the stress distribution at the crack-tip and/or modify the glass through which the crack-tip must propagate. Thus, the stress intensity and/or activity of water would determine the extent of water diffusion ahead of the crack-tip, and quite possibly, this water of hydration might dissociate - under stress - as the crack propagates. And in a qualitative sense, an interaction between the glass and environment 'ahead of the crack-tip' would explain the erratic behavior of the cracks in these glasses. In contrast to the behavior of silicate glasses during crack-growth experiments, the cracks in even well-annealed fluoride glasses seldom follow a path which is perfectly orthogonal to the applied moment. It is also found that once the crack has arrested - e.g. in and

below the threshold region of stress intensity - the crack will not re-propagate when the load is increased unless the specimen is 'tapped' to get it running.

6. SUMMARY

A detailed interpretation of the stress corrosion behavior in fluorozirconate glasses is only just beginning to emerge. The origin of the stress-intensity thresholds and velocity plateaus is not obvious, but clearly, an understanding of these features could contribute to the development of a model for stress corrosion in these materials. In this regard, it is noteworthy that the environments where velocity thresholds and plateaus are observed also happen to be those where the potential formation of HF reaction products can be proposed . Thus, the dependence of crack growth rates upon the ionic strength of $HF-H_2O$ mixtures would be useful information. In general, though, a more substantial data base concerning the surface chemistry and slow-crack growth characteristics of these glasses will be required, before a definitive model can be proposed and validated. This understanding will be necessary when evaluating the fatigue data yet to be reported for fluorozirconate optical fibers, and will be of great benefit in the design and development of more fatigue-resistant systems. And since these fluorozirconate materials represent a new and unique class of ionically-bonded glasses, the ability to compare their slow crack growth behavior with that of the more covalently-bonded silicate glasses could provide a more fundamental insight to stress-corrosion reactions in brittle solids.

ACKNOWLEDGEMENTS

The author thanks the Air Force Office of Scientific Research for their financial support (AFOSR-82-0013) and acknowledges his co-workers for their contributions: Armando Gonzalez, Cheryl Houser, Theresa McCarthy, Jack Mecholsky and Andrew Phelps.

REFERENCES

1. Pantano, C. G., "Surface Chemistry and Fracture of Fluoride Glasses", Materials Science Forum, 6, 285 (1985).
2. Becher, P. F. and Freiman, S. W., "Crack Propagation in Alkaline Earth Fluorides", J. Appl. Phys. 49, 3779 (1978).
3. McKinney, K. R., Mecholsky, J. J. and Freiman, S. W., "Delayed Failure in Chemically Vapor Deposited ZnSe", J. Am. Ceram. Soc., 62, 336 (1979).
4. Mecholsky, J. J., "Intergranular Slow Crack Growth in MgF_2", J. Am. Ceram. Soc., 64, 563 (1981).
5. Hillig, W. B. and Charles, R. J., "Surfaces, Stress-Dependent Surface Reactions and Strength", in High Strength Materials, (W. F. Zackey, Ed., Wiley, NY, 1965) pp 682-701.
6. Wiederhorn, S. M., "A Chemical Interpretation of Static Fatigue", J. Am. Ceram. Soc., 55, 81 (1972).
7. Michalske, T. A. and Freiman, S. W., "A Molecular Mechanism for Stress Corrosion in Vitreous Silica", J. Am. Ceram. Soc., 66, 284 (1983).
8. Simmons, C. J., Sutter, H., Simmons, J. H. and Tran, D. C., "Aqueous Corrosion Studies of a Fluorozirconate Glass", Mat. Res. Bull. 17, 1203 (1982).
9. Mitachi, S., "Chemical Durability of Fluoride Glasses in the BaF_2-GdF_3-ZrF_4 System", Phys. Chem. Glasses, 24, 146 (1983).
10. Barkatt, A. and Boehm, L., "The Corrosion Process of Fluoride Glass in Water and the Effects of Remelting and of Glass Composition", Mat. Lett., 3, 43 (1984).
11. Frischat, G. H. and Overbeck, I., "Chemical Durability of Fluorozirconate Glasses", J. Am. Ceram. Soc., 67, C-238 (1984).
12. Doremus, R. H., Murphy, D., Bansal, N. R., Lanford, W. A., and Burman, C., "Reaction of Zirconium Fluoride Glass with Water: Kinetics of Dissolution", J. Mater. Sci., 20, 4445 (1985).
13. Loehr, S. R., Bruce, A. J., Mossadegh, R., Doremus, R. H. and Moynihan, C. T., "IR Spectroscopy Studies of Attack of Liquid Water on ZrF_4-Based Glasses" Mater. Sci. Forum, 5, 311 (1985).
14. Simmons, C. J. and Simmons, J. H., "Chemical Durability of Fluoride Glasses" to appear.

15. McCarthy, T. A., Houser, C. A. and Pantano, C. G., "Dissolution and Surface Layer Formation in Fluorozirconate Glasses" to appear.
16. Amphlett, C. B., "The Adsorption of Water Vapour by Calcium Fluoride", Trans. Faraday Soc., 54, 1206 (1958).
17. Hall, P. G. and Tompkins, F. C., "Adsorption of Water Vapour on Insoluble Metal Halides", Trans. Faraday Soc., 58, 1734 (1962).
18. Barraclough, P. B. and Hall, P. G., "Adsorption of Water Vapour by Calcium Fluoride,, Barium Fluoride and Lead Fluoride", Trans. Faraday Soc., 71, 2266 (1975).
19. Palik, E. D., Gibson, J. W., Holm, R. T., "Internal Reflection Spectroscopy Study of Adsorption of Water on CaF_2 Surfaces", Surf. Sci., 84, 164 (1979).
20. Wojciechowska, M. and Fiedorow, R., "Surface Chemistry of Porous Magnesium Fluoride", J. Fluorine Chem., 15, 443 (1980).
21. Strecker, C. L., "Determination of the Heat of Adsorption for Water Vapor on Clean Calcium Fluoride Surfaces by Ion Scattering Spectroscopy", Ph.D. Dissertation, University of Dayton, 1985.
22. Freiman, S. W., Mulville, D. R. and Mast, D. W., "Crack Propagation Studies in Brittle Materials", J. Mater. Sci., 8, 1527 (1973).
23. Pantano, C. G., and Madey, T. E. "Electron Beam Damage in Auger Electron Spectroscopy", Appl. Surf. Sci., 6, 115 (1981).
24. Chikazawa, M. and Kanazawa, T., "The Adsorption Mechanism of Methanol on Alkali Halides", Bull. Chem. Soc. Japan, 50, 2837 (1977).
25. Tregoat, D., Fonteneau, G., Lucas, J. and Moynihan, C. T., "Corrosion of HMFG by H_2O Vapor", Mater. Sci. Forum, 5, 323 (1985).
26. Waters, T. N., "Some Investigations in the Zirconium Tetrafluoride-Water System", J. Inorg. Nucl. Chem., 15, 320 (1960).
27. Gutman, V. The Donor-Acceptor Approach to Molecular Interactions, Plenum Press, NY, 1978.
28. Gonzalez, A., Mecholsky, J. J. and Pantano, C. G., "Stress Corrosion Mechanisms in Fluorozirconate Glasses", to appear.

CHAPTER VII

ELASTIC MODULI OF SILICATE GELS PREPARED WITH TETRAETHOXYSILANE

by

M. J. Murtagh, E. K. Graham and C. G. Pantano

Department of Materials Science and Engineering

Pennsylvania State University

University Park, PA 16802

Accepted for publication in J. American Ceramic Society.

ABSTRACT

The elastic moduli of several organometallic silica gels were measured using pulse-superposition interferometry (PSP). A series of gels were prepared under acid-catalyzed conditions where the molar ratio of water to tetraethoxysilane in the sol was varied (4:1, 12:1, 16:1 and 24.1). It was found that the elastic moduli varied systematically with the hydrolysis conditions used to prepare the gels, as well as with the relative humidity used to equilibrate the gels before and during the PSP measurement. The experimental PSP data for the gels were evaluated using a composite model (matrix plus pores) and then the elastic moduli of the gel matrix were determined by applying a correction for porosity based on a self consistent scheme (SCS) approximation. The results show that the elastic moduli of the gel matrix also exhibit a systematic dependence upon the preparation conditions, but they always fall below the corresponding values for fused silica. Even when excess water was used to hydrolyze the TEOS, this did not lead to a fully polymerized silica matrix structure. It is suggested that the lowered matrix moduli values are due to the presence of residual hydroxy and ethoxy groups which are internal to a polymeric structure.

INTRODUCTION

The sol/gel method of glass formation is limited to the production of only small bodies because of the cracking and fragmentation which occurs during processing. This is especially evident in the case of organometallic sol/gel materials; that is, silica gels prepared by the hydrolysis of tetralkoxysilanes in non-aqueous solvents. It is well recognized that the mechanical stresses generated during drying and firing are responsible for the fracture, but there have been only a few attempts to model them in terms of the capillary forces, density gradients, and their dependence upon the rate of drying or firing. The development of such models requires information concerning the elastic modulus of the gel as a function of the textural parameters (i.e., the matrix structure and pore-size distribution) and the relative humidity (i.e., the effects of adsorbed/condensed water). And independent of their role in determining the mechanical integrity of these materials during drying and firing, the structure and mechanical properties of the 'gel matrix' are of fundamental interest.

This paper reports a systematic study concerning the effects of the solution composition upon the elastic moduli of silica gels; the dependence of the elastic moduli upon relative humidity is also presented. The structure of these silicon alkoxide gels consists of a silica-like matrix with microporosity whose volume fraction, distribution and connectivity varies with the hydrolysis conditions. The elastic moduli of the matrix phase were evaluated by modeling the composite elastic moduli in terms of the volume fraction of the gel matrix and the pore geometry.

EXPERIMENTAL PROCEDURE

Gel Preparation

A series of silicon alkoxide gels (with water: TEOS of 4:1, 12:1, 16:1, and 24:1) were prepared systematically (see Table 1) using TEOS ($Si(OC_2H_5)_4$), ethanol (C_2H_5OH), water and a 1M hydrochloric acid solution (1). These H_2O-to-TEOS ratios represent 1, 3, 4, and 6 times the theoretical quantity of water required for complete hydrolysis, respectively, and are hereinafter referred to as 1X, 3X, 4X and 6X. The solutions were cast in 16 mm x 150 mm pyrex test tubes and left to gel at room temperature. The gelation and drying were carried out over a period of several months.

Density

The bulk density of the gels was determined by Archimedes and dimensional methods. The bulk densities measured by the Archimedes method were conducted in water using a wax immersion technique approved by ASTM (2). Five determinations were made on each sample. The results are reported as an average value with 95% confidence intervals. The bulk densities measured by dimensional methods were carried out on cylindrical gel samples with the end faces polished flat and parallel with one micron diamond paste. The diameter and thickness were measured using a hand held micrometer, accurate to plus or minus 5 microns. Twenty determinations were made per sample and reported as an average with 95% confidence intervals.

The matrix density was determined by further drying the gels at 0% relative humidity. The dry weight was recorded and then the gels were saturated with deionized water. The volume of the matrix was determined in the following manner. The volume of the water in the pores, V_{H_2O}, is given by

Table 1. Sol/Gel Compositions (by volume).

Sol	$Si(OC_2H_5)$ %	C_2H_5OH %	H_2O %	Molar ratio of H_2O to $Si(OC_2H_5)_4$	Catalyst 1M HCl ml
1X *	43	43	14	4	0.4
3X	33.5	33.5	33.0	12	0.4
4X	30.2	30.2	39.6	16	0.4
6X	25.2	25.2	49.6	24	0.4

* the X denotes a H_2O to $Si(OC_2H_5)_4$ ratio of 4.

$$V_{H_2O} = \frac{A_s - A_m}{\rho_{H_2O}} \quad (1)$$

where V_{H_2O} is assumed equivalent to the volume of the pores in the gel samples, A_s is the saturated mass, A_m is the mass of the matrix, and ρ_{H_2O} is the density of water. Then,

$$V_m = V_b - V_{H_2O} \quad (2)$$

where V_m is the volume of the matrix and V_b is the volume of the bulk gel.

Elastic Moduli

The elastic moduli were determined using an acoustic interferometry technique known as ultrasonic pulse-superposition (PSP), as described by McSkimin (3). PSP utilizes an applied repetitive sequence of radio frequency pulses-in the range KHz to GHz-transmitted through a piezoelectric transducer which is bonded to the sample. The time interval during which the elastic wave propagates through the sample, from one face to the other and back, may be adjusted to equal precisely the repitition rate of the next RF pulse. When this is achieved, the applied pulses are superimposed upon the return echoes producing a constructive interference. The echoes then build up sufficient amplitude to be observed on an oscilloscope.

The samples were prepared as flat parallel cylinders 5-10 mm in diameter and 1-3 mm thick. X-cut and AC-cut (3 mm and 4.6 mm) quartz transducers were used to generate and determine the travel-time of the longitudinal (compressional) and transverse (shear) waves, respectively. The instrument used in this work had a frequency range of 15-25 MHz, but all of the gel measurements were made at 20 MHz.

The Young's elastic modulus was determined from the bulk density (ρ) of the

sample and the compressional (V_p) and shear wave (V_S) velocities by

$$E = \frac{3\rho V_p^2 - 4\rho V_s^2}{(V_p/V_s)^2 - 1} \quad . \tag{3}$$

The shear modulus was determined from the density of the samples and the shear wave velocities by

$$G = \rho V_s^2 \quad . \tag{4}$$

The bulk modulus (K) was determined via

$$K = \rho V_p^2 - {}^4/_3\, V_s^2 \quad , \tag{5}$$

and the Poisson's ratio (υ) was determined from the ratio of the Young's elastic modulus and the shear modulus using

$$\upsilon = \frac{E}{2G} - 1 \quad . \tag{6}$$

Controlled Humidity Measurements

Young's elastic modulus, the shear modulus, the bulk modulus, and Poisson's ratio were also determined as a function of the relative humidity at room temperature using the PSP method. Here, the relative humidity was controlled by mixing dry and saturated nitrogen gases in a one cubic foot dessicator. The humidity levels were recorded by a Bacharach hygrometer which is accurate to plus or minus two percent. The cylindrical gel samples were equilibrated at increments of ten percent relative humidity, and although not reported, the kinetics of equilibration were simultaneously monitored by the PSP travel-time measurements at five minute intervals up to one hour.

Model for Composite Moduli

A self consistency scheme (SCS) was developed by Budiansky, and also by Hill (4,5), to characterize the elastic properties of isotropic multi-phase composites. This model was used here to generate theoretical elastic moduli values for the saturated and dry gel composites assuming a 'fused' silica matrix. These values were then compared with the experimentally determined properties. The effective, or composite, moduli (M^*) are given by:

$$\frac{M^* - M_l}{M_m - M_l} = (1-n) \left[1 + \frac{n(M_m - M_l)}{M_l + F}\right]^{-1} \qquad (7)$$

where M^* is either the bulk modulus (K^*) or the shear modulus (G^*) for the composite, M_l is either K_l or G_l for the pore[++], M_m is either K_m or G_m for the gel matrix, and n is the volume fraction porosity. F depends on whether M^* is K^* or G^*, and the pore geometry, as follows;

Spherical Pores

For K^*

$$F = \frac{4}{3} G^*$$

For G^*

$$F = \frac{G^*(9K^* + 8G^*)}{6(K^* + 2G^*)} \qquad (9)$$

Needle Pores

For K^*

$$F = \frac{1}{3} (G_l + G^*)$$

For G^*

[++] In the present case, the pores are either dry or saturated with water.

$$F = 5\left[3(K_1 + {}^1/_3\, G_1 + G^*)^{-1} + \frac{2(2G_1 + G^* + g)}{(G_1 + G^*)(G_1 + g)}\right]^{-1} - G_1 \quad (11)$$

where

$$g = \frac{G^*(K^* + \frac{1}{3}G^*)}{K^* + \frac{2}{3}G^*} \quad (12)$$

Due to the nature of the foregoing relations, K^* and G^* must be evaluated by an iterative procedure (6).

The Young's elastic modulus, shear modulus, bulk modulus, and Poisson's ratio of the gel matrix were also evaluated using the SCS model since the abovementioned calculations showed the assumption of a 'fused silica' matrix to be false. The experimental values of the shear and bulk modulus of the gel composites were used in this calculation and the pore geometry was assumed to be needle-shaped. It is reasonable to believe that needle-shaped porosity is meaningful for these gel materials, and indeed, it is shown that the theoretical predictions of the composite properties where needle-shapes are assumed more closely match the experimental composite values. The shear modulus (G_m) and bulk modulus (K_m) of the gel matrix were determined using

$$M_m = \frac{M^* F}{F(1-n) - M^* n} \quad (13)$$

which follows directly from equation 7 using, in this case, $K_1 = G_1 = 0$. The experimental values for M^* (i.e. K^* or G^*) were used, and for K^*

$$F = G^*$$

and for G^*

$$F = 5\left[(3G^*)^{-1} + \frac{2(G^* + g)}{(G^*)(g)}\right]^{-1}$$

where g is given by equation 12. The Young's elastic modulus (E_m) and the Poisson's (υ_m) ratio of the gel matrix were then determined using the relations

$$E_m = \frac{G_m(3K_m)}{K_m + \frac{1}{3}G_m} \tag{16}$$

and

$$\upsilon_m = \frac{K_m - \frac{2}{3}G_m}{2(K_m + \frac{1}{3}G_m)} \tag{17}$$

RESULTS AND DISCUSSION

Density

The bulk densities for the 1X, 3X, 4X, and 6X acid catalyzed TEOS gels were determined by the Archimedes' method after equilibration at a constant humidity. It is important to emphasize that there was little correlation between the gel compositions, the measured densities and the measured wave velocities until the gels were equilibrated at a controlled humidity before or during any measurement. The attainment of equilibrium could be verified by measuring the wave velocities during this equilibration.

The average bulk densities as a function of relative humidity, the average matrix density, and the corresponding porosity, are presented for each gel composition in Table 2. The bulk densities were used to determine the elastic moduli of the gel composite as a function of relative humidity while the matrix densities were used in the evaluation of the matrix elastic moduli. The density measured at 0% relative humidity was assumed to be the actual bulk density of the dry gel.

Table 2. The average* bulk density as a function of relative humidity, the matrix density, and the percent porosity for 1X, 3X, 4X, and 6X gel specimens.

Gel	Relative Humidity										Matrix Density	Percent Porosity
	0.00	0.15	0.25	0.35	0.45	0.55	0.65	0.75	0.85	1.00		
1X	1.65 ±.025	– –	1.689 ±.025	– –	– –	1.736 ±.025	– –	1.759 ±.025	– –	1.79 ±.025	1.883	12.4
3X	1.55 ±.022	– –	1.608 ±.022	– –	1.672 ±.022	– –	1.736 ±.022	– –	– –	1.772 ±.022	1.986	21.9
4X	1.474 ±.014	1.514 ±.014	1.536 ±.014	1.586 ±.014	1.62 ±.014	1.662 ±.014	1.704 ±.014	1.727 ±.014	1.745 ±.014	1.763 ±.014	2.069	28.8
6X	1.388 ±.016	1.428 ±.016	1.479 ±.016	1.566 ±.016	1.599 ±.016	1.633 ±.016	1.664 ±.016	1.69 ±.016	1.724 ±.016	1.736 ±.016	2.195	36.7

* 95% confidence interval

Figures 1 and 2 illustrate the bulk and matrix density (at 0% relative humidity) as a function of the molar ratio of water to TEOS used in the gel processing. The matrix density is linearly proportional to the molar ratio of water to TEOS whereas the bulk density shows an inverse relationship. This type of behavior has been reported by others (7-9). This trend has been explained in terms of the relative rates of hydrolysis and condensation for different ratios of H_2O to TEOS and the corresponding structural units so-produced.

In an acid catalyzed silicon alkoxide gel, hydrolysis proceeds via electrophilic attack (8). At low molar ratios of water to TEOS (with a constant acid concentration), highly-extended polymers can be expected (1) The backbone of this polymer is based upon Si-O-Si bonding, but the 'chain' is framed with residual ethoxy and hydroxy groups. Upon drying the gel, the highly-extended, but weakly cross-linked, gel shrinks upon itself with little resistance. Thus, these gels dry to a relatively high bulk density, but the matrix density is low due to the high residual organic component.

Conversely, at high molar ratios of water to TEOS (again with a constant acid concentration), the polymer units in the gel contain a lower percentage of residual ethoxy groups, and correspondingly, are denser and probably more highly cross-linked. During the desiccation and drying of these gels, the more highly cross-linked polymer units (which can be particle-like at very high H_2O/TEOS) resist the shrinkage due to packing contraints and/or due to additional polymerization as the system concentrates. In either case, the result is a gel of lower bulk density but higher matrix density.

Gel Moduli and Their Humidity Dependence

Table 3 presents the average elastic wave velocities (compressional and shear) as a function of the relative humidity and the sol/gel composition. The

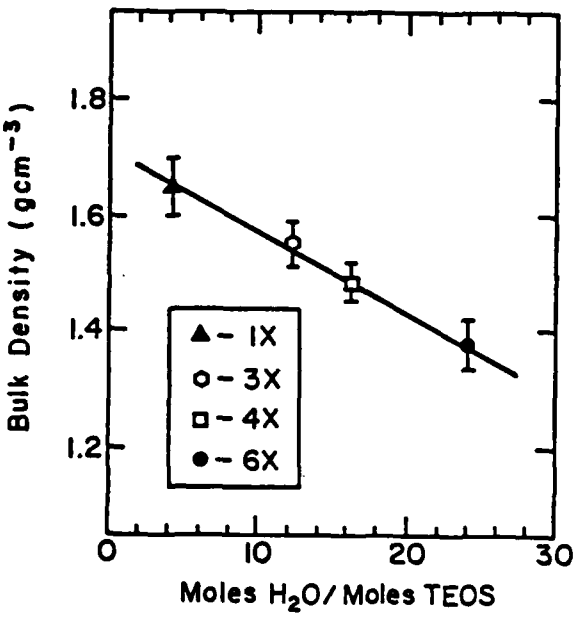

Figure 1. The variation in the bulk density at 0% relative humidity for 1X, 3X, 4X, and 6X acid catalyzed TEOS gels.

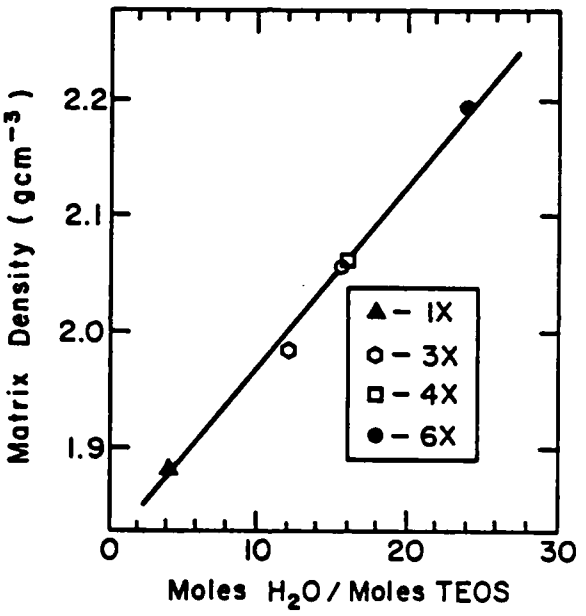

Figure 2. The variation in the average matrix density for 1X, 3X, 4X, and 6X acid catalyzed TEOS gels; the (o) data point is an independent density measurement for a 4X gel from reference (12).

AD-A170 243 SURFACE CHEMISTRY AND STRUCTURAL EFFECTS IN THE STRESS 3/3
CORROSION OF GLASS. (U) PENNSYLVANIA STATE UNIV
UNIVERSITY PARK DEPT OF MATERIALS SCI..
UNCLASSIFIED C G PANTANO ET AL. 31 MAR 86 F/G 11/2 NL

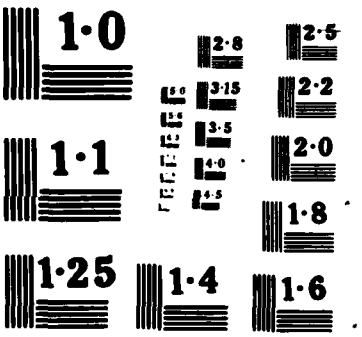
1·0
1·1
1·25
1·4
1·6
1·8
2·0
2·2
2·5
2·8
3·15
3·5
4·0
4·5

Table 3. The average wave velocities (km/sec) as a function of relative humidity, and the corresponding sample thickness (cm) for the 1X, 3X, 4X, and 6X gel specimens.

Gel	Wave Velocity	Relative Humidity 0.00	0.15	0.25	0.35	0.45	0.55	0.65	0.75	0.85	1.00	Sample Thickness
1X	V_p	2.678	-	2.747	-	-	2.809	-	2.845	-	2.892	0.1879
	V_s	1.553	-	1.545	-	-	1.537	-	1.538	-	1.541	
3X	V_p	2.512	-	2.576	-	2.623	-	2.651	-	-	2.712	0.1877
	V_s	1.496	-	1.488	-	1.484	-	1.482	-	-	1.482	
4X	V_p	2.412	2.441	2.489	2.518	2.534	2.545	2.561	2.578	2.59	2.62	0.1881
	V_s	1.473	1.451	1.448	1.443	1.445	1.445	1.447	1.448	1.449	1.452	
6X	V_p	2.32	2.291	2.339	2.382	2.413	2.436	2.454	2.473	2.491	2.507	0.1869
	V_s	1.419	1.397	1.388	1.385	1.386	1.387	1.391	1.392	1.395	1.4	

V_p - compressional wave velocity (km/sec)

V_s - shear wave velocity (km/sec)

elastic wave velocities listed in Table 3, and the densities given in Table 2, were used to determine the Young's elastic modulus (E), bulk modulus (K), shear modulus (G), and Poisson's ratio. The values for E, K, and G, as functions of relative humidity (P/P_o) for the 1X, 3X, 4X, and 6X gels, are shown in Figures 3 and 4. The elastic moduli and Poisson's ratios for the 'dry' gels are summarized in Table 4.

In general, the gels exhibit the expected trend of increasing elastic moduli with increasing density. The slopes of the E and K vs P/P_o plots also decrease with increasing density, presumably due to the decrease in pore volume with increasing density. The non-linearity in the E and K vs P/P_o curves at low relative humidity is probably due to an adsorbed water effect; and the fact that this inflection is enhanced for the higher porosity gels is consistent with a dependence upon surface area. The shear modulus shows a weaker dependence on relative humidity because of the negligible rigidity of the fluid phase.

Matrix Moduli as a Function of the H_2O/TEOS Ratio

Initially, the elastic moduli of the gel matrices were assumed to have the value for fused silica, and then the SCS model was utilized to generate theoretical wave velocities and moduli for 'fused silica' gel/composites. The compressional wave velocities for these theoretical 'fused silica' gel/composites are compared to the experimentally measured velocities of the bulk gels in Figure 5. The compressional wave velocity (and the elastic moduli) increase with density, in general, but the dependence upon density is quantitatively distinct for the 'fused silica' gel/composites versus the 'organometallic silica'-gel/composites. No manipulation of the model or pore geomety could be found which would reduce the compressional wave velocities of the 'fused silica'-gel to match (or approximate) those for the 'organometallic

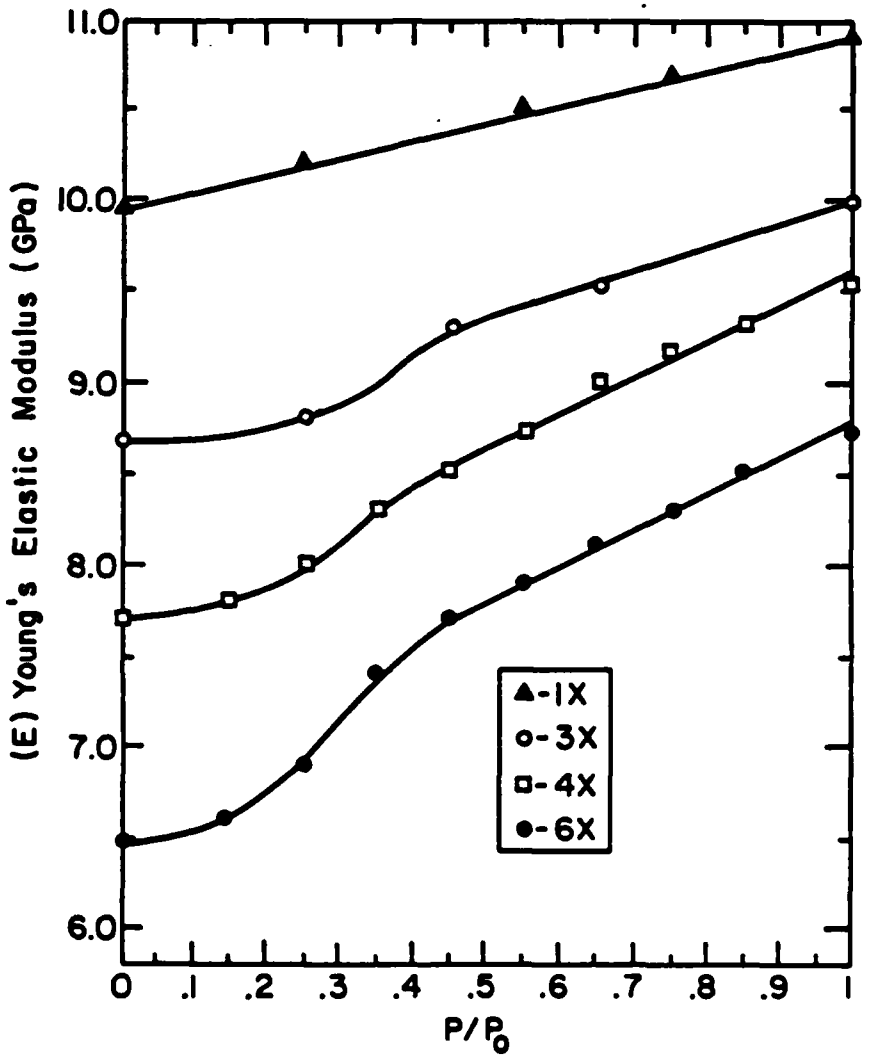

Figure 3. Variation in the Young's elastic modulus as a function of relative humidity for 1X, 3X, 4X and 6X acid catalyzed TEOS gels.

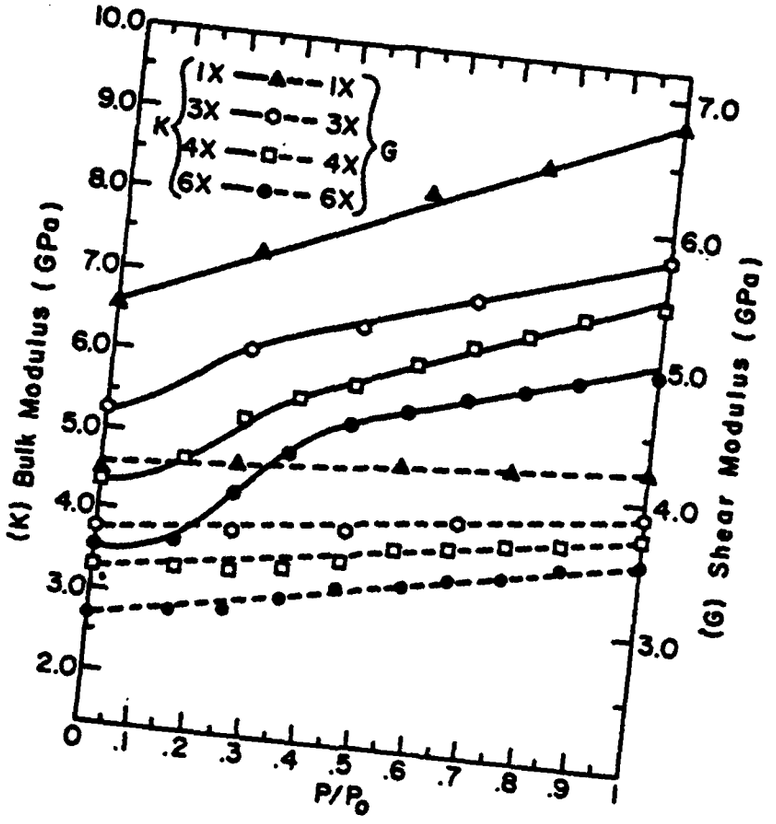

Figure 4. Variation in the bulk and shear modulus as a function of relative humidity for 1X, 3X, 4X, and 6X acid catalyzed TEOS gels.

Table 4. The average elastic moduli (GPa) and Poisson's ratio for 1X, 3X, 4X and 6X gel specimens at 0% relative humidity.

Gel	Young's Elastic Modulus*	Shear Modulus*	Bulk Modulus*	Poisson's Ratio*
1X	9.95	3.95	6.53	0.245
3X	8.72	3.54	5.28	0.228
4X	7.71	3.21	4.42	0.201
6X	6.55	2.83	3.51	0.192

* Average for 0% relative humidity

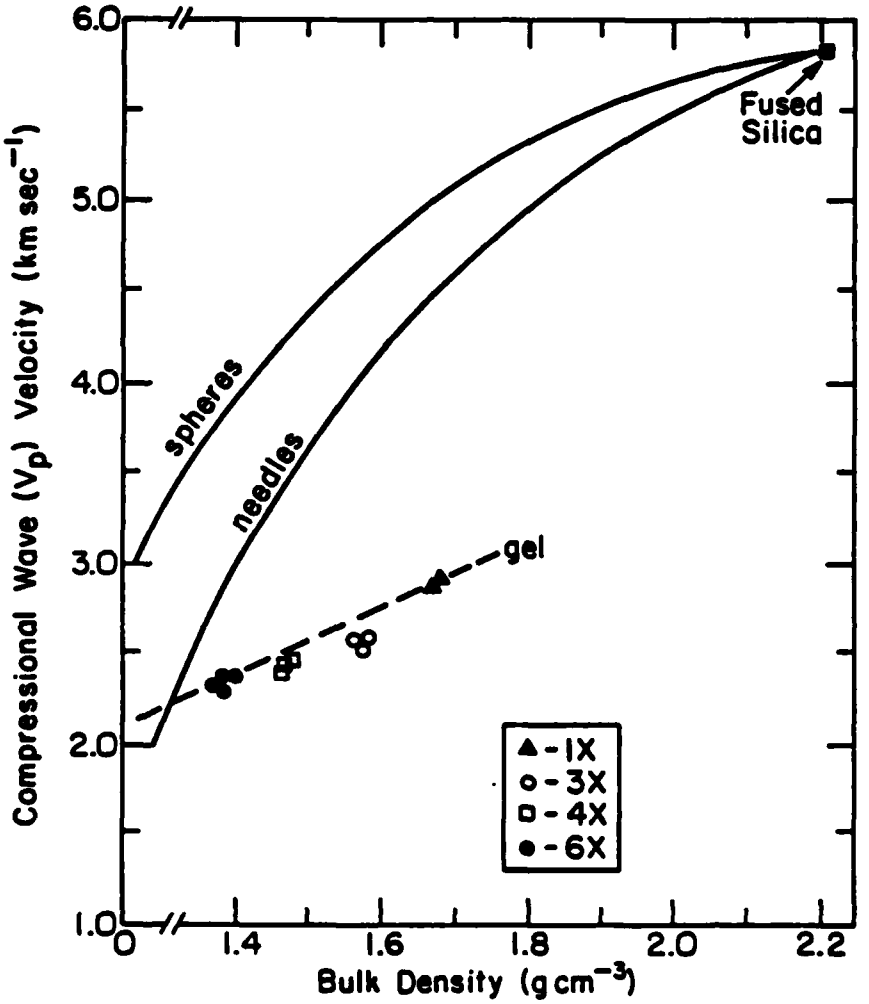

Figure 5. The compressional wave velocities for a hypothetical 'fused silica' gel/composite for needle and spherical pore geometries and the experimental values for 1X, 3X, 4X, and 6X acid catalyzed 'organometallic silica' gels as a function of bulk density; fused silica data from reference (11).

silica'-gel. One can only conclude that the matrix phase in silica gels prepared with TEOS does not exhibit the elastic properties of fused silica.

Figure 6 presents the average matrix elastic moduli (calculated according to equations 13-17) as a function of the molar ratio of H_2O to TEOS for the 1X, 3X, 4X, and 6X gels. It is clear that increasing the H_2O/TEOS ratio yields a matrix phase of increasing stiffness. This trend is consistent with the aforementioned polymer models for acid catalyzed TEOS gels (1, 7-10) which suggest the formation of more highly condensed silicates with increasing H_2O/TEOS ratios. But these data show clearly that although the elastic moduli of the matrix phase approach the values for fused silica, even the 6X gel falls short by a considerable amount. In simple terms, this means that the solid material which exists after equilibration of the gels at 0% relative humidity is not 'silica'. However, it is not possible to define a more precise structural interpretation with these data alone. The texture of the matrix, the concentration of residual ethoxy groups, and the extent of hydration all combine to determine the matrix density and moduli.

SUMMARY AND CONCLUSION

A series of silicate sol/gel materials were fabricated with varying ratios of water to TEOS. Under controlled atmosphere conditions, there is a clear trend in the density and elastic moduli of the gel composites as a function of percent relative humidity. The gels were treated as two-phase 'gel composites' wherein the solid phase is silica, or silica-like, while the other phase is a fluid-namely, dry air, moist air or water. Further characterization of the solid matrix-phase was then carried-out using a self-consistent scheme approximation (SCS) for interpretation of the elastic properties.

The matrix density for each gel composition was determined using the dry

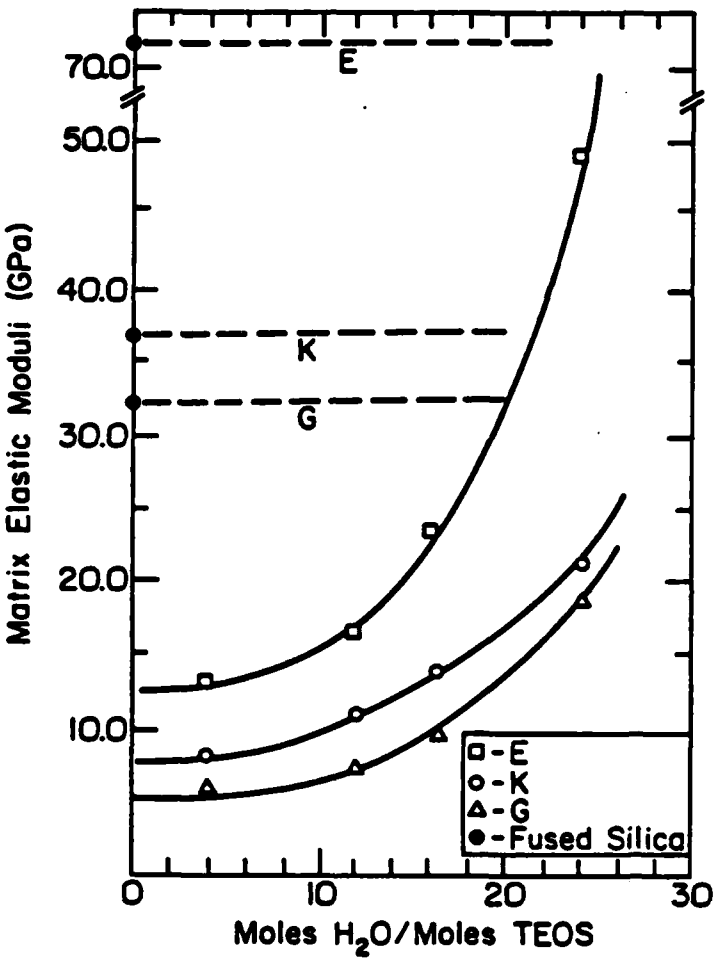

Figure 6. The variation in the matrix elastic moduli for 1X, 3X, 4X, and 6X acid catalyzed TEOS gels; fused silica data from reference (11).

gel composites; i.e., gels equilibrated at 0% relative humidity. The matrix density ranged from 1.88 gcm^{-3} to 2.19 gcm^{-3} for 4:1 to 24:1 gels (these may be compared to fused silica whose density is 2.2007 gcm^{-3}). A theoretical correction for porosity, based on the self consistent scheme (SCS) approximation, was applied to the gel composites to evaluate the elastic moduli of the gel matrix. The matrix values of the Young's elastic modulus varied from 13.8 GPa to 48.8 GPa, the shear modulus from 5.5 GPa to 21.5 GPa, the bulk modulus from 9.3 GPa to 23.3 GPa, and the Poisson's ratio from 0.24 to 0.16 over the range of compositions studied; these may be compared to the values for fused silica which are 72.8 GPa, 31.3 GPa, 36.2GPa and 0.16, respectively (11). It is important to emphasize, though, that the calculation of the matrix elastic moduli for the organometallic silica gel/composites assumed a uniform distribution of needle-shaped pores. However, it is also noteworthy that no manipulation of the model was sufficient to explain the organometallic silica gel/composite properties when a fused silica matrix was assumed.

The analysis of the matrix elastic moduli further supports the idea that the hydrolysis/condensation of tetraethoxysilane does not produce a 'fused-silica' matrix. The values of the elastic moduli for the gel matrix, over the range of the compositions studied, consistently fell below those of fused silica. This is presumably due to a limited degree of condensation during the solution-to-gel transition. Thus, there may be terminal hydroxy and ethoxy groups which not only 'frame' the matrix phase, but which are also internal to it. Nonetheless, the results show a trend towards increasing stiffness as the water necessary for hydrolysis is increased.

ACKNOWLEDGEMENT

The authors gratefully acknowledge the financial support of the Air Force Office of Scientific Research (AFOSR-82-0013).

REFERENCES

1. Brinker, J. C., Keefer, K. D., Schaefer, D. W., and Ashley, C. S., "Sol-Gel Transition in Simple Silicates," J. Non-Cryst. Solids, 48 (1) 47-64 (1982).

2. Standard Test Method, "Bulk Density of Volume of Solid Refractories by Wax Emersion," in Annual Book of ASTM Standards, (Edited by Priemon, R. A.) ASTM, Philadelphia, 15 (1) 448-499 (1983).

3. McSkimin, H. J., "Pulse Superposition Method for Measuring Ultrasonic Wave Velocities in Solids," J. Acoust. Soc. Am., 33 12-16 (1961).

4. Budiansky, B., "On the Elastic Moduli of Some Heterogeneous Materials," J. Mech. Phys. Solids, 13 (1) 223-227 (1965).

5. Hill, R., "Self-Consistent Mechanics of Composite Materials", J. of Mech. Phys. Solids, 13, 213-222 (1965).

6. Watt, P. J., Davies, G. F., O'Connell, R. J., "The Elastic Properties of Composite Materials," Review Geophys. Space Phys., 14 (4) 541-563 (1976).

7. Klein, L. C. and Garvey, G. J., "Drying and Firing Monolithic Silica Shapes from Sol-Gels", in Ultrastructure Processing of Ceramics, Glasses, and Composites, (Edited by Hench, L. L. and Ulrich, D. R.), John Wiley and Sons, Inc. New York, 88-99 (1984).

8. Keefer, K. D., "The Effect of Hydrolysis Conditions on the Structure and Growth of Silicate Polymers," in Better Ceramics through Chemistry, (Edited by Brinker, J. C., Ulrich, D. R., and Clark, D. E.), Elsevier-North Holland, New York, 15-25 (1984).

9. Brinker, C. J. and Scherer, G. W., "Relationships between the Sol-to-Gel and Gel-to-Glass Conversions," in Ultrastructure Processing of Ceramics, Glasses, and Composites, (Edited by Hench, L. L. and Ulrich, D. R.), John Wiley and Sons Inc., New York, 43-59 (1984).

10. Yoldas, B. E., "Introduction and Effect of Structural Variations in Inorganic Polymers and Glass Networks," J. Non-Cryst. Solids, 51 (1) 105-121 (1982).

11. M. H. Manghnani, "Pressure and Temperature Studies of Glass Properties Related to Vibrational Spectra", Final Report ONR-N00014-67-A-0387-0012, NR032-527, December 1974.

12. Klein, L. C., Gallo, T. A. and Garvey, G. J., "Densification of Monolithic Silica Gels Below 1000°C," J. Non-Cryst. Sol., 63, 23-33 (1984).

END

DTIC

8-86